Hydrothermal Systems of the Cascade Range, North-Central Oregon

Hydrothermal Systems of the Cascade Range, North-Central Oregon

By S.E. INGEBRITSEN, R.H. MARINER, *and* D.R. SHERROD

GEOHYDROLOGY OF GEOTHERMAL SYSTEMS

U.S. DEPARTMENT OF THE INTERIOR

BRUCE BABBITT, *Secretary*

U.S. GEOLOGICAL SURVEY

Robert M. Hirsch, *Acting Director*

CONTENTS

ILLUSTRATIONS

[Plates are in pocket]

Page

TABLES

Page

CONVERSION FACTORS

Multiply	By	To obtain
meter (m)	3.281	feet (ft)
kilometer (km)	0.6214	miles (mi)
gram (g)	0.03527	ounces (oz)
kilogram (kg)	2.205	pounds (lb)
liter (L)	0.03532	cubic feet (ft^3)
milligram per liter (mg/L)	6.243×10^{-5}	pounds per cubic foot (lb/ft^3)
liter per second (L/s)	0.03532	cubic feet per second (ft^3/s)
joule (J)	0.2389	calories (cal)
megawatt (MW)	5.692×10^4	British Thermal Units per minute (BTU/min)
milliwatt per square meter (mW/m^2)	0.02389	heat-flow units (hfu) (1 hfu = 1 μcal/cm$^2 \cdot$ s)
milliwatt per meter Kelvin (mW/m $\cdot$ K)	2.389	thermal-conductivity units (tcu) (1 tcu = 1×10^{-3} mcal/cm $\cdot$ s $\cdot$ °C)

For conversion of degrees Celsius (°C) to degrees Fahrenheit (°F), use the formula °F = 9/5°C + 32.

HYDROTHERMAL SYSTEMS OF THE CASCADE RANGE, NORTH-CENTRAL OREGON

By S.E. INGEBRITSEN, R.H. MARINER, and D.R. SHERROD

ABSTRACT

Quaternary volcanoes of the Cascade Range form a 1,200-kilometer-long arc that extends from southern British Columbia to northern California. The section of the Cascade Range volcanic arc in central Oregon is characterized by relatively high Quaternary volcanic extrusion rates and hot-spring discharge rates. Stable-isotope data and measurements of hot-spring heat discharge indicate that gravity-driven thermal fluid circulation transports about 1 MW (megawatt) of heat per kilometer of arc length from the Quaternary arc into Western Cascade rocks older than about 7 Ma (millions of years before present). Inferred flow-path lengths for the Na-Ca-Cl thermal waters of the Western Cascades are 10 to 40 kilometers (km), and an average topographic gradient as large as 0.1 separates the inferred recharge areas from the hot-spring groups. Thermal-fluid residence times are probably 10^2 to 10^4 years: sulfate-water isotopic equilibrium indicates residence times of more than 10^2 years, and our interpretation of stable-isotope data implies residence times of less than 10^4 years.

A large area of near-zero near-surface conductive heat flow occurs in the younger volcanic rocks of the central Oregon Cascades, due to downward and lateral flow of cold ground water. A heat-budget analysis shows that heat advected from areas where rocks younger than about 7 Ma are exposed could account for the anomalously high advective and conductive heat discharge measured in older rocks at lower elevations. Magmatic intrusion at rates ranging from 9 to 33 km^3 per kilometer arc length per million years could account for the total heat-flow anomaly.

Two alternative models for the high heat flow observed in older rocks on the flanks of the Cascade Range involve (1) an extensive midcrustal heat source or (2) a narrower deep heat source that is confined to the Quaternary arc and is flanked by a relatively shallow conductive heat-flow anomaly caused by regional ground-water flow. This lateral-flow model implies a more limited geothermal resource base, but a better-defined exploration target. Analysis of available regional gravity, magnetic, and electrical geophysical data does not clearly favor either of the two models.

We simulated ground-water flow and heat transport through two cross sections west of the Cascade Range crest: one in the Breitenbush area, where there is no major arc-parallel normal faulting, and one in the McKenzie River drainage, where major graben-bounding faults exist. Measured temperature profiles, hot-spring discharge rates, and geochemical inferences constrain the results. In the simulations, the alternative conceptual models for the deep thermal structure were represented as wide or localized deep heat sources. We found that either model can satisfy the observations. Thermal observations in the Breitenbush area seem to require significant advective heat transfer, whereas the sparser observations in the McKenzie River area can be satisfied with either advection- or conduction-dominated simulations. The numerical simulations provide some estimates of regional-scale permeabilities: simulated bulk permeabilities of about 10^{-14} m^2 (meter squared) in the youngest (0–2.3 Ma) rocks and 10^{-17} m^2 in the oldest (18–25 Ma) rocks allow the thermal observations to be matched. In general, permeability decreases downsection, but for rocks of any age, permeability at very shallow (less than about 50 m) depths may be much higher than the bulk permeability values required by the thermal observations: this is indicated by high recharge rates in 0- to 7-Ma rocks (greater than 1 meter per year) and well-test data from domestic wells in rocks older than 7 Ma (which indicate permeability values of 10^{-14} to 10^{-12} m^2).

The actual thermal structure is probably more complex than either of the models considered here. Deep drilling in areas of high heat flow in the older rocks would be the most definitive test of the models. Comparison of natural heat discharge from the central Oregon Cascade Range with that from the relatively well-explored Taupo volcanic zone suggests that published resource estimates for the Cascades are optimistic.

INTRODUCTION

The Cascade Range is a 1,200-km-long volcanic arc that extends from southern British Columbia to northern California. High-temperature igneous-related geothermal resources are assumed to exist in the Cascade Range (for example, Brook and others, 1979), but their magnitude and extent are poorly known. Several lines of evidence suggest relatively high geothermal potential in the central Oregon Cascade Range, a part of the arc characterized by relatively high rates of Quaternary volcanic extrusion (Sherrod and Smith, 1990), hot-spring discharge (Mariner and others, 1990), and conductive heat flow (Blackwell and others, 1982a, 1990a; Blackwell and Steele, 1987; Blackwell and Baker,

1988b). The central Oregon Cascade Range also includes several silicic volcanic systems that are probably young enough and large enough to retain substantial amounts of heat (R.L. Smith and Shaw, 1975, 1979). Extrusion rates and hot-spring discharge rates decrease north and south of the area, and conductive heat flow decreases to the north and possibly to the south.

The Cascade Range in Oregon is customarily divided into two physiographic subprovinces, the relatively uneroded High Cascades and the deeply dissected Western Cascades (Callaghan and Buddington, 1938). That distinction is useful here because of the fundamental control that topography exerts on regional hydrology. The High Cascades subprovince forms the crest of the range and is built mainly of permeable upper Pliocene and Quaternary volcanic rocks that create a broad ridge receiving heavy snowfall. The High Cascades are a regional ground-water recharge area; approximately half of the incident precipitation infiltrates and recharges ground-water systems. In contrast, the Western Cascades is a deeply incised terrane underlain by less permeable Oligocene to lower Pliocene volcanic and volcaniclastic strata. The boundary between the two subprovinces is controlled partly by volcanic onlap and partly by major normal faults. Topographically driven ground-water flow from the High Cascades feeds springs to the west and east. Most hot springs in the study area discharge at nearly the same elevation in deep valleys of the Western Cascades, as much as 20 km west of the High Cascades (fig. 1). One set of hot springs discharges east of the Cascade Range in a valley on the Deschutes-Umatilla Plateau. No hot springs are found in the High Cascades between latitudes 44° and 45°15' N.

Two end-member models describe the deep thermal structure of the Oregon Cascade Range: one model invokes an extensive, uniform midcrustal heat source, the other a relatively narrow, spatially variable heat source. The relative contribution of regional versus localized heat sources is important to understanding the accessible geothermal resource base of the Cascade Range, and the heat-budget analysis and numerical simulations discussed in this report demonstrate implications of each model.

This report is a chapter in the U.S. Geological Survey Professional Paper series "Geohydrology of Geothermal Systems." Previous chapters in this series describe hydrothermal systems at Long Valley, California; Hot Springs, Arkansas; Yellowstone National Park; Klamath Falls and Warner Valley, Oregon; and Ennis, Montana. The series also includes surveys of hydrothermal systems over broader areas (for example, the State of Utah and the Appalachians) and several related topical studies.

PURPOSE AND SCOPE

This report focuses on the hydrothermal systems of the Cascade Range in north-central Oregon. The geologic and hydrologic settings are described and geologic, geochemical, and geophysical data are interpreted in terms of the characteristics of the hydrothermal systems. Numerical simulation is used to investigate alternative conceptual models of the deep thermal structure. The study area includes a 135-km-long section of the arc between latitudes 44° and 45°15' N. It lies generally southeast of Portland, northeast of Eugene, and northwest of Bend and includes parts of the Cascade Range, Deschutes-Umatilla Plateau, and High Lava Plains physiographic provinces (fig. 1).

PREVIOUS INVESTIGATIONS

Some of the results presented in this report have been summarized elsewhere in abbreviated formats. Ingebritsen and others (1989) estimated a heat budget for the study area. Here, we present a slightly revised heat budget and discuss its implications in a more comprehensive fashion. Mariner and others (1989, 1990) used a chloride-flux method to determine the discharge of hot springs in the U.S. part of the Cascade Range. Their discharge estimates for hot springs in the study area are nearly identical to those presented here, but the repeated sets of measurements described in this report allow us to better assess the reproducibility of the results and to compare several solute-inventory methods.

Most hot springs of the Cascade Range in Oregon were described by Waring (1965), who reported approximate locations, discharge temperatures, and flow rates. Brook and others (1979) reported some additional discharge temperature and flow-rate data and also estimated reservoir temperature, volume, and thermal energy. Mariner and others (1980) reported the major-element chemistry and stable-isotope composition of the hot springs and calculated a suite of geothermometer temperatures. Blackwell and others (1978, 1982a) suggested several possible models for the relation between

hot-spring systems and the observed pattern of conductive heat flow. Ingebritsen and others (1988) compiled the publicly available heat-flow and water-chemistry data from the Cascade Range and adjacent areas between latitudes 43°40' and 45°20' N. Mariner and others (1990) reported revised hot-spring discharge rates derived from chloride-flux measurements, and Ingebritsen and others (1989) interpreted the stable-isotope composition of the thermal waters in terms of probable recharge areas.

Estimates of the accessible (less than 3 km depth) geothermal resource range as high as 180×10^{20} Joules (J) for Oregon and Washington (Bloomquist and others, 1985) and 170×10^{20} J for Oregon alone (Black and others, 1983), based on a uniformly high regional heat flow and the temperature-depth model of Blackwell and others (1982a). A more conservative estimate of 11×10^{20} J for the U.S. part of the Cascade Range excluding Newberry and Medicine Lake volcanoes (Brook and others, 1979) was influenced by estimates of the
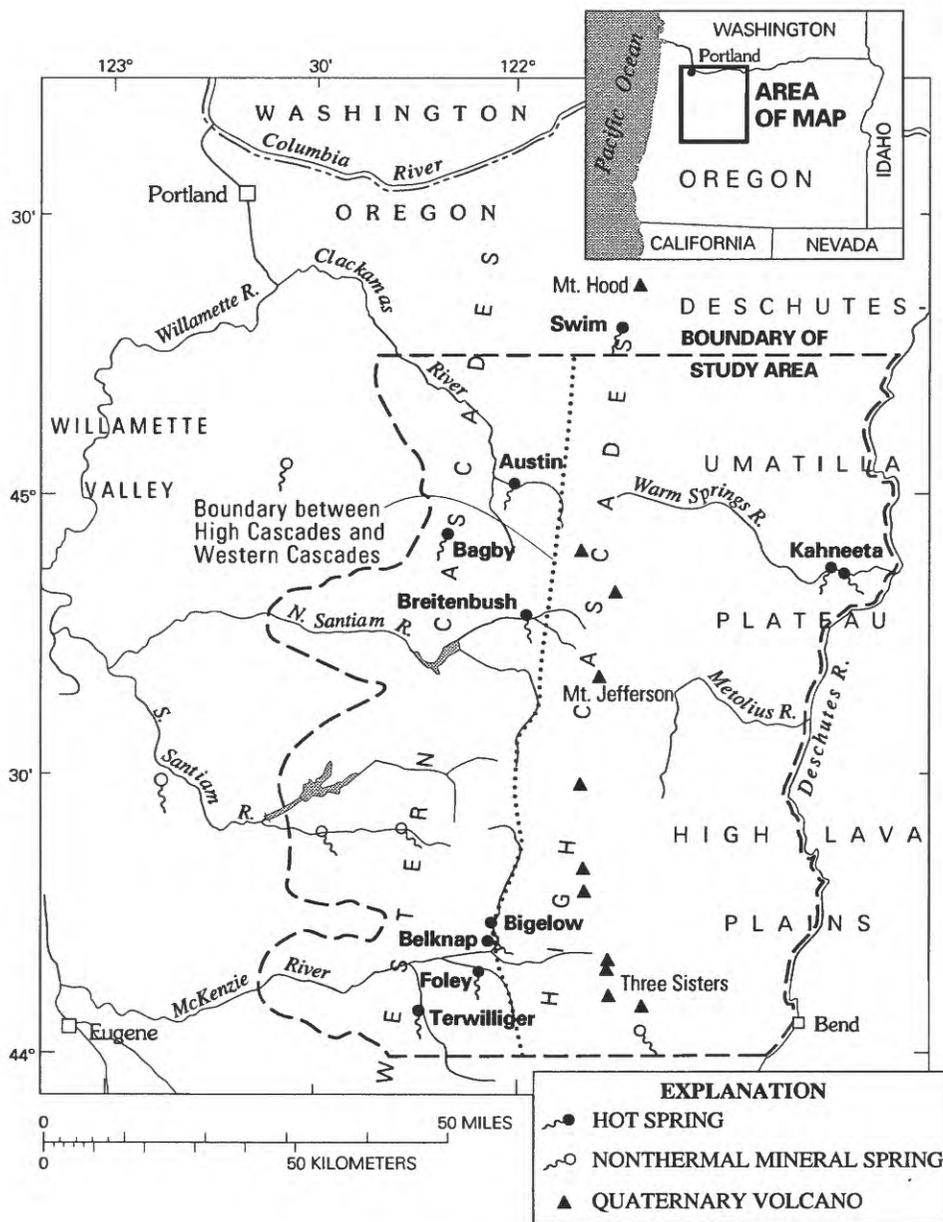
FIGURE 1.—Location of the study area in north-central Oregon. Physiographic provinces from Baldwin (1976), High Cascades-Western Cascades boundary (dotted line) from Callaghan (1933, fig. 1).

thermal energy localized in individual volcanic systems (R.L. Smith and Shaw, 1975). Relevant previous work is described in greater detail under the topical headings below.

GEOLOGIC SETTING

Cascade Range volcanism is related to subduction of the Juan de Fuca plate system beneath the North American plate (fig. 2). The Cascade Range has been an extensive, roughly north-south trending arc since at least late Eocene time (about 45 Ma). The record of Eocene Cascade Range-related volcanism is spotty, but by 30 or 35 Ma the arc was a well-developed volcanic system from central Oregon to northern California (J.G. Smith, 1989; Sherrod and Smith, 1989). About 17 Ma volcanism abated along all but the central Oregon part of the arc, becoming concentrated from about the latitude of Mount Hood south to Crater Lake. Strata in the central Oregon Cascade Range indicate a more or less continuous volcanic record from about 14 Ma to the present (Sherrod and Smith, 1989). The Washington and northern California parts of the arc became volcanically active again beginning in late Pliocene and early Quaternary time.

The Quaternary arc has changes in volcanic style along its length. Numerous small (3–20 km^3) basaltic to andesitic shield volcanoes have built up the broad crest of the central Oregon Cascade Range. From north of Mount Jefferson to south of Crater Lake, diffuse Quaternary volcanism has built a broad, continuous ridge. In contrast, Quaternary volcanism in Washington has resulted in large isolated stratovolcanoes and relatively few mafic shields (fig. 2). The largest stratovolcanoes are Mounts Shasta (345 km^3), Adams (210 km^3), and Rainier (140 km^3) (Sherrod and Smith, 1990). Although the volcanoes in central Oregon are relatively small, their cumulative eruptive products represent a significant part of the total Quaternary volcanic production of the Cascade Range.

The change in volcanic style north of Mount Jefferson is generally attributed to a transition from horizontal compressional tectonics (to the north) to extensional tectonics (for example, Muffler and others, 1982; Weaver and Smith, 1983), but the cause of this change in the crustal stress regime remains uncertain. Sherrod and Smith (1990) noted that the change in volcanic style north of Mount Jefferson corresponds approximately with the northwestward projection of the Brothers fault zone (fig. 2), which accommodates differential extension along the northern margin of the Basin and Range province. South of Crater Lake, where there is a similar transition from diffuse to localized volcanism, there is no corresponding structural feature.

The study area lies in the central part of the Cascade Range volcanic arc, where volcanism and sedimentation have been active since about 30–35 Ma. Although the distribution of Quaternary volcanic and intrusive rocks is perhaps most important to understanding the source and amount of geothermal energy presently available, older rocks and structures exert significant control on hydrothermal circulation and redistribution of heat in the shallow crust. Therefore the following summary discusses the stratigraphic and structural setting of the study area rather broadly. A geologic map (fig. 3) shows generalized lithologic units (from Sherrod and Smith, 1989), and a chart (table 1) shows the correlation between the stratigraphic nomenclature used here and other named units of central Oregon.

STRATIGRAPHY

Pre-Oligocene (older than 35 Ma) rocks are not exposed in the study area. Lower and middle Eocene (about 44–55 Ma) volcanic and marine sedimentary rocks likely extend beneath the study area, however, because they are exposed in the Coast Range to the west (Wells and Peck, 1961) and at the Hay Creek anticline about 70 km east of Mount Jefferson (Wareham, 1986). The nature of the pre-Tertiary crust is essentially unknown but worthy of speculation because thermal waters from the study area have an unusual chemical signature, which among North American thermal waters is shared only by waters from the Columbia embayment (Oregon and Washington) and the Salton Trough (California). The study area is near the southern limit of the Columbia embayment, a poorly delineated region presumably underlain by Cenozoic oceanic crust (Hamilton and Myers, 1966). The embayment's margin in Oregon is defined by a northeast-southwest trending gravity gradient that projects through the Cascade Range near the Three Sisters (Riddihough and others, 1986); Paleozoic and Mesozoic crust is exposed south of but not in the embayment.

The oldest rocks exposed in the study area are continental volcaniclastic strata of approximately 25 to 35 Ma age that interfinger westward with fluviodeltaic and marine sedimentary rocks (fig. 3, unit Ts_4) (Miller and Orr, 1984a, 1984b; Orr and Miller, 1984, 1986a, 1986b; Walker and Duncan, 1989). Along the axis of the Western Cascades, 17- to 25-Ma basaltic to dacitic volcanic and
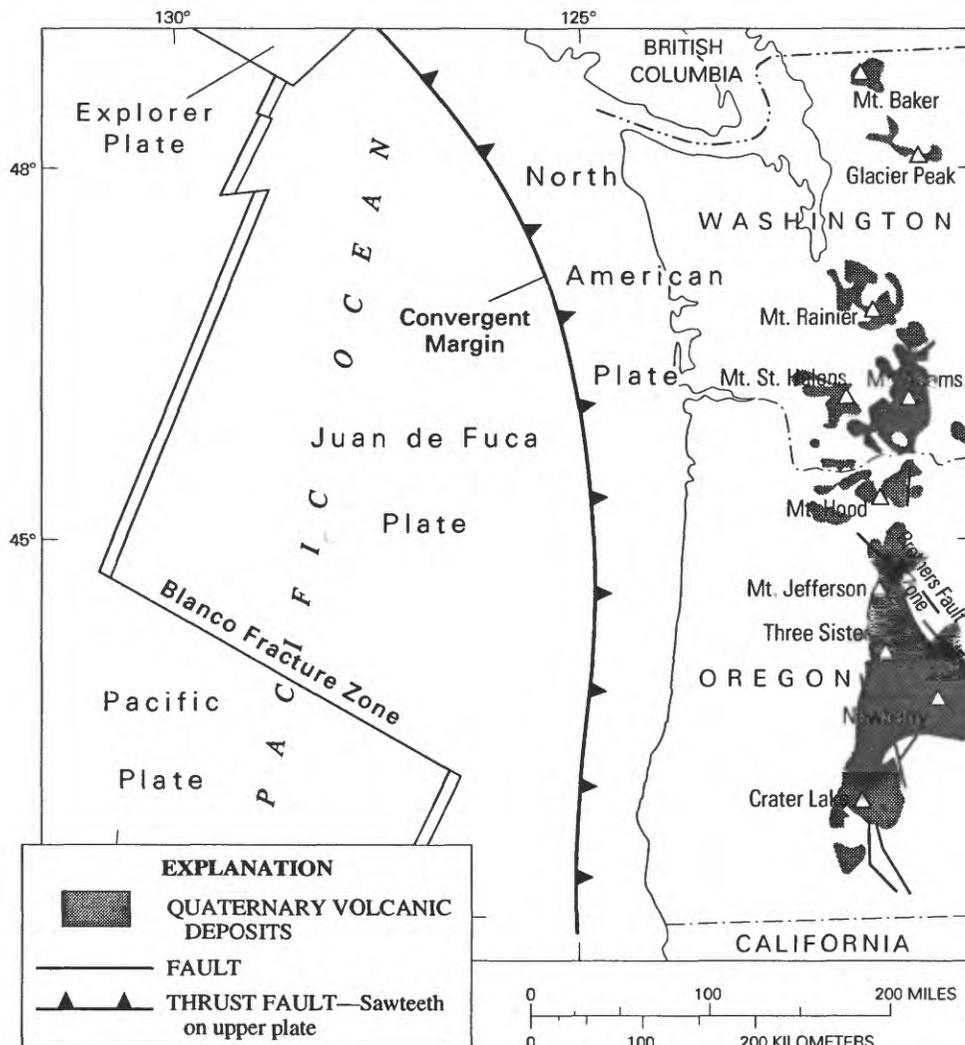
FIGURE 2.—Generalized setting of the Cascade volcanic arc in Washington and Oregon, and extent of Quaternary volcanic deposits (modified from Sherrod and Smith, 1990, figs. 1 and 2).
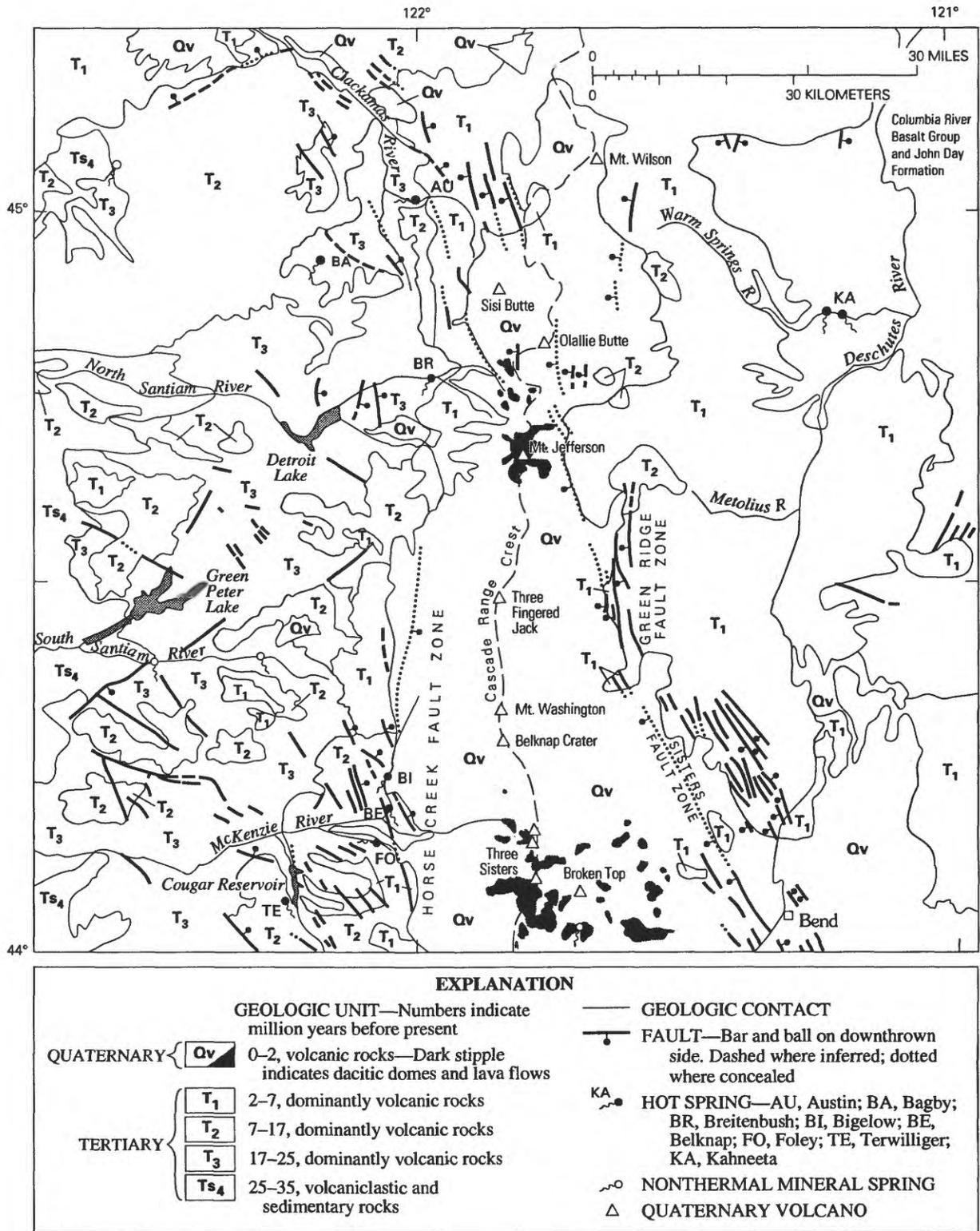
FIGURE 3.—Generalized geologic map of the Cascade Range and adjacent areas of north-central Oregon between latitudes 44° and 45°15' N. (modified from Sherrod and Smith, 1989).

TABLE 1.—*Stratigraphic nomenclature applied to rocks in study area and correlation with other named units of central Oregon*

[Ma, millions of years before present]

Period	Units modified from Sherrod and Smith (1989)[a]							Priest and others' (1983) informal time-stratigraphic units	Age-equivalent rock-stratigraphic units[b]
	Sedimentary rocks	CRBG	Volcanic rocks[c] bas.	and.	dac.	rhy.	Intrusive rocks		
QUATERNARY — 0 Ma — 2 Ma	Qs		Qb	Qa	Qd	Qr	Qi	Late High Cascade	
TERTIARY — 7 Ma	Ts_1		Tb_1	Ta_1	Td_1	Tr_1		— 4 Ma — Early High Cascade	Yonna and Troutdale Formations, Sandy River Mudstone (Ts_1); Deschutes Formation[d] (Ts_1, Tb_1, Td_1)
— 17 Ma	Ts_2	$\dfrac{Tcu}{Tcl}$	Tb_2	Ta_2	Td_2	Tr_2	Ti	— 7.5 Ma — Late Western Cascade	Dalles Formation (Ts_2, Ta_2), Rhododendron Formation (Ta_2), Sardine Formation (Tb_2, Ta_2)
— 25 Ma	Ts_3		Tb_3	Ta_3	Td_3	Tr_3		Early Western Cascade	Breitenbush Tuff[d] (Tb_3, Ta_3), Little Butte Formation[d] ($Ts_3, Tb_3, Ta_3, Td_3, Tr_3$), John Day Formation ($Ts_3$)
— 35 Ma	Ts_4		Tb_4	Ta_4	Td_4	Tr_4			Little Butte Formation ($Ts_4, Tb_4, Ta_4, Td_4, Tr_4$), John Day Formation ($Tr_4$)
SiO$_2$ content, in percent			57	62	70				

[a]Not all of Sherrod and Smith's (1989) map units are shown here; they divide the Quaternary (0–2 Ma) into five age units and also map middle and upper Eocene (35–45 Ma) rocks, which are not exposed in our study area.

[b]Modified from Sherrod and Smith (1989).

[c]Volcanic rocks: CRBG, Columbia River Basalt Group; bas., basaltic; and., andesitic; dac., dacitic; rhy., rhyolitic.

[d]Usage follows that of the Oregon Department of Geology and Mineral Industries.

volcaniclastic rocks are widely exposed (fig. 3, unit T_3) (Priest and others, 1987, 1988; Black and others, 1987; Walker and Duncan, 1989). Rocks of this age include thick ash-rich sequences such as the Breitenbush Tuff[1] of Priest and others (1987), which underlies the area around Breitenbush Hot Springs. The tuffaceous rocks are commonly altered to zeolite and clay minerals, and primary permeability is much reduced; however, the upper 300–600 m is unaltered at least locally. An ash-flow tuff in the upper part of the Breitenbush Tuff has been proposed to control a thermal aquifer on the basis of lithologic correlation and updip projection from a drill hole to Breitenbush Hot Springs (Priest and others, 1987).

Lava flows and tuff breccia, broadly andesitic in composition, were deposited between 17 and 7 Ma along the eastern edge of the Western Cascades subprovince (fig. 3, unit T_2). These rocks are less than 100 m thick in the central part of the study area (Black and others, 1987), but thicken to the north and south, where as much as 1.5 km of stratigraphic thickness is preserved (Priest and others, 1988; Sherrod and Conrey, 1988). Regionally, they form part of a middle and late Miocene volcanic arc that was limited mainly to Oregon. These rocks overlie the older, chiefly volcaniclastic sequence along a pronounced angular unconformity.

Since about 7 Ma, basaltic andesite and basalt lava have erupted from widespread, small shield volcanoes exposed eastward from the eastern edge of the Western Cascades into the Deschutes basin and the Basin and Range (fig. 3, units T_1 and Qv). The base of this stratigraphic interval approximately coincides with the "early High Cascade episode" of Priest and others (1983), whereas the youngest part corresponds to the Quaternary volcanoes of the modern arc. Volcanism of intermediate and silicic composition has been only locally important, but includes now-buried Miocene and Pliocene volcanoes that erupted ash flows preserved in the Deschutes Formation[2] east of the High Cascades (G.A. Smith and others, 1987) as well as andesitic to rhyodacitic lava erupted throughout the Quaternary in the vicinity of the Three Sisters (Taylor and others, 1987) and Mount Jefferson (R.M. Conrey, in Sherrod and Smith, 1989). All rocks younger than about 7 Ma are generally unaltered or altered only at the base of very thick stratigraphic sections.

The Quaternary rocks (0–2 Ma) are shown separately not because of any major structural or stratigraphic break but because high-temperature geothermal resources are often related to Quaternary magmatism. Pre-Quaternary intrusions with volumes less than about 1,000 km[3] generally have cooled to ambient temperatures (R.L. Smith and Shaw, 1979). Most Quaternary rocks in the study area are found in the High Cascades subprovince, where they form the crest of the range from Mount Wilson south (fig. 3, unit Qv). Quaternary silicic rocks are of particular interest because silicic magmas are probably erupted from storage chambers in the upper crust, whereas basic magmas generally do not form large high-level storage chambers (R.L. Smith and Shaw, 1975). Quaternary dacite and rhyolite are confined to the areas between Mount Jefferson and Olallie Butte and between Three Sisters and the Sisters fault zone (fig. 3).

STRUCTURE

The prominent structural features in the study area are en echelon, north-south-striking normal faults that parallel the Quaternary arc (fig. 3). The greatest offset has occurred along the Horse Creek and Green Ridge fault zones, which define the margins of the central Oregon High Cascade graben (G.A. Smith and Taylor, 1983). Farther north and south the High Cascades subprovince is bounded on either the east or west by normal faults but a subsided central block seems to be absent (Sherrod and Smith, 1989).

Displacement on the Green Ridge and Horse Creek fault zones took place in late Miocene and early Pliocene time. Motion along the Green Ridge fault zone isolated the Deschutes basin from volcanic centers in the High Cascades beginning about 5.4 Ma (G.A. Smith and others, 1987). Rocks as young as about 5 Ma are exposed at the top of the 650-m escarpment of Green Ridge (Armstrong and others, 1975), whereas the downthrown block is mantled by Quaternary and Pliocene sedimentary deposits. Displacement is at least 1 km, on the basis of ages of about 1.49 and 1.81 Ma from drill core in the downthrown block (Priest and others, 1989; B.E. Hill, oral commun., 1991). Total displacement along the fault and depth to the 5-Ma strata in the downthrown block are unknown. The Horse Creek fault zone has displaced 5- to 6-Ma strata as much as 670 m down along one trace north of the McKenzie River (Brown and others, 1980b); cumulative mapped offset is as much as

---

[1] [2]Usage follows that of the Oregon Department of Geology and Mineral Industries.

850 m south of the McKenzie River (Priest and others, 1988). Subsequent headward erosion by the McKenzie River breached the escarpment by late Pliocene time, and the basalt of Foley Ridge flowed from a source in the High Cascades westward across the fault trace and along the McKenzie River valley sometime between 2.2 and 1.7 Ma (Flaherty, 1981; Priest and others, 1988). The fault has been inactive since the emplacement of the basalt of Foley Ridge. Thus, demonstrable graben subsidence is about 1 km; larger estimates require buried intragraben faults, which are neither supported or refuted by the available data.

The Sisters fault zone (fig. 3) strikes northwest-southeast into the Cascade Range and is perhaps an extension of basin-range faults such as the Brothers fault zone (E.M. Taylor, 1981; MacLeod and Sherrod, 1988). The Sisters fault zone is characterized by relatively small displacement, measured in meters or tens of meters. Pleistocene lava, pyroclastic flows, and gravel deposits are locally deformed along the Tumalo fault segment of the Sisters fault zone (E.M. Taylor, 1981), making it one of the youngest known faults of the Cascade Range in central Oregon.

Consortium for Continental Scientific Profiling (COCORP) seismic reflection lines crossed the Cascade Range between latitudes 44°10' and 44°15' N. The seismic lines have high noise-to-signal ratios and fail to establish the offset of the Horse Creek fault zone (Keach and others, 1989). They stop short of the Sisters fault zone.

Pre-late Miocene and older rocks exposed on either side of the High Cascades generally dip toward the High Cascades, perhaps forming a synform beneath the High Cascades (Wells and Peck, 1961). Such a regional-scale synform could result from flexural loading of the elastic lithosphere by the growing Cascade arc (G.A. Smith and others, 1989).

Development of graben-bounding faults was accompanied by isostatic rebound west and east of the breaks and intragraben subsidence (G.A. Smith and others, 1989). Early Pliocene uplift in the Western Cascades and on the Deschutes-Umatilla Plateau led to deep entrenchment of the major streams. Priest (1990) estimated that there was up to 1 km of uplift west of the Horse Creek fault zone between about 5.1 and 3.3 Ma.

Although early workers (for example, Thayer, 1936; Peck and others, 1964) mapped a series of anticlines in the Western Cascades, only the 12- to 18-Ma northeast-trending Breitenbush anticline has been confirmed by subsequent mapping and radiometric dating (Sherrod and Pickthorn, 1989). Within the study area there are also a number of 11- to 17-Ma (Sherrod and Pickthorn, 1989) northeast-trending folds on the Deschutes-Umatilla plateau. (Folds are not shown on fig. 3; see Sherrod and Smith [1989] for locations.)

QUATERNARY EXTRUSION RATES

The intrusion rate at shallow crustal levels contributes significantly to accessible geothermal energy. The intrusion rate is unknown, but several lines of evidence support the idea that Cascade Range extrusion rates are indices of the overall rate of magmatism. First, there is a close positive correlation between Quaternary extrusion rates and regional conductive heat flow (Sherrod and Smith, 1990). Second, there is a positive correlation between extrusion rates and the heat discharged by hot springs in various segments of the arc (Mariner and others, 1990). Finally, there is a worldwide positive correlation between volcanic productivity and plate convergence rates (Wadge, 1984). This implies a correlation between the volumes of intrusive and eruptive rock if one assumes that the overall rate of magmatism is also correlated with the plate convergence rate.

Quaternary extrusion rates vary along the length of the Cascade Range volcanic arc, and perhaps the highest long-term rates are found in the area between Mount Jefferson and Crater Lake, Oregon (Sherrod and Smith, 1990). Sherrod (1986) drew a number of cross sections and calculated a 0- to 3.5-Ma extrusion rate of 3 to 6 km^3/km arc length/m.y. for this area. He also calculated shorter-term extrusion rates (0.25–0.72 Ma and 0–0.25 Ma) between latitudes 43° and 44° N., and concluded that the extrusion rate had not fluctuated measurably in the last 3.5 Ma.

Rate estimates by Priest (1990) for the central Oregon part of the Cascade Range are much higher, ranging from 9.9 km^3/km arc length/m.y. for 0.73- to 3.9-Ma to as high as 15.8 km^3/km arc length/m.y. for 0- to 0.73-Ma. The contradictory rate estimates are attributable largely to a difference of opinion regarding total graben subsidence and volcanic fill. We note, however, that Priest's (1990) very high short-term rate requires rocks younger than 0.73 Ma to have an average thickness of 350–400 m over the area that they cover (the area shown in fig. 7 of Priest, 1990). This great average thickness seems unlikely in view of the scattered outcrops of reversely polarized volcanic rocks

at or near the range crest (Sherrod and Smith, 1989). Also, dated core samples from one drill hole in the High Cascades northwest of Mount Jefferson show that approximately 600 m of volcanogenic rocks were deposited during the last 3 m.y. or so (Conrey and Sherrod, 1988). Assuming a constant extrusion rate, this thickness-to-age relation suggests that only about 145 m of 0- to 0.73-Ma rocks are present. Cross sections by Black and others (1987) from the Santiam Pass area are consistent with this lesser thickness, indicating an average thickness of about 480–620 m for the entire Quaternary and upper Pliocene sequence.

HYDROLOGIC SETTING

The western half of the study area (west of the Cascade Range crest) is drained by the Clackamas, North Santiam, South Santiam, and McKenzie rivers, all of which are tributaries of the Willamette River. The eastern half of the study area is drained by the Deschutes River and its major tributaries, the Warm Springs and Metolius rivers. Both the Willamette and Deschutes rivers are tributaries of the Columbia River, which forms the Washington-Oregon border north of the study area (fig. 1).

The Metolius and Deschutes rivers are fed by large springs rising from aquifers in Pliocene and Quaternary volcanic rocks, and their natural flow is characterized by relatively low seasonal variability. This characteristic is shared to some extent by the McKenzie and North Santiam rivers. The annual maximum daily flow of the Metolius near its confluence with the Deschutes is typically only 2 to 4 times as great as the minimum daily flow. The other major streams in the study area have a greater degree of seasonal variability that is typical of snowmelt-fed mountain streams where ground-water storage is less significant. The South Santiam River exhibits the most extreme seasonal variability; its maximum daily flow above the dams near the study area boundary (fig. 1) is typically 100 to 400 times as great as the minimum flow.

PRECIPITATION

The Cascade Range forces air masses moving generally west-to-east to ascend and release moisture. Average annual precipitation in the study area ranges from more than 100 inches in parts of the Western and High Cascades to less than 10

inches along the lower Deschutes River[3]. Precipitation decreases abruptly east of the Cascade Range crest (fig. 4). The western slope is densely vegetated with forests dominated by Douglas fir (*Pseudotsuga menziesii*). The drier eastern slope is more sparsely vegetated; common plant species include yellow (Ponderosa) pine (*Pinus ponderosa*) and several species of sagebrush (*Artemisia* sp.).

West of the Cascade Range about half of the total precipitation falls from December through February. Most of the remainder falls in the autumn and spring, with very little in the summer. East of the Cascade Range about 90 percent of the precipitation falls in autumn, winter, and spring, and about 10 percent in the summer (National Oceanic and Atmospheric Administration, 1985).

The sodium (Na^+) and chloride (Cl^-) contents of precipitation in the study area are of interest relative to the chloride-flux studies discussed in the section "Thermal Waters." There are no precipitation-chemistry data from the study area itself, but published data are available from sites that surround it. Junge and Werby (1958) reported average Na^+ and Cl^- values at Salem (lat 44°55' N., long 123° W.) and Medford (lat 42°22' N., long 122°52' W.) for the period of July 1955 to June 1956, and since 1984 the U.S. Geological Survey has collected weekly precipitation chemistry data at Bull Run Reservoir (lat 45°26'55" N., long 122°08'45" W.) and Silver Lake (lat 43°07'01" N., long 121°04' W.). The U.S. Geological Survey data are included in annual reports entitled "Water Resources Data for Oregon." The available Na^+ and Cl^- data (in milligrams per liter) are tabulated below. The average composition of seawater is also shown for comparison:

Location	Date	Average Na^+	Average Cl^-	Average Na^+/Cl^-
Bull Run Res.	1984–1986	0.37	0.67	0.55
Salem	1955–1956	.48	.68	.71
Medford	1955–1956	.15	.22	.68
Silver Lake	1984–1986	.11	.15	.72
Seawater	—	10,500	19,000	.55

STABLE-ISOTOPE DATA

Stable isotopes are commonly used to infer ground-water source areas and mixing patterns. The mean isotopic composition of precipitation at a particular location is approximately constant over time periods that are long enough to minimize the effects of seasonal variations and short enough to

---

[3]We report precipitation values in U.S. Customary units because our precipitation data are obained from a non-SI isohyetal map.

preclude the effects of significant climate change. There are two stable isotopes of hydrogen: ^1H and ^2H (deuterium or D), and three of oxygen: ^{16}O, ^{17}O, and ^{18}O, of which ^{16}O and ^{18}O are the more abundant. Because the vapor pressure of water molecules is inversely proportional to their masses, water vapor is depleted in the heavier isotopes D and ^{18}O relative to coexisting liquid water (Faure,
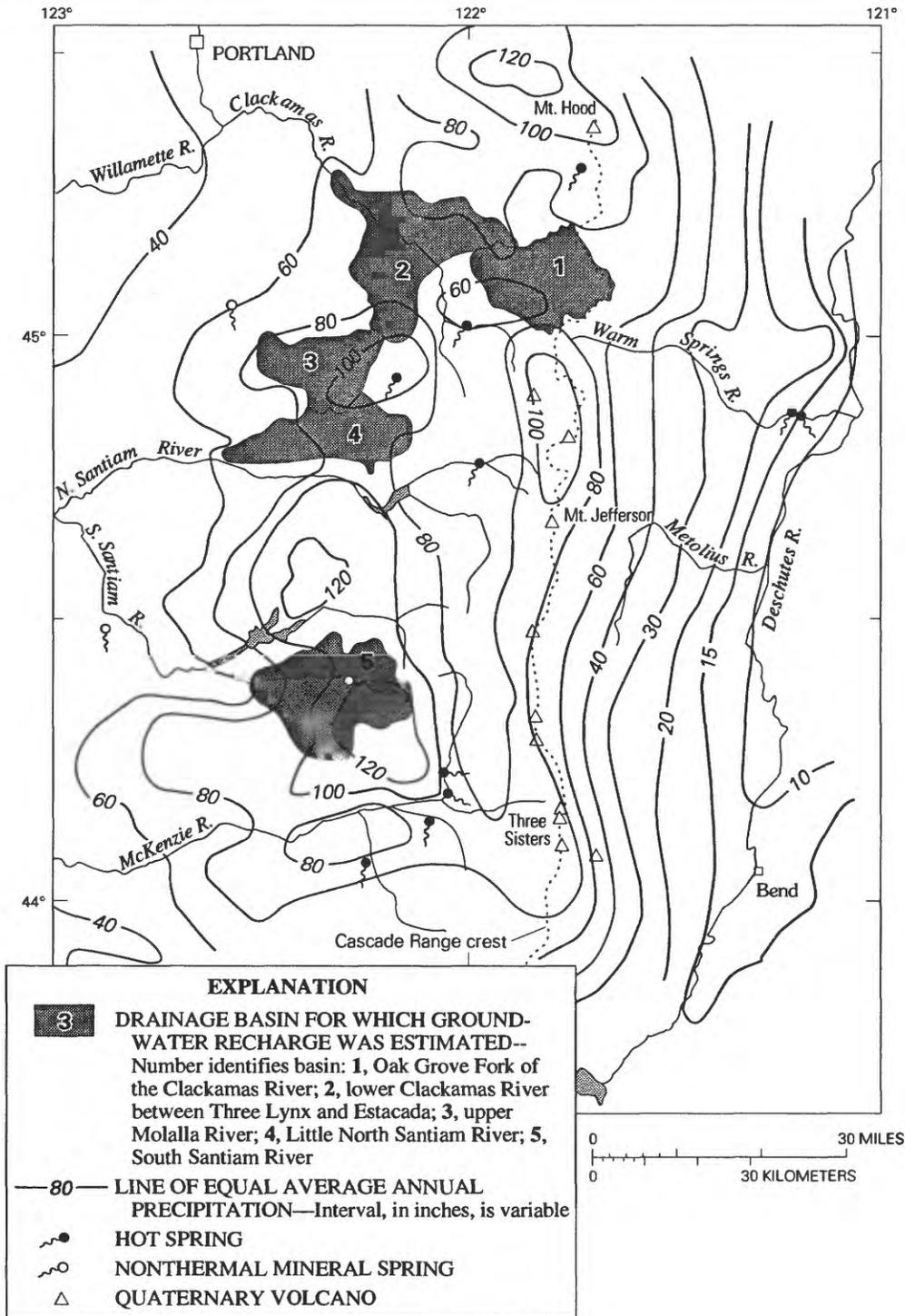
FIGURE 4.—Average annual precipitation in and near study area (generalized from U.S. Department of Agriculture, Soil Conservation Service, 1964) and location of areas for which ground-water recharge is estimated.

1986). The D and ^{18}O content of water is conventionally reported in "δ-notation" relative to Craig's (1961b) Standard Mean Ocean Water (SMOW):

$$\delta = [(R_{sample}/R_{SMOW}) - 1] \times 1,000$$

where R is the D/H or $^{18}O/^{16}O$ ratio and the units of δ are permil (o/oo). The δD and $\delta^{18}O$ values of water vapor in an air mass become progressively more negative as precipitation falls from it. Stable-isotope data collected west of the Cascade Range crest reflect the progressive depletion in D and ^{18}O of generally east-moving marine storm systems and, in the section "Thermal Waters," are used to infer the provenance of the thermal waters in the Western Cascades. Most of the data are from low-salinity springs or wells in zero- or first-order (unchanneled or headwater) basins, and represent time-integrated samples of the local precipitation.

Deuterium (δD) values range from about –65 o/oo near the western edge of the study area to less than –115 o/oo east of the Three Sisters and near the Deschutes River (table 2, pl. 1). Corresponding $\delta^{18}O$ values range from about –9 to –15 o/oo. Craig (1961a) showed that meteoric waters worldwide define the relation $\delta D = 8\delta^{18}O + 10$, and the data from the study area generally fall close to Craig's meteoric water line (fig. 5). However, isotopic data for cold springs and wells east of the Cascade Range crest plot both above and below the Craig line. Possible causes for this scatter include evapo-

ration of precipitation as it falls through dry air, mixing of air masses from continental and marine sources, or a storm track different from the marine pattern shown on the western side of the Cascade Range.
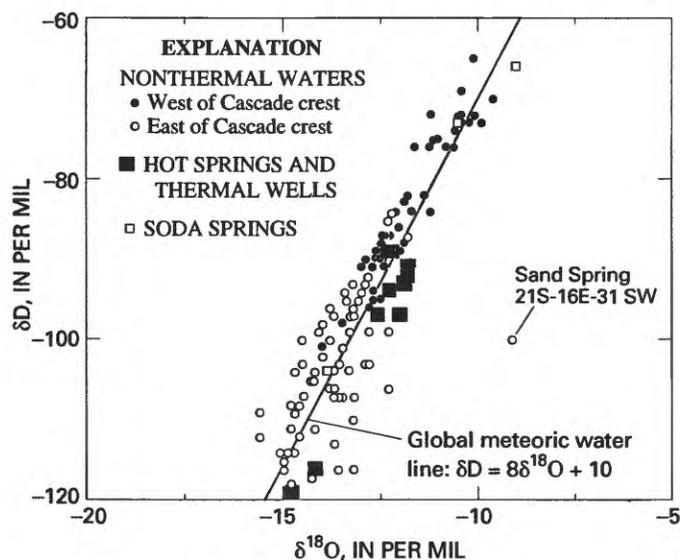
West of the Cascade Range crest, δD values (fig. 6) and $\delta^{18}O$ values for nonthermal waters show an inverse correlation with elevation. East of the crest, there is a weak but statistically significant positive correlation between elevation and δD values (fig. 6) and $\delta^{18}O$ values, as samples from the lowlands of the Deschutes basin tend to be more depleted in D and ^{18}O than those from the High Cascades.

Friedman and Smith (1970) measured the D content of snow cores from the Sierra Nevada, another area where moist Pacific air overrides a generally north-south-trending mountain range. They noted that (1) the D content of snow west of the Sierra Nevada crest is clearly a function of altitude, but the relation east of the crest is less clear; (2) the D content is not an obvious function of latitude; (3) the snow west of the Sierra Nevada crest tends to contain 10–50 o/oo more D than snow east of the crest; and (4) the snow east of higher segments of the Sierra Nevada crest is more depleted in D than snow east of lower segments of the crest. Each of these observations is qualitatively consistent with the data reported here, although our observations differ from Friedman and Smith's (1970) in some details. For example, the Friedman and Smith (1970) data show δD decreasing at the rate of about 40 o/oo per 1,000 m west of the Sierra

FIGURE 5.—Relation between deuterium and oxygen-18 contents for waters sampled in and near study area. Sand Spring is a nonflowing spring on the flank of Newberry Volcano; water sampled there was probably affected by low-temperature evaporation.
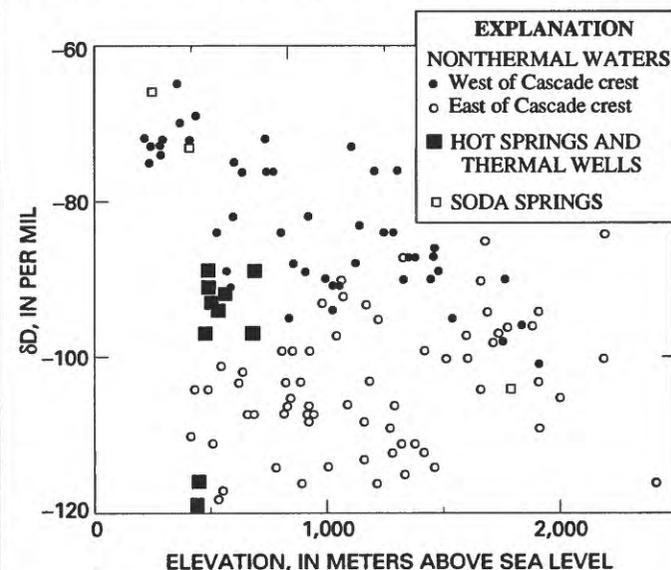
FIGURE 6.—Relation between deuterium content and elevation for waters sampled in and near study area.

TABLE 2.—*Stable-isotope, sodium, and chloride values for selected springs, wells, streams, and lakes in Cascade Range of northern and central Oregon*

[Well names are from well logs on file with the Oregon Department of Water Resources. Wells denoted "(well)" have no well log available. Dashes indicate the absence of data. Values followed by "e" are approximate. Sites are ordered by township, range, and section. Sites with this information in parentheses are in unsurveyed areas and cadastral location is approximated from U.S. Forest Service maps. Isotope values are reported in permil notation relative to standard mean ocean water (SMOW). For additional information about most of these sites, see Ingebritsen and others (1988). >, greater than; <, less than]

T-R-Sec. 1/4	Longitude	Latitude	Name	Elev. (m)	Depth (m)	Date (mo/d/yr)	Na (mg/L)	Cl (mg/L)	δD (o/oo)	$\delta^{18}O$ (o/oo)
			Cold springs and wells west of the Cascade crest							
3S-4E-21 NE	122°18'53"	45°17'47"	(well)	280	17	06/24/86	5e	—	-73	-9.9
3S-5E-32 SE	122°12'52"	45°15'33"	unnamed spring	411	—	06/30/86	6e	—	-72	-10.4
3S-5E-36 SE	122°08'08"	45°15'56"	unnamed spring	732	—	06/30/86	1e	—	-72	-10.5
3S-6E-33 SE	122°04'29"	45°15'53"	unnamed spring	1,103	—	06/30/86	1e	—	-73	-10.2
5S-4E-01 SW	122°16'10"	45°09'30"	unnamed spring	631	—	06/30/86	3e	—	-76	-10.6
5S-7E-12 NE	121°53'37"	45°09'24"	High Rock Spring	1,378	—	07/03/86	3e	—	-87	-12.5
5S-8.5E-11 SE	121°44'59"	45°08'53"	unnamed spring	991	—	10/01/87	2.6	0.5	-90	-12.9
5S-8.5E-35 NE	121°44'42"	45°05'51"	(well)	1,019	43	07/09/86	3e	—	-94	-12.7
6S-5E-14 NE	122°09'23"	45°03'03"	unnamed spring	743	—	07/01/86	2e	—	-76	-10.6
(6S-8E-32 N)	121°51'31"	45°00'31"	Fire Springs	1,024	—	08/15/81	2.0	<1	-91	-13.0
7S-5E-28 SE	122°12'05"	44°55'42"	unnamed spring	765	—	07/09/86	2e	—	-76	-11.2
7S-6E-09 NW	122°05'24"	44°58'38"	(well)	567	—	02/23/87	220	170	-89	-12.5
(7S-7E-09 SW)	121°57'48"	44°58'36"	unnamed spring	1,280	—	08/15/81	1.7	<1	-84	-12.1
8S-8E-20 SW	121°51'18"	44°51'54"	Cub Spring	1,120	—	08/21/79	3.6	.8	-88	-12.5
9S-2E-17 NE	122°34'53"	44°47'41"	(well)	216	81	08/01/86	430	920	-72	-11.2
9S-2E-24 NW	122°30'28"	44°46'41"	unnamed spring	437	—	08/07/86	5e	—	-69	-10.4
9S-3E-28 SE	122°26'27"	44°45'35"	(well)	287	>90e	06/25/86	470	690	-74	-10.6
9S-6E-21 SE	122°04'37"	44°46'25"	Willamette Nat. For.	597	45	08/31/87	5.9	.7	-82	-11.4
9S-6E-35 SE	122°02'21"	44°44'32"	unnamed spring	1,140	—	07/15/86	83	.4	-83	-12.1
(9S-7E-03 NE)	121°56'24"	44°49'30"	unnamed spring	1,359	—	04/25/88	—	—	-83	-11.7
(9S-7E-09 SW)	121°57'45"	44°48'10"	unnamed spring	914	—	10/17/79	2.6	.4	-87	-12.2
(9S-7E-12 SE)	121°53'24"	44°48'12"	unnamed spring	902	—	07/15/86	101	1.3	-82	-12.1
(9S-7E-29 SE)	121°58'12"	44°45'48"	unnamed spring	853	—	04/25/88	—	—	-81	-11.4
(9S-8E-02 NE)	121°47'36"	44°49'30"	Big Spring	1,460	—	10/17/79	4.6	2.4	-86	-12.0
10S-3E-09 NE	122°26'15"	44°43'22"	unnamed spring	370	—	07/13/86	2.8	*1.7	-70	-9.6
10S-6E-22 NW	121°49'36"	44°41'43"	Green Veneer well	527	183	08/01/87	120	89	-84	-11.7
(10S-8E-04 SW)	121°51'18"	44°43'54"	unnamed spring	1,830	—	09/18/82	—	—	-96	-12.8
(10S-8E-05 NE)	121°49'00"	44°44'24"	unnamed spring	1,330	—	10/17/79	1.6	.4	-90	-12.4
(10S-8E-15 SW)	121°43'10"	44°42'12"	unnamed spring	1,760	—	08/14/81	1.4	<1	-90	-12.5
(11S-5E-17 SE)	122°13'10"	44°36'46"	unnamed spring	1,201	—	07/12/86	2e	—	-76	-10.8
11S-7E-06 NE	121°59'42"	44°38'50"	unnamed spring	1,244	—	07/12/86	2e	—	-84	-12.1
11S-7E-27 SW	121°56'45"	44°35'11"	unnamed spring	1,052	—	06/20/86	3e	—	-91	-12.4
13S-2E-36 SW	122°38'50"	44°23'24"	Munts well	243	38	07/21/87	270	200	-73	-10.4
13S-7.5E-23 SE	121°52'49"	44°25'18"	(well)	1,441	<10e	07/18/86	1e	—	-90	-12.6
14S-2E-02 NE	122°31'25"	44°23'17"	Betts well	357	107	07/09/86	7.7	1.3	-65	-10.1
14S-4E-10 NE	122°18'26"	44°22'02"	unnamed spring	1,299	—	07/21/86	1e	—	-76	-11.6
14S-7E-20 NE	121°59'50"	44°20'38"	Icecap Spring	833	—	10/18/79	3.9	.6	-95	-12.5
(15S-6E-09 NE)	122°05'51"	44°17'10"	unnamed spring	802	—	10/18/79	2.4	.6	-84	-11.2
(15S-7.5E-25 NW)	121°50'36"	44°14'42"	unnamed spring	1,540	—	10/18/79	1.7	.4	-95	-12.7
16S-2E-29 SE	122°35'26"	44°08'31"	Toy well	235	67	08/12/86	260	420	-75	-11.0
16S-4E-09 SE	122°19'53"	44°11'57"	unnamed spring	601	—	08/15/86	3e	—	-91	-11.1
16S-6E-24 SE	122°01'12"	44°09'42"	unnamed spring	585	—	10/18/79	5.0	1.8	-95	-12.7
17S-2E-02 NE	122°03'54"	44°07'19"	unnamed spring	297	—	08/13/86	1e	—	-72	-10.1
(17S-8E 18)	121°48'54"	44°06'00"	unnamed spring	1,905	—	08/12/81	4.2	1.0	-101	-14.0
(17S-8E 19)	121°48'54"	44°04'54"	unnamed spring	1,750	—	08/12/81	5.2	<1	-98	-13.5

TABLE 2.—Stable-isotope, sodium, and chloride values for selected springs, wells, streams, and lakes in Cascade Range of northern and central Oregon—Continued

T-R-Sec. 1/4	Longitude	Latitude	Name	Elev. (m)	Depth (m)	Date (mo/d/yr)	Na (mg/L)	Cl (mg/L)	δD (o/oo)	δ18O (o/oo)
Cold springs and wells west of the Cascade crest—Continued										
(18S-6E-02 SE)	122°02'28"	44°01'47"	unnamed spring	1,453	—	08/14/86	1e	—	-87	-12.4
(18S-6.5E 25)	121°57'07"	43°58'38"	Bill Gott Spring	1,475	—	09/02/86	2e	—	-89	-12.6
Cold springs, wells, streams, and lakes east of the Cascade crest										
3S-10E-20 SW	121°34'54"	45°17'23"	unnamed spring	1,658	—	10/06/87	1.7	.6	-90	-12.7
3S-11E-18 NE	121°27'50"	45°18'41"	Sunrise Springs	1,596	—	10/06/87	2.9	.6	-97	-13.7
3S-13E-34 NW	121°10'09"	45°16'05"	unnamed spring	512	—	09/30/87	9.1	1.8	-111	-14.2
3S-14E-31 NW	121°06'38"	45°16'12"	unnamed spring	488	—	10/08/87	11	3.2	-104	-13.7
4S-9E-17 SW	121°14'39"	45°13'14"	Mt. Hood N.F. well	1,676	73	10/01/87	2.9	.5	-85	-12.3
4S-10E-15 SE	121°31'21"	45°12'58"	unnamed spring	1,219	—	10/07/87	2.3	.9	-95	-13.4
4S-12E-22 NW	121°17'12"	45°12'33"	Harvey & Jensen well	546	101	04/25/88	13	6	-101	-13.5
4S-12E-32 SW	121°20'09"	45°10'22"	Lichtenberger well	642	198	04/25/88	26	9	-102	-14.0
5S-12E-06 NE	121°20'27"	45°10'18"	Thompson well	664	>152	04/25/88	106	130	-107	-13.2
5S-15E-09 NE	120°56'17"	45°09'15"	unnamed spring	620	—	04/24/88	11	6	-103	-12.9
(6S-10E-19 SW)	121°35'53"	45°02'02"	unnamed spring	1,167	—	10/16/87	3.5	.6	-93	-13.2
6S-11E-08 SE	121°26'56"	45°03'40"	Coyote Spring	832	—	10/16/87	19	2.3	-106	-13.7
6S-12E-27 NW	121°17'38"	45°01'24"	Nena Spring	814	—	10/13/87	28	11	-107	-14.5
7S-10E-35 SW	121°31'07"	44°55'00"	Nellie Spring	843	—	10/15/87	5.6	1.7	-105	-14.3
7S-14E-08 NW	121°05'11"	44°58'55"	unnamed spring	433	—	10/15/87	32	2.0	-104	-13.3
7S-15E-11 NW	120°54'03"	44°58'37"	unnamed spring	923	—	04/24/88	11	5	-99	-12.8
8S-13E-10 SW	121°10'01"	44°53'11"	unnamed spring	555	—	10/15/87	40	5.2	-117	-14.3
8S-14E-21 NE	121°03'14"	44°51'54"	unnamed spring	418	—	07/14/89	44	4.9	-110	-13.2
8S-15E-15 SW	120°55'30"	44°52'01"	unnamed spring	823	—	04/24/88	13	6	-103	-12.8
9S-10E-31 NW	121°35'32"	44°44'45"	unnamed spring	1,183	—	10/16/87	4.7	.9	-103	-14.5
9S-11E-34 NW	121°24'53"	44°45'02"	Seymore Springs	882	—	10/16/87	6.1	.6	-103	-13.6
9S-13E-06 SW	121°13'48"	44°49'03"	unnamed spring	536	—	10/11/87	29	5.8	-118	-14.8
(10S-8E-24 SE)	121°45'58"	44°40'51"	unnamed stream	1,999	—	06/27/88	—	—	-105	-14.2
(10S-8E-35 NE)	121°47'16"	44°39'23"	unnamed lake	2,182	—	06/26/88	—	—	-100	-14.5
(10S-8E-35 NE)	121°47'15"	44°39'23"	unnamed stream	2,185	—	06/26/88	—	—	-84	-12.2
(10S-8E-36 NE)	121°39'30"	44°39'30"	unnamed stream	1,902	—	06/26/88	—	—	-94	-13.0
(10S-8.5E-25 SW)	121°44'38"	44°40'09"	Parker Creek	1,658	—	06/26/88	—	—	-104	-14.7
(10S-8.5E-25 SE)	121°43'56"	44°40'19"	unnamed spring	1,597	—	06/26/88	—	—	-100	-13.8
(10S-8.5E-26 NW)	121°45'37"	44°40'40"	Milk Creek	1,902	—	06/27/88	—	—	-109	-14.7
(10S-8.5E-26 NW)	121°45'37"	44°40'39"	unnamed stream	1,902	—	06/27/88	—	—	-103	-14.5
(10S-8.5E-26 SE)	121°44'47"	44°40'01"	unnamed stream	1,686	—	06/26/88	—	—	-94	-13.4
(10S-8.5E-35 NE)	121°45'07"	44°39'42"	unnamed stream	1,768	—	06/26/88	—	—	-96	-13.8
10S-9E-28 NE	121°40'06"	44°40'35"	unnamed spring	1,530	—	05/25/88	1.6	.4	-95	-13.1
10S-9E-33 NW	121°40'27"	44°39'55"	unnamed spring	1,658	—	09/26/87	2.0	.4	-104	-14.2
10S-11E-30 SW	121°28'32"	44°40'42"	Peters Spring	937	—	09/26/87	5.2	.5	-107	-13.7
(11S-8E-04 NE)	121°46'28"	44°38'54"	unnamed spring	1,878	—	06/26/88	—	—	-96	-13.2
(11S-8E-23 N)	121°44'42"	44°36'18"	unnamed spring	1,731	—	09/27/86	—	—	-97	-13.3
11S-12E-08 NE	121°19'04"	44°38'16"	Pipp Spring	689	—	10/14/87	17	3.2	-107	-13.6
11S-14E-02 NE	121°00'48"	44°38'35"	Monner Spring	850	—	04/24/88	32	12	-99	-12.3
11S-14E-34 SW	121°02'03"	44°34'13"	North Combs Spring	889	—	07/15/89	48	16	-116	-13.2
11S-15E-25 SE	121°52'20"	44°35'01"	unnamed spring	1,090	—	07/15/89	17	2.6	-106	-12.3
12S-10E-18 NE	121°34'42"	44°32'12"	unnamed spring	1,292	18	08/11/87	4.2	1.1	-106	-13.9
13S-8E-27 NE	121°45'26"	44°25'05"	Lovegren well	1,061	20	04/23/88	4.2	3	-90	-12.7
13S-8E-27 SW	121°46'10"	44°24'40"	Blue Lake	1,067	40	08/13/87	3.8	.6	-93	-12.6
			Blue Lake		60	08/13/87	3.7	.6	-91	-12.7
			Blue Lake		80	08/13/87	3.7	.6	-90	-12.6
			Blue Lake		81.7	08/13/87	3.7	.6	-94	-13.0

TABLE 2. — Stable-isotope, sodium, and chloride values for selected springs, wells, streams, and lakes in Cascade Range of northern and central Oregon—Continued

T-R-Sec. 1/4	Longitude	Latitude	Name	Elev. (m)	Depth (m)	Date (mo/d/yr)	Na (mg/L)	Cl (mg/L)	δD (o/oo)	δ18O (o/oo)
Cold springs, wells, streams, and lakes east of the Cascade crest—Continued										
13S-9E-22 NE	121°38'18"	44°26'03"	Metolius Spring	920	—	09/27/86	9.2	1.6	-108	-14.8
13S-12E-29 NW	121°19'42"	44°24'53"	Clevenger well	805	96	04/24/88	15	7	-99	-13.3
14S-9E-35 SW	121°38'01"	44°18'38"	Cold Spring	1,036	—	07/09/87	4.1	.5	-97	-13.2
14S-10E-21 SE	121°32'15"	44°20'24"	Indian Ford L&C Co. w.	975	12	04/23/88	11	7	-93	-12.9
14S-12E-16 NW	121°18'19"	44°21'39"	unnamed spring	779	—	07/15/89	12	5.9	-114	-14.7
15S-11E-20 NE	121°26'13"	44°15'31"	(well)	921	—	07/16/89	17	11	-107	-13.5
15S-12E-23 SW	121°16'01"	44°15'16"	(well)	920	75	04/24/88	19	8	-106	-13.9
15S-16E-27 SW	120°48'06"	44°14'05"	unnamed spring	1,154	—	07/14/89	28	9.2	-113	-13.7
16S-9E-13 NW	121°36'16"	44°11'43"	Melvin Spring	1,329	—	09/29/86	5.0	.2	-115	-15.0
16S-9E-14 NE	121°36'47"	44°11'46"	Black Pine Spring	1,317	—	08/01/87	5.0	.7	-111	-14.8
16S-11E-24 SW	121°21'15"	44°10'20"	(well)	1,000	190	04/23/88	13	7	-114	-14.9
16S-14E-12 SW	121°00'12"	44°11'45"	Picket Spring	1,214	—	07/14/89	8	17	-116	-15.0
(17S-9E-29 NE)	121°41'00"	44°04'45"	unnamed spring	2,410	—	08/13/81	1.3	<1	-116	-13.6
17S-11E-18 NE	121°26'56"	44°06'28"	Bull Spring	1,164	—	08/19/87	—	—	-108	-14.6
18S-8E-03 SW	121°45'44"	44°02'23"	unnamed spring	1,710	—	08/13/81	—	—	-103	-14.0
						07/29/84	—	—	-96	-14.0
						08/15/87	2.6	.2	-96	-14.1
19S-8E-34 SW	121°45'59"	43°52'51"	unnamed spring	1,414	—	04/23/88	3.6	1	-99	-14.1
19S-10E-02 SE	121°29'04"	43°57'03"	Kiwa Spring	1,460	—	09/29/86	2.6	.4	-114	-15.1
19S-10E-13 NW	121°29'00"	43°55'56"	Coyote Spring	1,416	—	08/15/87	—	—	-112	-15.6
(20S-8E-20)	121°47'42"	43°50'06"	unnamed spring	1,372	—	08/01/85	4.5	<1	-111	-14.2
20S-10E-01 SW	121°28'30"	43°51'54"	unnamed spring	1,274	—	09/28/86	9.3	2.3	-112	-14.6
20S-10E-26 NE	121°29'11"	43°49'06"	(well)	1,271	209	04/23/88	40	3.0	-109	-15.6
21S-16E-31 SW	120°50'45"	42°29'58"	Sand Spring	1,506	—	07/16/89	3.0	1.6	-100	-9.1
22S-8E-18 SE	121°48'45"	43°39'27"	unnamed spring	1,329	—	04/23/88	3.7	1	-87	-11.8
Hot springs and thermal wells										
6S-7E-30 NW	122°00'30"	45°01'18"	Austin Hot Springs	509	—	07/28/84	305	390	-93	-11.9
(7S-5E-27 NE)	122°10'21"	44°56'09"	Bagby Hot Springs	692	—	09/18/77	53	14	-89	-12.4
9S-7E-20 NE	121°58'32"	44°46'52"	Breitenbush H. Sprs.	682	—	08/21/79	745	1,200	-97	-12.6
15S-6E-26 NW	122°03'30"	44°14'21"	Bigelow Hot Spring	561	—	07/26/84	675	1,250	-92	-11.8
15S-6E-11 NE	122°02'54"	44°11'39"	Belknap Springs	493	—	07/27/84	660	1,200	-91	-11.8
16S-6E-10 SW	122°04'33"	44°11'06"	Bigelow well	481	209	09/29/86	670	1,400	-97	-12.0
16S-6E-28 NW	122°05'51"	44°09'12"	Foley Springs	536	—	07/27/84	555	1,350	-94	-12.3
						03/29/90	510	1,330	-97	-12.2
(17S-5E-20 NW)	122°14'00"	44°04'57"	Terwilliger Hot Spring	530	—	07/26/84	405	790	-89	-12.2
8S-13E-19 NW	121°13'42"	44°52'02"	Kahneeta Sprs. (west)	451	—	10/17/87	410	230	-116	-14.2
						03/30/90	370	230	-120	-14.4
8S-13E-20 E	121°12'00"	44°51'42"	Kahneeta Hot Spring	440	—	08/—/79	325	155	-119	-14.8
Soda springs										
13S-3E-32 NW	122°28'28"	44°23'48"	unnamed spring at Cascadia	244	—	09/19/77	2,200	3,300	-66	-9.0
13S-4E-26 SE	122°17'03"	44°24'17"	unnamed spring at Upper Soda	414	—	09/19/85	2,200	3,500	-73	-10.5
18S-9E-06 S	121°41'48"	44°02'24"	unnamed spring on Soda Ck.	1,783	—	08/19/79	50	5	-104	-13.9

Nevada crest, whereas our data show δD decreasing at only about 16 o/oo per 1,000 m west of the Cascade Range crest.

GROUND-WATER RECHARGE ESTIMATES

Late-summer stream discharge (baseflow) in the Cascade Range consists almost entirely of ground-water contributions. The unit baseflow (baseflow per unit area), an index of ground-water recharge, has been estimated for five basins west of the Cascade Range crest (fig. 4). These basins encompass diverse rock units (fig. 7). Within each basin, stream flow is either unregulated by artificial structures or regulated in such a way that diversions and reservoir storage can be accounted for. Hydrographs of monthly mean discharge for each basin are shown in figure 8.
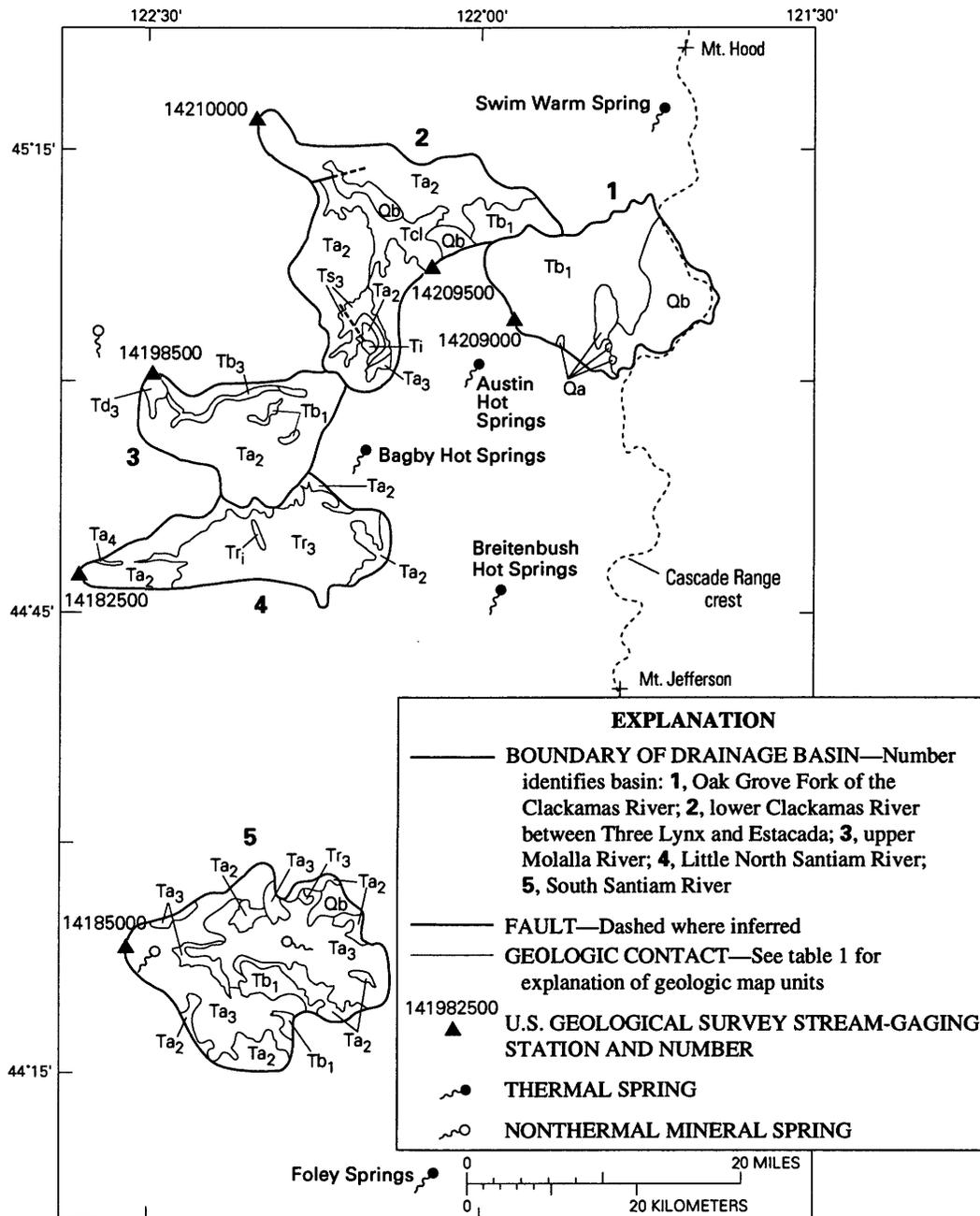
FIGURE 7.—Surficial geology and locations of streamflow-gaging stations for basins where ground-water recharge was estimated. Geology from Sherrod and Smith (1989).

Baseflow estimates are based on low-flow values for the period 1981–85, a time when annual runoff in the Willamette River basin ranged from 83 to 130 percent of the long-term mean value (U.S. Geological Survey, 1983a, 1983b, 1984, 1986b, 1987b). The lowest monthly mean flow for each basin generally occurs in August or September, and the low-flow values are fairly consistent from year to year (fig. 8). Late summer baseflow is a minimum estimate of the ground-water contribution to stream flow, which may be considerably larger in fall, winter, and spring.

Dividing the baseflow (m^3/s) by the basin area (m^2) provides an estimate of the minimum ground-water recharge rate per unit area (m/s). The estimated recharge rates show a rough inverse correlation with the age of the rocks exposed in each basin (table 3). Estimated recharge rates vary by more than an order of magnitude, ranging from 1.1×10^{-9} m/s in the South Santiam basin (figs. 4 and 7, area 5), where 17- to 25-Ma volcanic rocks are widely exposed, to 26×10^{-9} m/s in the 0- to 7-Ma rocks of the Oak Grove Fork basin (area 1). The relatively low recharge rate calculated for the South Santiam basin is about 1 percent of the annual precipitation; the rate for the Oak Grove Fork basin represents about 50 percent of the annual precipitation (see fig. 4 for average annual precipitation). These rates provide some constraints on near-surface permeability; they are compared with simulated hydrologic fluxes in the section "Numerical Simulations".

The inverse correlation between recharge rate and age of rocks probably reflects loss of primary
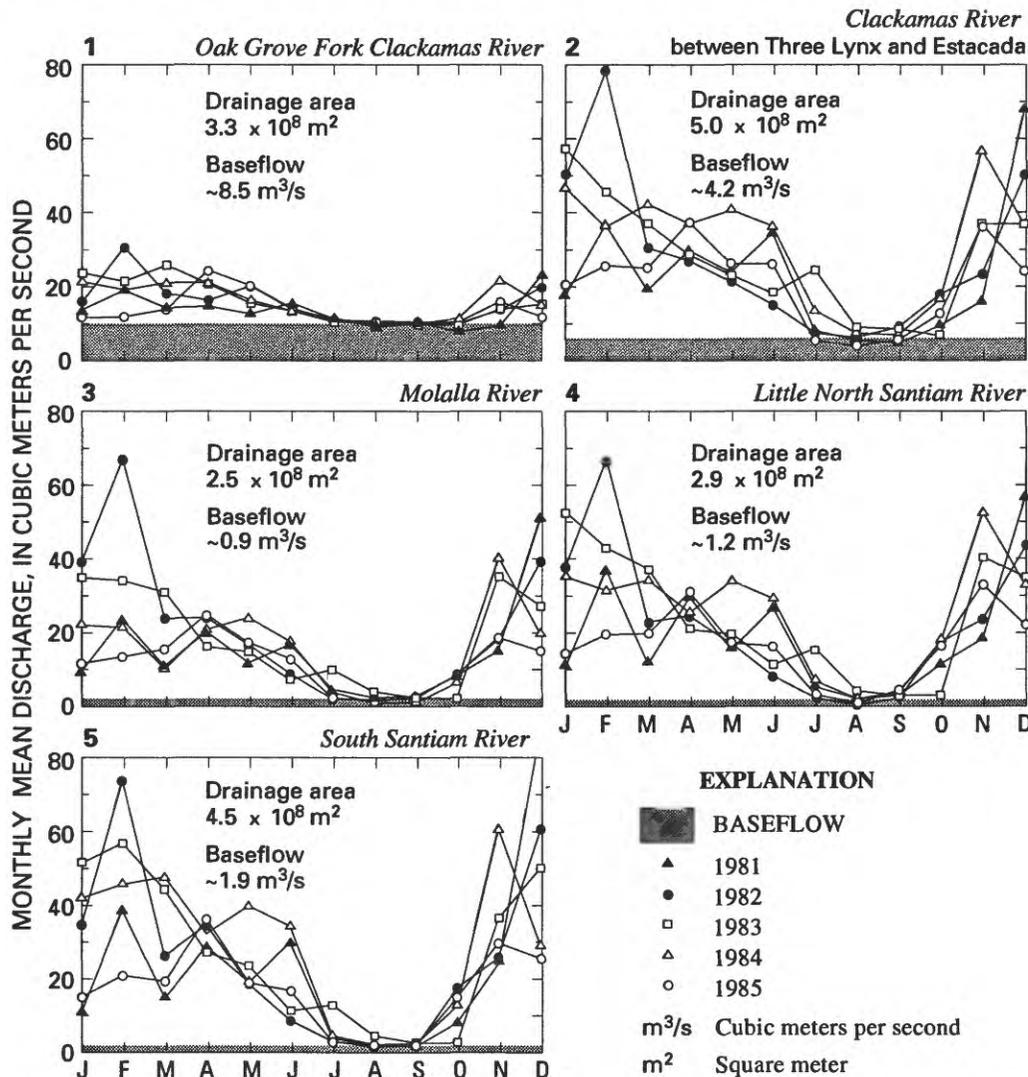
FIGURE 8.—Monthly mean discharge of major streams in basins for which ground-water recharge was estimated. See figures 4 and 7 for locations.

TABLE 3.—*Estimated minimum ground-water recharge rates for selected basins west of Cascade Range crest*

[See figure 4 for basin locations and annual precipitation, figure 7 for surficial geology, and figure 8 for stream hydrographs. m^2, square meter; m/s, meter per second; <, less than; Ma, million years before present]

Number	Basin	Area (10^8 m^2)	Approximate rock age and dominant lithology	Minimum ground-water recharge[a] (m/s × 10^{-9})
(1)	Oak Grove Fork Clackamas River[b]	3.3	<7 Ma andesite	26
(2)	Clackamas River between gaging stations 14209500 and 14210000	5.0	7–17 Ma andesite	4.9[c]
(3)	Molalla River	2.5	7–17 Ma andesite (volcanic diamicton)	3.7
(4)	Little North Santiam River	2.9	17–25 Ma andesite	4.2
(5)	South Santiam River	4.5	17–25 Ma andesite	1.1[c]

[a] Baseflow per unit area.

[b] Stream flow at U.S. Geological Survey gaging station 14209000 was adjusted for changes in storage at Timothy Lake.

[c] Estimated rate for >7 Ma rocks only, obtained by assuming that the unit baseflow for the <7 Ma rocks in the basin is the same as that calculated for the Oak Grove Fork basin (26 × 10^{-9} m/s).

porosity and permeability in the older volcanic rocks; the relatively steep topography in areas where older rocks are exposed may also tend to reduce infiltration. We believe that reduced permeability is the more important factor, because the heat-flow data discussed in the section "Conductive Heat Flow" also support the inference that the older rocks are much less permeable than the younger ones.

NONTHERMAL GROUND-WATER CHEMISTRY

Areal variations in nonthermal ground-water chemistry reflect the copious recharge in the High Cascades. The shallow nonthermal ground water is commonly mixed cation-bicarbonate water, with concentrations of total dissolved solids ranging from less than 100 mg/L in the High Cascades to about 300 mg/L elsewhere in the study area. Nonthermal ground water has been sampled at about 625 springs and wells in and near the study area. The major-element chemistry for 125 sites is listed in table 4, and partial analyses (Na only or Na and Cl) for about 500 additional sites were reported by Ingebritsen and others (1988).

In general, the nonthermal waters are very different chemically from the thermal waters in the study area, most of which are Na-Cl or Na-Ca-Cl waters with dissolved solids concentrations ranging up to about 3,000 mg/L (fig. 9). Relatively saline non-thermal ground water (greater than 300 mg/L dissolved solids) was sampled in parts of the Western Cascades where 25- to 35-Ma sedimentary rocks are exposed, in the lower Deschutes basin, and at a few other sites. These more saline waters include Na-Cl waters (table 4, analyses 8, 10, 27, 36), Na-Ca-Cl waters (analysis 7), Na-HCO$_3$ waters (analyses 9, 11, 13, 20, 60, 63, 72, 78, 80), and Na-mixed anion waters (analyses 3, 17). Other unusual samples include more dilute Na-Cl waters from west of the Cascade Range crest (analyses 21, 28, 30) and two Ca-SO$_4$ waters from the upper Deschutes basin (analyses 103, 104).

Most of the relatively saline Na-Cl and Na-Ca-Cl waters sampled in the study area were obtained from wells drilled into 25- to 35-Ma sedimentary rocks in the Western Cascades (fig. 10). Na-Ca-Cl waters have sodium and chloride as the dominant cation and anion, but they also have the peculiar characteristic that some of the calcium (Ca^{2+}) present is electrically balanced by chloride (Cl$^-$). That is,

$$2m_{Ca} > 2m_{SO_4} + m_{HCO_3} + 2m_{CO_3}$$

where m is in molal units (moles solute/kg water). This is the same characteristic that Hardie (1983) used to define calcium-chloride brines; none of our samples is sufficiently saline to classify as a brine. The major-element geochemistry of the nonthermal Na-Ca-Cl sample (analysis 7) is very similar to several of the thermal waters in the study area (fig. 9). Nonthermal Na-Ca-Cl waters are common southwest of the study area in interlayered volcanic and sedimentary rocks of the lower Eocene marine Umpqua Formation (for example, Robison, 1974; Robison and Collins, 1977; Frank, 1979).

FIGURE 9.—Trilinear diagram showing analyses of nonthermal ground waters and hot
springs expressed as percentage of total milliequivalents per liter. Waters in
which more than 50 percent of cations are Mg, Na+K, or Ca are described as Mg,
Na, or Ca waters, respectively. Similarly, waters in which more than 50 percent of
anions are SO_4, Cl, or CO_3 +HCO_3 are described as SO_4, Cl, or HCO_3 waters. Any
simple mixture of hypothetical waters A and B will plot on line AB on diamond-
shaped plotting field.

TABLE 4.—*Chemical composition of ground water in Cascade Range of northern and central Oregon. Most of the data are from nonthermal springs and wells. Data from one lake (analysis 90) and previously published data from several of the hot springs in the Kahneeta Hot Springs area (analyses 64–66) are also included for completeness*

[Well names are from well logs on file with the Oregon Department of Water Resources. Dashes indicate the absence of data. Sites are ordered by township, range, and section; in parentheses where unsurveyed. Codes: W, well; SP, spring; LK, lake. Concentrations are in milligrams per liter (mg/L). Different levels of precision reported for various dissolved constituents reflect the fact that the analyses were done in several laboratories. In general, cations were determined by inductively coupled plasma; bicarbonate by acid titration; chloride by colorimetry or mercurimetric titration; sulfate by turbidimetry; silica by turbidimetry; silica by atomic adsorption and molybdate blue; fluoride by ion-selective electrode; and boron by dianthrimide. <, less than]

Number	T-R-Sec.	Name	Code	Temp. (°C)	pH	Calcium (Ca)	Magnesium (Mg)	Sodium (Na)	Potassium (K)	Bicarbonate (HCO$_3$)	Chloride (Cl)	Sulfate (SO$_4$)	Silica (SiO$_2$)	Fluoride (F)	Boron (B)	Lithium (Li)
								West of the Cascade crest								
1.	3S-5E-28	—	W	18	9.0	1.8	0.61	71	0.4	106	42	5.4	26	0.4	0.11	0.029
2.	(6S-8E-32)	Fire	SP	7	6.9	5.5	3.2	2.0	.2	37	<1	<1	21	<.1	—	—
3.	7S-6E-09	—	W	14	9.7	5.0	.04	230	3.5	83	160	180	16	1.1	1.8	.02
4.	(7S-7E-09)	unnamed	SP	3	7.1	3.2	1.1	1.7	.6	19	<1	<1	17	<.1	—	—
5.	8S-4E-31	—	W	23	7.3	31	.78	11	.1	66	6.3	39	14	.1	.17	.004
6.	(8S-8E-20)	Cub	SP	6	7.7	4.4	1.3	3.6	1.4	29	.8	<1	29	<.1	—	—
7.	9S-2E-17	—	W	17	8.9	160	<.1	480	2.8	14	1,000	11	17	.3	1.0	.02
8.	9S-2E-27	—	W	15	8.1	39	.9	330	1.9	127	560	30	33	.6	2.3	.03
9.	9S-3E-11	Ceri	W	15	8.9	8.5	1.4	110	.9	260	37	10	17	.2	.67	.004
10.	9S-3E-28	—	W	18	8.4	53	13	470	1.6	288	670	40	29	.2	2.5	.15
11.	9S-6E-35	unnamed	SP	9	9.9	1.0	.10	86	.5	228	1.1	2.1	31	.4	.22	.015
12.	(9S-7E-03)	unnamed	SP	4	7.1	6.6	1.3	2.6	.2	32	.4	<1	15	—	—	—
13.	(9S-7E-09)	unnamed	SP	8	9.0	2.9	.57	100	2.2	293	5.9	3.9	33	.3	.04	.057
14.	(9S-7E-14)	unnamed	SP	7	7.2	7.2	1.1	4.7	.4	40	.5	<1	17	—	—	—
15.	(9S-7E-29)	unnamed	SP	8	7.7	10	3.6	3.8	.8	59	.4	<1	26	—	—	—
16.	(9S-8E-02)	Big	SP	5	6.6	7.3	2.6	4.6	1.4	44	2.4	<1	42	—	—	—
17.	10S-6E-22	Green Veneer	W	14	7.7	5.3	2.0	120	1.0	158	89	30	31	.7	.28	.033
18.	(10S-8E-05)	unnamed	SP	5	6.5	2.5	.3	1.6	.8	16	.4	<1	23	—	—	—
19.	(10S-8E-15)	unnamed	SP	6	6.6	2.1	.1	1.4	.3	12	<1	<1	12	<.1	—	—
20.	13S-2E-36	Munts	W	12	6.7	36	11	250	.6	520	170	30	40	.8	2.3	.2
21.	13S-4E-32	—	W	11	6.5	36	2.1	52	.2	66	100	5.1	19	.4	1.0	.047
22.	13S-5E-32	—	W	12	5.8	14	3.6	12	.6	63	16	2.0	26	.2	.14	.004
23.	13S-7E-32	—	W[a]	25	8.0	—	.1	32	2.6	73	4.2	1.0	48	—	1.0	—
24.	14S-7E-20	Icecap	SP	4	7.7	3.5	1.8	3.9	1.2	30	.6	<1	26	—	—	—
25.	(15S-6E-04)	unnamed	SP	7	7.1	6.2	2.3	2.4	1.0	35	.6	<1	22	—	—	—
26.	(15S-7.5E-25)	unnamed	SP	5	6.3	2.1	.7	1.7	.6	12	.4	<1	12	—	—	—
27.	16S-2E-29	Toy	W	18	7.8	32	7.2	300	6.7	160	430	13	16	1.3	1.2	.19
28.	16S-5E-21	Bowman	W	14	6.2	14	3.1	12	.7	31	26	6.4	29	.1	.09	<.004
29.	16S-6E-24	unnamed	SP	6	7.1	3.1	1.6	5.0	1.1	27	1.8	<1	24	—	—	—
30.	(16S-7E-21)	—	W	14	7.3	6.8	5.0	45	3.2	68	54	4.1	25	.1	.15	.007
31.	(17S-8E-18)	unnamed	SP	3	6.7	2.2	1.4	4.2	1.2	19	1	2	31	<.1	—	—
32.	(17S-8E-19)	unnamed	SP	3	6.7	1.5	1.2	5.2	1.3	22	<1	2	31	<.1	—	—
								East of the Cascade crest								
33.	4S-12E-22	Harvey&Jensen	W	9	8.09	9.4	7.5	13	2.1	94	6.0	<1	65	.2	—	—
34.	4S-12E-32	Lichtenberger	W	7	8.26	5.4	2.8	26	6.5	90	9.0	<1	72	.4	.11	—
35.	5S-11E-35	Kelly	SP[b]	14.5	7.5	16	3.2	18	4.3	103	2.0	2.5	—	.2	—	—
36.	5S-12E-06	Thompson	W	9	7.68	12	10	106	8.0	115	130	<1	71	6.9	2.0	—
37.	6S-9E-21	Willow	SP[b]	11.5	7.5	3.1	3.4	1.8	.1	26	.8	1.1	19	<.1	—	—
38.	6S-11E-03	Daniel	SP[b]	15.5	7.2	37	.4	15	3.7	158	2.2	1.6	73	.1	—	—
39.	6S-11E-08	Coyote	SP[b]	15.5	7.6	41	8.4	17	.8	210	2.8	1.9	44	.2	—	—

TABLE 4.—Chemical composition of ground water in Cascade Range of northern and central Oregon. Most of the data are from nonthermal springs and wells. Data from one lake (analysis 90) and previously published data from several of the hot springs in the Kahneeta Hot Springs area (analyses 64–66) are also included for completeness—Continued

Number	T-R-Sec.	Name	Code	Temp. (°C)	pH	Calcium (Ca)	Magnesium (Mg)	Sodium (Na)	Potassium (K)	Bicarbonate (HCO₃)	Chloride (Cl)	Sulfate (SO₄)	Silica (SiO₂)	Fluoride (F)	Boron (B)	Lithium (Li)
							East of the Cascade crest—Continued									
40.	6S-11E-27	Log	SP^b	17.5	7.3	12	7.8	12	3.7	100	2.4	1.0	69	.1	—	—
41.	6S-12E-27	Nena	SP^b	10.5	7.6	23	1.9	27	3.5	109	16	6.6	72	.1	.01	—
42.	7S-10E-07	Big	SP^b	9.5	7.9	8.5	4.4	5.4	1.5	66	1.3	2.0	38	.1	—	—
43.	7S-10E-25	Wally^d	W^b	—	7.1	6.8	6.5	6.7	7.5	67	2.5	2.6	30	.2	.25	—
44.	7S-11E-32	Comedown^d	W^b	10.5	7.3	9.4	5.6	1.9	1.3	58	1.6	2.1	39	.1	.02	—
45.	7S-11E-33	unnamed	SP^b	10.0	—	11	4.7	5.1	.7	70	1.4	2.1	35	.7	.004	—
46.	7S-12E-07	Simnasho^d	W^b	—	—	19	1.8	19	.7	105	1.5	6.2	33	.3	.01	—
47.	7S-12E-34	Suppah^d	W^b	—	—	10	3.8	13	1.4	72	2.8	2.6	40	1.0	—	—
48.	7S-13E-17	Eagle	SP^b	11.8	7.5	7.0	2.6	9.5	1.7	54	3.6	1.1	43	.1	—	—
49.	7S-14E-08	unnamed	SP^b	16.8	7.7	15	.8	31	.6	124	2.4	4.1	35	.9	—	—
50.	7S-14E-17	unnamed	SP^b	17.0	7.7	5.2	1.1	13	1.3	44	1.3	4.1	46	.2	—	—
51.	8S-11E-06	Sidwalter^d	W^b	—	—	9.9	6.8	8.8	1.8	83	6.0	1.8	48	.1	.01	—
52.	8S-11E-16	Guerin^d	W^b	—	—	9.4	6.0	11	1.5	85	1.4	1.8	49	.3	.003	—
53.	8S-11E-25	Quinn^d	W^b	14.3	7.6	12	5.7	16	3.0	95	3.3	3.4	48	.3	.01	—
54.	8S-11E-33	Wells^d	W^b	14.0	8.0	12	5.4	8.8	2.7	82	1.5	1.6	34	1.0	<.01	—
55.	8S-12E-03	unnamed	SP^b	17.0	7.0	9.1	4.9	7.8	1.2	60	2.5	2.6	40	.1	.02	—
56.	8S-12E-03	Schoolie Flat	W^b	—	—	23	9.6	19	2.2	166	4.5	4.4	54	.3	.01	—
57.	8S-12E-04	Schoolie Flat	W^b	—	—	18	7.6	13	2.2	115	4.7	2.9	59	.3	.01	—
58.	8S-12E-14	Kuckup	SP^b	—	—	15	6.0	22	2.0	117	7.9	3.3	65	.6	.01	—
59.	8S-12E-29	Buck^d	SP^b	15.0	8.2	9.8	5.5	4.8	1.1	73	1.3	1.3	38	.1	.03	—
60.	8S-13E-01	unnamed	SP^b	17.0	8.4	12	3.3	130	6.5	368	16	17	73	1.1	.02	—
61.	8S-13E-07	Wire Corral^d	SP^b	16.0	7.6	8.6	2.1	14	1.3	60	2.9	6.0	45	.5	.02	—
62.	8S-13E-11	Charley^d	SP^b	13.5	7.6	7.2	1.2	43	5.5	129	5.2	7.0	80	.7	—	—
63.	8S-13E-17	Charley^d	W^b	17.5	7.5	11	.4	100	.9	263	11	11	43	1.0	—	—
64.	8S-13E-19	unnamed	SP^b	83.5	8.1	13	.3	400	11	603	240	31	78	21	5.6	—
65.	8S-13E-20	Kahneeta	SP^b	47.0	8.2	3.8	.0	320	3.8	504	150	34	51	23	2.6	—
66.	8S-13E-20	unnamed	SP^b	55.5	8.8	5.2	.2	380	1.3	595	220	39	58	27	—	—
67.	8S-13E-30	unnamed	SP^b	13.5	7.8	32	4.2	27	4.8	168	4.7	18	67	.4	—	—
68.	8S-13E-32	McKinley^d	W^b	15.5	7.5	14	3.9	35	5.1	138	6.7	6.9	76	.5	<.01	—
69.	8S-13E-33	Frank^d	W^b	—	8.2	12	1.4	60	4.0	179	9.1	11	51	.7	.07	—
70.	8S-13E-35	Culpus^d	SP^b	16.6	7.8	17	2.0	46	7.6	162	7.8	10	88	.7	.05	—
71.	8S-14E-20	Rattlesnake^d	SP^b	6.5	8.1	7.9	2.3	14	5.3	54	2.1	8.4	42	.2	—	—
72.	8S-14E-20	Heath^d	W^b	—	7.5	8.2	.3	96	14	164	6.5	91	57	.3	.04	—
73.	8S-14E-31	unnamed	SP^b	13.0	8.1	31	13	23	4.2	188	6.9	8.9	54	.6	—	—
74.	(9S-8E-11)	—	W^b	7.5	7.4	3.1	1.9	2.7	.9	25	1.7	1.5	13	<.1	—	—
75.	9S-12E-01	unnamed	SP^b	13.0	7.6	21	3.3	34	6.6	157	6.9	6.5	77	.6	<.01	—
76.	9S-12E-03	Tohet^d	SP^b	13.0	7.9	21	5.6	25	6.6	135	4.8	6.8	77	.4	—	—
77.	9S-12E-10	unnamed	SP^b	16.5	7.7	13	5.4	16	4.4	100	7.9	4.1	69	.3	—	—
78.	9S-12E-13	unnamed	SP^b	10.5	7.5	28	6.3	78	4.4	263	15	23	70	.8	—	—
79.	9S-12E-31	unnamed	SP^b	9.3	7.6	20	10	20	4.1	164	3.6	3.5	73	.4	—	—
80.	9S-12E-32	Switzler^d	W^b	—	7.7	20	.4	65	7.4	229	5.5	7.6	51	.4	<.01	—
81.	10S-9E-33	unnamed	SP^b	3.0	7.5	4.3	1.0	1.7	.3	21	.6	.5	21	<.1	.04	—
82.	10S-10E-04	unnamed	SP^b	3.5	7.5	9.4	4.9	3.2	.9	62	1.4	3.6	34	.1	—	—
83.	10S-11E-30	Peters	SP^b	10.3	7.1	12	6.9	4.1	1.3	83	1.1	2.3	44	.1	—	—
84.	10S-12E-15	Smith^d	W^b	—	7.8	16	6.3	20	3.4	122	4.2	5.3	63	.1	.006	—
85.	10S-12E-29	Johnson^d	W^b	—	7.1	17	12	14	4.3	159	1.8	2.4	55	.2	—	—
86.	10S-12E-30	Miller^d	W^b	—	7.4	15	8.9	21	6.2	152	2.8	2.8	69	.2	<.01	—

TABLE 4.—*Chemical composition of ground water in Cascade Range of northern and central Oregon. Most of the data are from nonthermal springs and wells. Data from one lake (analysis 90) and previously published data from several of the hot springs in the Kahneeta Hot Springs area (analyses 64–66) are also included for completeness—Continued*

Number	T-R-Sec.	Name	Code	Temp. (°C)	pH	Calcium (Ca)	Magnesium (Mg)	Sodium (Na)	Potassium (K)	Bicarbonate (HCO3)	Chloride (Cl)	Sulfate (SO4)	Silica (SiO2)	Fluoride (F)	Boron (B)	Lithium (Li)
									East of the Cascade crest—Continued							
87.	11S-12E-02	Simtustus Park	W[b]	13.0	8.3	8.7	6.4	20	3.0	107	2.9	5.4	20	.2	—	—
88.	11S-12E-18	Estabrook	W[b]	—	7.6	17	9.2	20	3.9	144	4.1	4.4	45	.5	<.01	—
89.	12S-12E-33	Upper Opal	SP[c]	—	8.1	—	—	15	2.0	93	3.9	4.7	—	—	—	—
90.	13S-8E-27	Blue Lake	LK	15	7.0	5.2	2.1	4.0	1.4	28	.4	.2	26	.1	.01	.004
91.	13S-8E-27	Lovegren	W	8	7.82	6.2	2.8	4.2	1.6	46	3.0	<1	32	.08	<.05	<.04
92.	13S-12E-29	Clevenger	W	7	7.80	29	23	15	3.9	155	7.0	28	54	.2	<.05	<.04
93.	13S-13E-34	unnamed	SP[c]	6	8.1	—	—	15	2.3	115	3.5	4.7	—	—	—	—
94.	14S-10E-21	Indian Fd. L&C	W	13	7.10	18	14	11	1.6	120	7.0	5.2	50	.2	—	—
95.	14S-13E-31	—	W[c]	12	7.8	43	4.8	22	4.4	150	9.0	11	—	—	—	—
96.	15S-10E-36	McCulley	W[c]	10.5	7.8	13	6.2	9.0	3.1	90	1.5	2.1	45	.3	—	—
97.	15S-12E-23	—	W	7	8.10	15	11	19	4.4	126	8.0	8.9	44	.1	—	—
98.	16S-11E-15	—	W[c]	—	8.0	9.6	7.2	14	2.8	85	2.6	3.5	43	.2	.01	—
99.	16S-11E-24	Kautz	W	10	8.41	15	11	13	1.7	110	7.0	9.2	55	.3	—	—
100.	16S-11E-30	—	W[c]	11.0	7.8	6.2	5.7	13	1.9	69	2.2	1.7	38	.2	.07	—
101.	16S-12E-29	—	W[c]	12	7.9	21	16	19	4.6	131	4.0	6.0	—	—	—	—
102.	17S-9E-20	unnamed	SP	10	7.0	2.3	.8	1.3	.4	16	<1	<1	17	<.1	—	—
103.	17S-9E-28	unnamed	SP	3	6.04	13	4.0	4.3	.5	25	.3	49	44	.1	<.01	<.004
104.	17S-9E-28	unnamed	SP	6	6.34	16	5.7	4.1	.6	10	.4	53	47	.1	<.01	<.004
105.	17S-11E-02	—	W[c]	10.5	7.9	6.3	5.6	11	1.7	69	2.0	1.9	38	.1	.05	—
106.	17S-11E-03	unnamed	SP[c]	9.5	7.7	4.0	3.7	7.8	1.5	44	1.1	1.3	37	.1	.01	—
107.	17S-11E-13	unnamed	SP[c]	10.5	6.8	9.5	6.4	7.5	1.1	64	1.2	5.9	59	.2	.004	—
108.	17S-11E-13	—	W[c]	10.0	7.5	23	15	31	1.8	170	3.6	23	51	.5	.05	—
109.	17S-11E-23	—	W[c]	10.5	7.8	5.9	5.4	10	2.0	69	2.0	1.3	39	.1	.05	—
110.	17S-11E-23	—	W[c]	10.5	7.8	5.6	5.1	10	1.8	66	2.0	1.0	37	.1	.05	—
111.	17S-11E-25	—	W[c]	—	—	9.2	6.8	8.5	—	114	4.5	1.2	17	.2	—	—
112.	17S-12E-17	—	W[c]	—	7.4	8.8	12	8.4	1.3	69	2.0	2.0	40	—	—	—
113.	17S-12E-18	—	W[c]	12	8.0	9.6	5.3	6.0	2.4	50	1.0	1.0	—	—	—	—
114.	17S-12E-20	—	W[c]	12.4	8.2	7.8	6.3	9.4	3.2	80	1.6	1.7	40	.1	.02	—
115.	18S-8E-03	unnamed	SP	3	6.4	1.1	0.6	2.3	0.9	13	<1	<1	27	<.1	—	—
116.	18S-10E-10	—	W[c]	7.9	7.6	6.1	2.6	5.7	1.9	45	.5	.3	41	.1	—	—
117.	18S-11E-23	—	W[c]	10.9	7.7	8.2	4.5	7.4	—	70	1.3	.9	50	.1	—	—
118.	18S-11E-23	—	W[c]	11.2	7.6	5.3	4.3	7.9	1.8	63	1.5	1.0	37	.1	.04	—
119.	19S-8E-34	—	SP	6	7.93	2.3	1.4	3.6	.9	23	1.0	<1	27	.1	—	—
120.	19S-11E-31	unnamed	SP[c]	8.8	7.6	7.4	5.5	12	2.2	74	3.8	1.6	40	.1	.07	—
121.	20S-10E-01	—	W[c]	7.0	7.9	5.6	3.8	9.8	1.5	57	2.8	.8	38	.1	.06	—
122.	20S-10E-01	unnamed	SP[c]	7.0	8.0	5.3	3.6	10	1.5	57	3.0	1.4	34	.1	.06	—
123.	20S-10E-26	—	W	8.0	8.00	12	10	40	3.8	219	3	<1	37	.4	<.05	<.04
124.	20S-11E-06	—	W[c]	8.5	8.2	6.2	5.0	16	2.6	81	2.7	1.3	27	.1	.05	—
125.	22S-8E-18	unnamed	SP	9	7.55	4.1	1.6	3.7	1.4	30	1	<1	13	.07	<.05	<.04

[a] Raw, unfiltered sample; pH determined in laboratory.
[b] Robison and Laenen (1976).
[c] Unpublished data, J.B. Gonthier, U.S. Geological Survey, Portland, Oregon.
[d] Names from Robison and Laenen (1976).
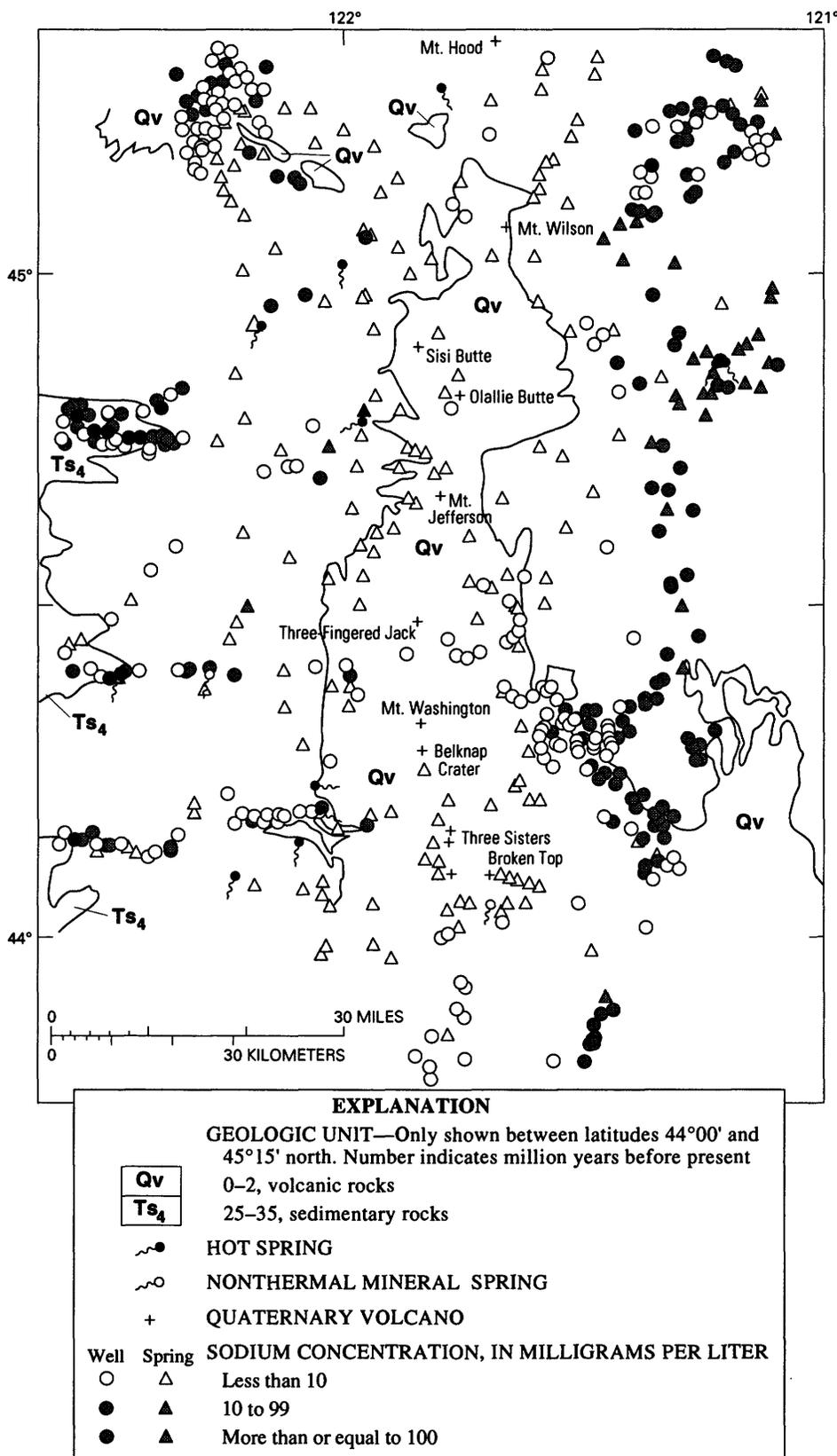
FIGURE 10.—Sodium concentrations in waters sampled in and near study area. Most samples with sodium in concentrations of 100 mg/L or more are waters from unit Ts$_4$, near west edge of study area. Data from Ingebritsen and others (1988).

Sodium-bicarbonate (Na-HCO$_3$) waters that were sampled at several widely separated sites in the Western Cascades and on the Deschutes-Umatilla Plateau do not appear to be associated with a particular near-surface lithology. These waters are characterized by a predominance of sodium over other cations that ought to be observed in water that has dissolved albite (Hem, 1985). Two unusual low-discharge springs in the Breitenbush Hot Springs area (analyses 11, 13) are characterized by Na exceeding 95 percent of total cations and HCO$_3$ exceeding 95 percent of total anions (fig. 9).

Mixing of Na-Ca-Cl thermal water with dilute mixed cation-bicarbonate water may explain the major-element geochemistry of the more dilute Na-Cl waters sampled west of the Cascade Range crest (analyses 21, 28, 30). Such a process is perhaps the most plausible explanation for the sample from a 62-m-deep well in the Quaternary arc about 7.5 km east-southeast of Belknap Springs (analysis 30). Surface waters in the vicinity have somewhat elevated Cl concentrations, and a well about 2.2 km west of Belknap Springs discharges Belknap-equivalent thermal water (Ingebritsen and others, 1988), suggesting a "leaky" thermal system in the area.

THERMAL WATERS

In this section, we present data suggesting that gravitationally driven thermal fluid circulation transports significant amounts of heat from the Quaternary arc into Western Cascade rocks older than about 7 Ma. Inferences regarding the generalized pattern of thermal fluid circulation are based on the locations of the hot springs relative to regional topography, geologic structures, and possible heat sources and on the isotopic composition of the thermal waters. Estimates of the heat transported by various hot-spring systems are based on chemical geothermometry and hot-spring discharge measurements.

LOCATION OF HOT SPRINGS

Hot springs in the study area discharge from Miocene or Oligocene rocks at elevations of 440–680 m (see table 2 for hot-spring elevations). With the exception of Bagby Hot Springs, they are found near major streams that originate in the Quaternary arc, in deeply incised valleys that focus the discharge from regional ground-water flow systems (fig. 11). The presence of hot springs within a relatively narrow elevation range implies that topography is a major control on thermal-water discharge.

Most and perhaps all of the hot springs are located near the surface exposures of structurally or stratigraphically controlled permeable conduits. The four hot springs in the McKenzie River drainage (fig. 11) are located near faults or fracture zones that likely interrupt the flow of ground water down the hydraulic gradient from the Quaternary arc (Priest and others, 1988). Three of the four are close to and probably associated with the Horse Creek fault zone (fig. 11); the fourth and westernmost is near the older (older than 6.3 Ma), down-to-the-east Cougar Reservoir fault zone (Priest and others, 1988). Austin, Breitenbush, Bagby, and Kahneeta Hot Springs are not directly associated with any mapped structures. However, Sherrod and Conrey (1988) suggest that a zone of northwest-southeast-trending faults (fig. 11) may connect Austin Hot Springs to the Mount Jefferson area.

Drill-hole data suggest the presence of a stratigraphically controlled thermal aquifer in the Breitenbush Hot Springs area. Thermal fluid was encountered in a well 3 km south-southeast of Breitenbush Hot Springs (Priest, 1985) in the same stratigraphic unit as the hot-spring orifices (Priest and others, 1987). Both the aquifer and the hot springs are found in the upper part of Sherrod and Smith's (1989) map unit Ta$_3$ (see table 1 for description of map units). Additional evidence for a stratigraphically controlled thermal aquifer in the Breitenbush area is provided by temperature-gradient data that define a 30-to 50-km^2 area of anomalously high heat flow south and east of the hot springs (Blackwell and Baker, 1988b). Terwilliger Hot Spring issues at approximately the same stratigraphic position as the thermal aquifer in the Breitenbush area (fig. 3).

Bagby Hot Springs is unique among the Western Cascade hot springs in that it is isolated from the Quaternary arc by major drainage divides. Its location and chemical composition (discussed under "Thermal Water Chemistry") suggest that Bagby is the product of relatively local deep circulation, rather than regional-scale lateral ground-water flow.

The Kahneeta Hot Springs group is in the Deschutes-Umatilla Plateau physiographic province and includes a number of springs along a 3-km reach of the Warm Springs River (fig. 11). Kahneeta is the only hot-spring group in the study area that lies east of the Quaternary arc, and it is more areally extensive than any hot-spring group in the Cascade Range. The deeply incised valley of the Warm Springs River may be a regional

discharge area for generally north-moving ground-water flow in the Deschutes basin and (or) generally west-to-east flow from the Quaternary arc (see the water-table configuration in fig. 11). Kahneeta may also be the product of more localized circulation, although its large discharge (discussed under "Hot-Spring Discharge Rates") suggests a relatively extensive system.

EXPLANATION

Qv   QUATERNARY VOLCANIC ROCKS—Dark stipple indicates dacitic and rhyolitic rocks

⸻•⸻   FAULT—Bar and ball on downthrown side. Dotted where buried. Dashed where inferred

– –2400– –   WATER-TABLE CONTOUR—Shows altitude of water table. Contour interval 200 feet. Datum is sea level

—2500—   TOPOGRAPHIC CONTOUR—Shows altitude of land surface. Contour interval 2500 feet. Datum is sea level

27 MW•   HOT SPRING—Number indicates heat output in megawatts

⌐O   NONTHERMAL MINERAL SPRING

△   QUATERNARY VOLCANO

FIGURE 11.—Location of hot springs, generalized topography, selected geologic structures, Quaternary volcanic rocks, water-table elevations in Deschutes basin, and amount of heat transported advectively by hot-spring systems. Geologic data from Sherrod and Smith (1989); water-level information from Black (1983), J.B. Gonthier (U.S. Geological Survey, unpublished data), and Bolke and Laenan (1989).

Many high-temperature hydrothermal systems are associated with Quaternary silicic magmatism (Smith and Shaw, 1975). R.L. Smith and Shaw (1975) suggested that the Breitenbush Hot Springs system might be related to silicic domes in the Mount Jefferson area and, as noted above, Sherrod and Conrey (1988) suggested a structural connection between Austin Hot Springs and the Mount Jefferson area. The hot springs in the McKenzie River drainage might be linked to silicic magmatism in the Three Sisters area, on the basis of geographic proximity and a favorable topographic gradient (fig. 11). Any relation between Kahneeta Hot Springs and Quaternary silicic magmatism is much more speculative, but lateral flow from the areas of silicic volcanism along the upper Deschutes River or from the Mount Jefferson area seems hydraulically possible (fig. 11).

STABLE-ISOTOPE DATA

The isotopic composition of thermal waters in the Western Cascades suggests that they were recharged at relatively high elevations. Figure 12 shows the relation between δD and elevation for thermal and nonthermal waters sampled west of the Cascade Range crest. Oxygen-18 contents show a similar pattern because there is little oxygen shift in the thermal waters. In figure 12 we have omitted nonthermal data obtained from relatively saline waters (>70 mg/L Na) and (or) from high-order drainage basins, where the source of
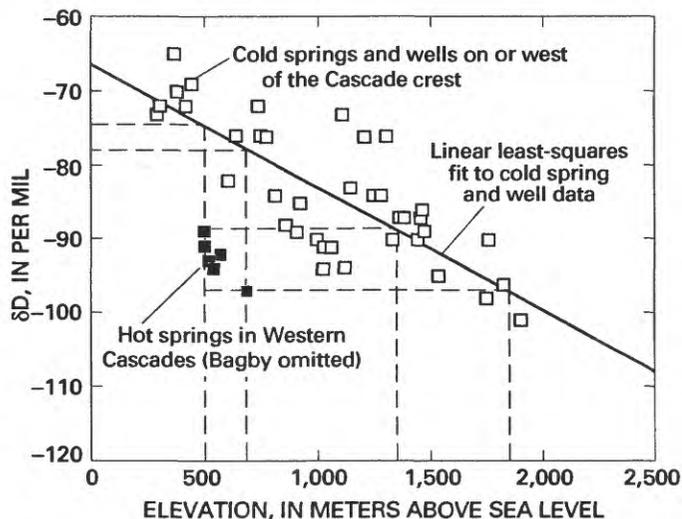
FIGURE 12.—Relation between deuterium content and elevation for waters on or west of Cascade Range crest.

recharge is unclear. The remaining samples presumably represent local meteoric water, and the strong inverse correlation between δD and elevation is much clearer than in figure 6, which included all of the data from the study area.

On the basis of a linear least-squares fit to the nonthermal data, the range of δD values measured in the thermal waters (–97 to –89 o/oo) is best matched by that of meteoric waters at elevations of 1,350 to 1,850 m above sea level (fig. 12). This suggests that recharge takes place within the Quaternary arc, because only very limited areas outside the Quaternary arc reach such elevations. Extensive areas at elevations above 1,500 m (5,000 ft) are found only in the highlands around Mount Jefferson and the Three Sisters (pl. 1). The hot springs in the Western Cascades are at elevations of 490 to 680 m above sea level (table 2), so a significant elevation difference is available to drive the thermal circulation systems. The average topographic gradient between the inferred recharge areas and the hot springs is as large as 0.1.

It is arguable that the Western Cascade thermal waters are local meteoric waters, but that the isotopic composition of precipitation has changed significantly since they were recharged. This could be the case if the thermal waters were recharged in the Pleistocene. The average thermal water contains about 17 o/oo less deuterium than average meteoric water at the same elevation (fig. 12). Few if any paleotemperature data are available for the Cascade Range, but a decrease of about 3–4°C in mean annual air temperature would probably be sufficient to decrease the deuterium content of precipitation by 17 o/oo (Dansgaard, 1964; Gat, 1980). In South Kazakhstan, late Pleistocene (12–30 ka) ground water contains up to about 13 o/oo less deuterium than younger ground water (Ferronsky and others, 1983), and ice-core data from the Arctic and Antarctic indicate much larger isotopic variations related to the Wisconsin glaciation (Faure, 1986).

There does not appear to be any absolute way to estimate residence times for the Western Cascade thermal waters. Carbon-14 dates would be inaccurate because the reactions that produce Na-Ca-Cl waters result in precipitation of calcite. Magmatic sources of CO_2 are presumably present in the Quaternary volcanic arc and would also preclude carbon-14 dating. Crude estimates of relative circulation times might be obtained from total dissolved helium (Andrews, 1983). The results would be

uncertain because this technique requires knowledge of the porosity, density, and thorium and uranium contents of the rock through which the waters have circulated. The available helium isotope data indicate appreciable ^{3}He, which in this environment probably comes from the mantle, and correcting for a mantle component would create additional uncertainty. Chlorine-36 has been used as a dating tool for very old ground water (for example, Bentley and others, 1986), but the high chloride content of the Western Cascade thermal waters would complicate chlorine-36 dating.

Because the hot springs in the Western Cascades are located at sites expected to capture regional ground-water flow from the Quaternary arc, we prefer to explain the isotopic composition of these thermal waters in terms of higher-elevation recharge during the Holocene. Relatively high ^{3}He/^{4}He ratios (table 5) are further suggestive evidence that these thermal waters originate in areas of Quaternary volcanism (Craig and others, 1978; Tolstikhin, 1978).

The isotopic composition of Kahneeta thermal waters is best matched by meteoric waters in the upper Deschutes basin east of the Three Sisters or on the flanks of low mountains immediately north and south of the hot springs (pl. 1). Thermal waters from the Kahneeta Hot Springs group are much more depleted isotopically than meteoric waters near the Cascade Range crest to the west (pl. 1); this seems to rule out Holocene recharge in the Mount Jefferson area.

Ground waters of meteoric origin may be enriched in ^{18}O by water-rock interaction at high temperatures (Craig, 1963), whereas deuterium values remain largely unaffected because of the low hydrogen content of most rocks. The thermal waters from the study area have relatively small "oxygen shifts" of about 1 o/oo (fig. 5), perhaps because they do not reach very high temperatures and (or) their residence time is short. The size of the oxygen shift can be used to calculate a quantitative index of the degree of water-rock interaction (H.P. Taylor, 1971; Blattner, 1985). This "water-rock ratio" is an apparent mass ratio of water to rock, based on a material balance. Water-rock ratios for hot-spring systems in the study area are 3±1, assuming open-system (R_∞) behavior. These open-system values are comparable to those obtained for other active and fossil hydrothermal systems (Blattner, 1985; Larson and Taylor, 1986; White and Peterson, 1991).

TABLE 5. — *Chemical composition, geothermometer temperatures, and discharge data for hot springs in study area*

[Dashes indicate the absence of data. Concentrations are in milligrams per liter (mg/L), and were determined by the methods described at the head of table 4]

Name of spring	pH	Ca	Mg	Na	K	HCO$_3$	Cl	Br	SO$_4$	SiO$_2$	T_d^a (°C)	T_g^b (°C)	Q_t^c (L/s)	^{3}He/^{4}He $(R/R_a)^d$
Austin	7.4	35	0.10	305	6.4	36	390	1.2	130	81	86	186	120±6	5.7
Bagby	9.4	3.3	<.05	53	.7	69	14	—	42	74	58	52	1	1.2
Breitenbush	7.0	95	1.1	745	31	137	1200	4.2	140	163	84	174	13±2	6.5
Bigelow	7.8	195	.53	675	15	22	1250	3.8	140	73	59	155	—	—
Belknap	7.6	210	.34	660	15	20	1200	3.9	150	91	73	152	20±3[e]	—
Foley	8.0	510	.08	555	8.7	20	1350	4.0	510	63	79	100	11±4	—
Terwilliger	8.5	215	.07	405	6.1	21	790	2.2	240	47	46	135	5	—
Kahneeta	8.1	13	.05	400	11	603	240	.8	31	78	83	137	50±5	—

[a] Discharge temperature.
[b] Chemical geothermometer temperatures based on anhydrite saturation, except for Kahneeta and Bagby, which are based on the silica (quartz) and cation geothermometers. The solubility of anhydrite (CaSO$_4$) provides a geothermometer which indicates maximum temperature (Ellis and Mahon, 1977). Anhydrite saturation values for the Na-Cl and Na-Ca-Cl waters that discharge in the Western Cascades correlate well with sulfate-water isotope temperatures (Mariner and others, 1993). The temperatures listed for Kahneeta and Bagby are averages of the quartz and cation geothermometers. These and other geothermometers are discussed by Fournier (1981).
[c] Discharge based on chloride-flux measurements, except for Bagby Hot Spring, where discharge was measured directly.
[d] ^{3}He/^{4}He ratio (R) normalized by the atmospheric ratio (R_a).
[e] Combined discharge of Bigelow and Belknap hot springs.

THERMAL-WATER CHEMISTRY

Most of the thermal waters in the study area are Na-Cl or Na-Ca-Cl waters of near-neutral pH. Austin Hot Springs discharges Na-Cl waters; Breitenbush Hot Springs and the hot springs in the McKenzie River drainage (Bigelow, Belknap, Foley, and Terwilliger) discharge Na-Ca-Cl waters; Bagby Hot Springs discharges Na-mixed anion waters; and Kahneeta Hot Springs discharges Na-HCO_3 waters (table 5, fig. 9).

The definition of Na-Ca-Cl waters ($2m_{Ca} > 2m_{SO_4} + m_{HCO_3} + 2m_{CO_3}$) implies that at least part of the Ca^{2+} is electrically balanced by Cl^-. The presence of a $CaCl_2$ component is an unusual chemical signature shared by many rift-zone hydrothermal brines, some oil-field brines, fluid inclusions in ore minerals, and a few saline lakes (Hardie, 1983). In North America, thermal Na-Ca-Cl waters occur primarily in the Salton Trough and in the Columbia embayment, which encompasses northwest Oregon and southwest Washington and may be built on Cenozoic oceanic crust (Hamilton and Myers, 1966).

A number of processes have been suggested to explain the origin of Na-Ca-Cl waters. Hardie (1983) presented a strong empirical case for origin by basalt-seawater interaction for the Reykjanes, Iceland, hydrothermal system. There, Na-Ca-Cl waters appear to develop from Na-Cl waters by albitization of plagioclase:

anorthite
$$CaAl_2Si_2O_8 + 2Na^+ + 4H_4SiO_4 =$$
$$albite$$
$$2NaAlSi_3O_8 + Ca^{2+} + 8H_2O$$
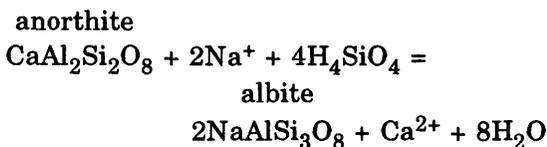
where anorthite represents the calcium component of intermediate plagioclase. The resulting increase in dissolved calcium causes precipitation of calcite ($CaCO_3$) and anhydrite ($CaSO_4$). Calcite precipitation can lead to very low HCO_3 concentrations (table 5), unless a source of CO_2 is present. Another possible control on Na/Ca ratios in Na-Ca-Cl waters is conversion of plagioclase or calcium-bearing zeolites to analcime ($NaAlSi_2O_6 \cdot H_2O$) (Mariner and others, 1993). In either case (albitization or analcimization), Na-Ca-Cl thermal waters can be regarded as having evolved from Na-Cl waters by alteration of a calcium-bearing mineral.

Mariner and others (1980) and Ingebritsen and Sorey (1985) suggested that Na-Cl and Na-Ca-Cl thermal waters of the Cascade Range obtain high concentrations of Na and Cl by circulating through rocks deposited in a marine environment. However,

Conrey and Sherrod (1988) described xenoliths from the Cascade Range that appear to have lost Na and Cl during recrystallization to quartz, potassium feldspar, and illite, and suggested that the source of these constituents in the thermal waters could be altered volcanic glass. Mariner and others (1989) noted that bromide to chloride weight ratios in the thermal waters (table 5) are similar to those in seawater (3.5×10^{-3}) rather than volcanic ash (1.5×10^{-3} for Mount St. Helens ash), and again suggested a "marine" Cl source. However, the Br/Cl ratio in Japanese volcanic rocks varies within a range that brackets the seawater ratio ($1-6 \times 10^{-3}$; Brehler and Fuge, 1978).

Mass-balance considerations imply the presence of a source of chloride in addition to the volcanic rocks. The chlorine contents of Cascade Range volcanic rocks are highly variable and poorly known, but probably quite low. H.N. Elsheimer (U.S. Geological Survey, written commun., 1990) obtained values of 160 ± 230 mg/kg for nine samples of Eocene or younger volcanic rocks. About 70 km^3/km arc length/m.y. of volcanic rocks with an average Cl content of 160 mg/kg would be required to supply the current flux of chloride from hot springs (about 120 g/s distributed over the 135 km of arc length in the study area). This rate is more than an order of magnitude greater than the long-term volcanic production rate of 3–6 km^3/km arc length/m.y. (Sherrod and Smith, 1990).

A large discrepancy between chlorine-based water-rock ratios and those based on ^{18}O also suggests that only a minor amount of the chloride in the thermal water is derived from leaching of volcanic rock. Lithophile elements that are not major components in secondary minerals (including Cl, B, and Li) can be used to calculate water-rock ratios analogous to those calculated on the basis of ^{18}O contents (White and Peterson, 1991). For the Long Valley, California, hydrothermal system, White and Peterson (1991) showed that chlorine contents (Cl_{rock}/Cl_{water}) give a range of water-rock ratios (1.1 to 2.5) very similar to the range calculated on the basis of ^{18}O composition (1.5 to 2.3). They also showed a general relation between fluid and rock chlorine contents for hydrothermal systems contained principally in Quaternary rhyolitic tuffs, with Cl_{rock}/Cl_{water} ratios falling in the range of 0.5 to 2. Again taking 160 mg/kg as representative of the rock chlorine content, Cl_{rock}/Cl_{water} ratios for the study area range from 0.1 to 0.4, whereas the water-rock ratios based on ^{18}O contents are 3 ± 1.

The most probable sources of chloride are marine rocks and magmatic volatiles. As noted under

"Stratigraphy," lower and middle Eocene (about 44–58 Ma) marine rocks likely extend beneath the study area. A magmatic source also seems feasible: relatively high ^{3}He/^{4}He values for the Na-Ca-Cl thermal waters (table 5) indicate that some dissolved constituents are of magmatic origin, and most magmatic chloride will partition to an aqueous phase. If we assume conservatively that the chloride content of the magma is 0.1 weight percent (Burnham, 1979), an intrusion rate of 10 km^3/km arc length/m.y. could supply the current flux of chloride from the hot-spring systems of the study area (about 1 g/s per km arc length). This intrusion rate is within the range of rates (9–33 km^3/km arc length/m.y.) calculated in the "Heat Budget" section.

Bagby Hot Springs discharges dilute high-pH Na-mixed anion waters (table 5) and is also unique among the Western Cascade hot springs in that it is isolated from the Quaternary arc by major drainage divides. This location, chemical composition, and a relatively low ^{3}He/^{4}He ratio (table 5) suggest that Bagby is the product of relatively local deep circulation. Its Na-mixed anion waters are similar to thermal waters associated with granitic rocks of the Idaho batholith (Mariner and others, 1980). Tertiary granitic or dioritic rocks are locally exposed in the Bagby Hot Springs area (Walker and others, 1985) and may be more widespread at depth. The chloride-rich Na-HCO$_3$ waters of Kahneeta Hot Springs are also markedly different from other thermal waters in the study area. Their chemical composition somewhat resembles that of several hot springs in the Long Valley-Mono Lake area, California (Mariner and others, 1977).

GEOTHERMOMETRY

Many different chemical and isotopic reactions are used as geothermometers (geochemical thermometers) in order to estimate fluid temperatures in the deep parts of active hydrothermal systems (see, for example, the review by Fournier, 1981). Those most commonly used, listed in table 6, are based on the temperature-dependent solubility of silica, temperature-dependent exchange reactions that control the ratios of certain cations in solution, or the temperature-dependent fractionation of oxygen isotopes between water and dissolved sulfate.

The quartz, cation (Na-K-Ca), and SO$_4$-H$_2$O geothermometers give disparate results when applied to the Na-Cl and Na-Ca-Cl waters of the study area. Only for Breitenbush Hot Springs are all three geothermometers in reasonably good

agreement (within 30°C). For the other Na-Cl and Na-Ca-Cl springs the Na-K-Ca temperatures are 45–84°C, the silica (quartz) temperatures are 99–132°C, and the SO$_4$-H$_2$O temperatures are 117–181°C (Mariner and others, 1993). The rates of the SO$_4$-H$_2$O exchange reactions are very slow relative to silica geothermometry and cation exchange reactions; if equilibrium is attained at high temperatures there is little reequilibration as the water cools during movement to the surface (Fournier, 1981).

The retrograde solubility of anhydrite can provide another geothermometer that indicates maximum temperature (Ellis and Mahon, 1977). Because excess calcium is produced by alteration of plagioclase, the Na-Cl and Na-Ca-Cl thermal waters are likely to be saturated with anhydrite at depth. Using anhydrite solubility to estimate aquifer temperatures is not straightforward because the solubility depends on two species (Ca^{2+} and SO$_4{}^{2-}$) that can enter into complexes and whose activities depend upon the temperature and ionic strength of the water. Mariner and others (1993) used the solution-mineral equilibrium code SOLMINEQ.88 (Kharaka and others, 1988) to determine the temperatures at which the Na-Cl and Na-Ca-Cl thermal waters were saturated with anhydrite.

Calculated anydrite saturation temperatures agree remarkably well with the SO$_4$-H$_2$O temperatures of the Na-Cl and Na-Ca-Cl waters in the study area (to within 13°C; Mariner and others, 1993). The SO$_4$-H$_2$O and anhydrite geothermometers are completely independent, so their close agreement is good evidence that the temperatures estimated by these methods are correct.

Anhydrite has not been reported from drill holes in the study area, but most drilling has been too shallow to encounter zones of thermal fluid circulation. In general, it is rare to recover anhydrite in cuttings from geothermal wells, because anhydrite will dissolve in the relatively cool drilling fluids.

In table 5 we list anhydrite saturation temperatures for the Na-Cl and Na-Ca-Cl waters, and an average of the silica and Na-K-Ca temperatures for the Na-mixed anion (Bagby) and Na-HCO$_3$ (Kahneeta) waters. For Bagby and Kahneeta the silica and Na-K-Ca temperatures are in good agreement. The anhydrite saturation temperatures are significantly higher, but these relatively low-calcium waters may never have been saturated with anhydrite.

Mariner and others (1993) suggested three possible explanations for the low temperature estimates

TABLE 6.—*Commonly used geothermometers*

Geothermometer	Equation	Reference
Quartz (no steam loss)	$T = \dfrac{1{,}309}{5.19 - \log C} - 273.15$ where C is dissolved silica concentration, in mg/L	Fournier and Rowe, 1966
Na-K-Ca	$T = \dfrac{1{,}647}{\log(Na/K) + \beta[\log(\sqrt{Ca}/Na) + 2.06] + 2.47}$ where $\beta = 4/3$, $T < 100°C$ $\quad\quad = 1/3$, $T > 100°C$ and Na, K, and Ca concentrations are in mg/L	Fournier and Truesdell, 1973
$\Delta^{18}O(SO_4^{2-} - H_2O)$	$1{,}000 \ln\alpha = 2.88(10^6 T^{-2}) - 4.1$ where $\alpha = \dfrac{1{,}000 + \partial^{18}O(HSO_4^-)}{1{,}000 + \partial^{18}O(H_2O)}$ and T is in kelvins	Mizutani and Rafter, 1969

yielded by the Na-K-Ca geothermometer: (1) that the Na-Cl and Na-Ca-Cl waters are lower in P_{CO_2} than the waters from which the geothermometer was empirically derived; (2) that the relatively high calcium concentrations cause anomalously low temperature estimates; or (3) that potassium concentrations were decreased by lower-temperature water-rock interaction as the thermal fluid moved laterally in an outflow structure and cooled. They noted that the Na-K-Ca temperature of the relatively CO_2 -rich Breitenbush Hot Springs waters ($P_{CO_2}\sim$ 0.01 bar) is about 70°C hotter than those estimated for the other Na-Cl and Na-Ca-Cl springs ($P_{CO_2}\sim$ 0.001 bar at the anhydrite saturation temperatures). The low P_{CO_2} may be related to the elevated calcium concentrations, which force precipitation of calcite as well as anhydrite and may ultimately remove virtually all of the dissolved carbon. The K-Mg geothermometer of Giggenbach (1986) resets quickly to lower temperatures. The relatively low K-Mg and silica geothermometer temperatures for thermal waters in the study area may represent temperatures in an outflow structure (Mariner and others, 1993).

RESIDENCE TIMES

As noted above, there does not appear to be any absolute way to estimate residence times for the Western Cascade thermal waters. The precipitation of calcite that accompanies the evolution of Na-Ca-Cl waters precludes carbon-14 dating, as does the probable presence of magmatic sources of CO_2. The high chloride content of the Western Cascade thermal waters would complicate chlorine-36 dating. However, residence times can be constrained indirectly on the basis of other geochemical indicators.

Our interpretation of stable-isotope data in terms of Holocene recharge suggests maximum residence times of about 10,000 years, and the kinetics of sulfate-water oxygen-isotope equilibration can be used to calculate minimum residence times for the Na-Cl and Na-Ca-Cl thermal waters. Calculated equilibration times for hot-spring waters of the study area range from 40 years (Austin Hot Springs) to 2,000 years (Foley Springs). The time required for equilibration decreases with increasing reservoir temperature and increases with increasing pH (log $t_{1/2}$= 2.54 [$10^3/T$] + b, where $t_{1/2}$ is the

half time of exchange in hours, T is absolute temperature, and b is –1.17 at pH 7 and 0.25 at pH 8: McKenzie and Truesdell, 1977).

HOT-SPRING DISCHARGE RATES

The discharge rates of hot springs in the study area were determined on the basis of downstream increases in the sodium and chloride loads of nearby streams. The central Oregon Cascade Range is an ideal environment for application of this "solute inventory" method, because the thermal waters are rich in sodium and chloride (table 5) and the streams are generally very dilute (Ingebritsen and others, 1988). Mariner and others (1990) presented solute-inventory discharge estimates for most of the hot springs in the U.S. part of the Cascade Range. Here we discuss a more detailed set of measurements from the study area, where repeated determinations allow us to compare several solute-inventory methods and to assess the reproducibility of the results.

Earlier published discharge values for hot springs in the study area (Waring, 1965; Brook and others, 1979) were based on visual estimates or direct measurements of individual orifices, and tend to be lower than the solute-inventory values reported here, perhaps because these other methods cannot account for diffuse discharge or leakage directly into streams. Most thermal springs in the Cascade Range discharge from multiple orifices near major streams, and thermal water often discharges directly into the streams.

The chloride-inventory method was first used at Wairakei, New Zealand, to measure pre-exploitation discharge (Ellis and Wilson, 1955). The discharge rate of a hot-spring group (Q_t) is calculated from the chloride concentration upstream (Cl_u) and downstream (Cl_d) of the hot springs, the chloride concentration in the thermal water (Cl_t), and the discharge rate of the stream (Q_s):

$$Q_t = \frac{Q_s(Cl_d - Cl_u)}{(Cl_t - Cl_u)}$$

The concentration of sodium can be substituted for chloride concentration to obtain an independent, though less reliable, check of the hot-spring discharge rate. Sodium concentrations in streams are roughly an order of magnitude higher than those in precipitation, indicating that water-rock reactions occurring at relatively shallow depths release significant amounts of sodium. In contrast, chloride concentrations in streams above the hot-spring groups are within or near the range of average values in precipitation at sites that surround the study area (0.15–0.68 mg/L; see the discussion of precipitation in the "Hydrologic Setting" section). Because there is a significant nonthermal source of sodium, the discharge estimates based on chloride increases are considered to be more reliable, particularly where the upstream and downstream sampling sites are widely separated.

Grab samples or integrated samples were collected both upstream and downstream from each hot-spring group, and the discharge rate of the stream was measured at the downstream sample site. The "grab" samples were collected at a single point in the stream, whereas "integrated" samples were collected across the entire width of the stream. For well-mixed streams these methods will give identical results. Many of the downstream sample sites are near permanent U.S. Geological Survey stream-gaging stations; elsewhere, stream discharge was measured by standard wading techniques (Buchanan and Somers, 1969). Most of the stream discharge values are accurate to within ±10 percent. Where possible, additional samples were collected 15 to 40 km downstream from the hot-spring groups to detect leakage of thermal or mineral waters away from obvious spring sites.

The values listed in table 5 represent our best estimates of the hot-spring discharge rates, but in some cases there is a considerable degree of uncertainty (table 7). The discharges of Terwilliger, Austin, and Kahneeta Hot Springs have been established to within ±10 percent; the values cited for Bigelow and Belknap (combined) and Breitenbush Hot Springs may be ±15 percent, and the discharge of Foley Springs is known only to within ±40 percent.

From each complete set of downstream measurements (table 7), hot-spring discharges were calculated in three ways: (1) by the sodium increase; (2) by the chloride increase; and (3) by using a two-component mixing model. In the mixing-model approach, the Na/Cl ratio of the thermal component was assumed to be that of the nearest hot spring. The Na/Cl ratio of the nonthermal component was assumed to be 5.4. This background ratio is obtained from a linear least-squares fit to the stream-chemistry data of Ingebritsen and others

TABLE 7.—*Sodium, chloride, and discharge data from hot-spring areas in Cascade Range of northern and central Oregon*

[Dashes indicate the absence of data. Values followed by "e" are approximate. Sample locations are reported by township, range, and section; locations in parentheses are unsurveyed. In general, sodium was determined by inductively coupled plasma and chloride by colorimetry or mercurimetric titration. Most stream-discharge data are from U.S. Geological Survey streamflow-gaging stations; at a few sites stream discharge was measured by standard wading techniques using the method described by Buchanan and Somers (1969). Hot-spring discharge values are based on the downstream increase in sodium and chloride concentrations and on downstream Na/Cl ratios. For additional information about most of these sites, see Ingebritsen and others (1988). <, less than]

T-R-Sec.	Longitude	Latitude	Date (mo/d/yr)	Na (mg/L)	Cl (mg/L)	Stream discharge (L/s)	Hot-spring discharge (L/s) From Na increase	From Cl increase	Based on Na/Cl ratio
Austin Hot Springs (Clackamas River)				305	390				
Upstream									
6S-7E-26 SE	122°55'00"	45°01'00"	7/—/84	—	.6	—			
	122°55'10"	45°01'00"	10/16/84	3.5	.7	9,850			
(8S-8E-07 SE)	121°53'23"	44°54'48"	8/21/85	3.4	<1	1,850			
Downstream									
5S-6E-21 NE	122°04'18"	45°07'30"	7/—/84	—	2.8	—			
			10/16/84	4.1	2.2	30,500	60	120	130
			9/28/89	4.8	2.9	18,700	80	110	110
6S-6E-22 SE	122°03'30"	45°02'00"	7/—/84	—	4.7	—			
	122°03'31"	45°01'56"	10/16/84	6.6	4.9	—			
	122°03'23"	45°01'55"	8/15/85	7.4	5.5	9,400	120	120	120
Breitenbush Hot Springs (Breitenbush River)				745	1,200				
Upstream									
(9S-7E-21 NW)	121°57'54"	44°46'48"	7/—/84	—	.4	—			
	121°58'01"	44°46'52"	10/16/84	2.7	.4	—			
	121°57'47"	44°46'48"	8/31/85	<3e	—	1,250 (North Fork)			
	121°57'47"	44°46'44"	8/31/85	<3e	—	1,500 (South Fork)			
Downstream									
9S-5E-36 NE	122°07'40"	44°45'10"	10/16/84	4.3	2.9	6,250	13	13	12
			9/27/89	6.2	4.7	3,110	15	11	10
9S-6E-29 NW	122°06'24"	44°45'54"	7/—/84	—	2.2	—			
(9S-7E-19 NE)	121°59'35"	44°46'47"	7/—/84	—	2.7	—			
(9S-7E-19 SE)	121°59'41"	44°46'43"	10/16/84	5.0	3.9	—			
			9/24/85	6.0	5.4	3,300	15	14	13
Bigelow and Belknap Hot Springs (McKenzie River)				660	1,200 (Belknap)				
Upstream									
14S-7E-31 NW	122°01'32"	44°18'42"	10/08/85	5.2	<1	2,000			
(15S-6E-01 NE)	122°01'48"	44°17'54"	7/—/84	—	.9	—			
(15S-6E-13 NW)	122°02'55"	44°16'05"	10/15/84	4.3	.7	20,500			
(15S-6E-23 SE)	122°02'59"	44°14'33"	11/17/89	4.1	.8	—			
Downstream									
16S-6E-18 NW	122°07'48"	44°10'42"	7/—/84	—	1.2	—			
			10/15/84	4.6	1.4	35,000	16	18	18
			9/26/89	4.6	1.6	28,300	17	19	20
			11/17/89	4.5	1.6	34,000	21	23	24

TABLE 7.—*Sodium, chloride, and discharge data from hot-spring areas in Cascade Range of northern and central Oregon*—Continued

T-R-Sec.	Longitude	Latitude	Date (mo/d/yr)	Na (mg/L)	Cl (mg/L)	Stream discharge (L/s)	Hot-spring discharge (L/s)		
							From Na increase	From Cl increase	Based on Na/Cl ratio
Foley Springs (Horse Creek)				555	1,350				
Upstream									
16S-6E-27 NE	122°04'03"	44°09'01"	1/19/89	4.0	1.4	—	(Below Separation Creek)		
16S-6E-35 NW	122°03'05"	44°08'29"	9/26/89	5.5	1.9	—	(Do.)		
(17S-6E-01 NW)	122°02'01"	44°07'27"	11/17/89	5.6	1.6	—	(Separation Creek)		
	122°02'09"	44°07'27"	10/15/84	3.0	.8	—	(Above Separation Creek)		
	122°02'09"	44°02'21"	11/17/89	2.6	.6	—	(Do.)		
Downstream									
16S-5E-24 SW	122°09'05"	44°09'45"	10/15/84	5.3	1.9	11,500	48	9	9
			1/19/89	4.1	1.9	18,000	36	16	17
			9/26/89	5.6	2.3	7,300	34	9	5
			11/17/89	5.4	2.4	—	—	—	—
Terwilliger Hot Spring (Rider Creek)				405	790				
Downstream									
17S-5E-20 NW	122°14'00"	44°05'00"	9/19/85	380	700	5.1	5	5	—
McKenzie River near Vida				660	1,200 (Belknap Springs)				
Upstream						.8 ± .2 (assumed)			
Downstream									
17S-3E-05 NW	122°28'10"	44°07'30"	10/15/85	3.8	1.3	98,500	—	8–74	53
			9/27/89	3.6	1.2	70,800	—	0–47	34
			11/17/89	3.7	1.5	64,300	—	16–59	48
Kahneeta Hot Springs (Warm Springs River)				400	240				
Upstream									
8S-12E-24 NE	121°14'21"	44°51'53"	9/19/85	4.6	.5				
8S-12E-24 SW	121°14'48"	44°51'35"	11/17/89	4.7	.9				
Downstream									
8S-13E-20 SE	121°12'18"	44°51'36"	9/19/85	8.1	2.6	7,850	69	69	52
8S-13E-23 SW	121°08'55"	44°51'24"	9/27/89	8.0	2.6	5,660	48	49	39
			11/17/89	7.7	2.7	6,680	50	50	54

(1988), if samples obtained downstream from known sources of thermal or mineral water are omitted. A typical hot-spring-discharge calculation is summarized in figure 13.

There are several possible reasons for the discrepancies among the various calculated discharge values (table 7). Analytical accuracy is a significant factor for relatively large streams where the downstream sodium and chloride values are relatively low. The Cl values listed in table 7 are probably accurate to ±0.15 mg/L and the Na values to ±0.1 mg/L. There is also uncertainty regarding the actual upstream Na and Cl values in a number of cases where simultaneous upstream samples are unavailable, and Na and Cl increases were calculated based on average upstream values or upstream values from other dates. There may be significant seasonal fluctuation in these background values. Incomplete mixing of thermal and nonthermal waters may be a factor in cases where grab-sample data were used. Finally, there may be some seasonal variation in the amount of thermal water entering the streams. M.L. Sorey and G.W. Moeckli (U.S. Geological Survey, written commun., 1990) observed significant seasonal variation in the discharge of hot springs south of Lassen Volcanic National Park, California, during the period 1983–88. For example, Q_t averaged 19.5 L/s at their site MC–36, but maximum wintertime Q_t values approached 25 L/s and minimum summertime values were near 14 L/s. Sorey and Moeckli attributed
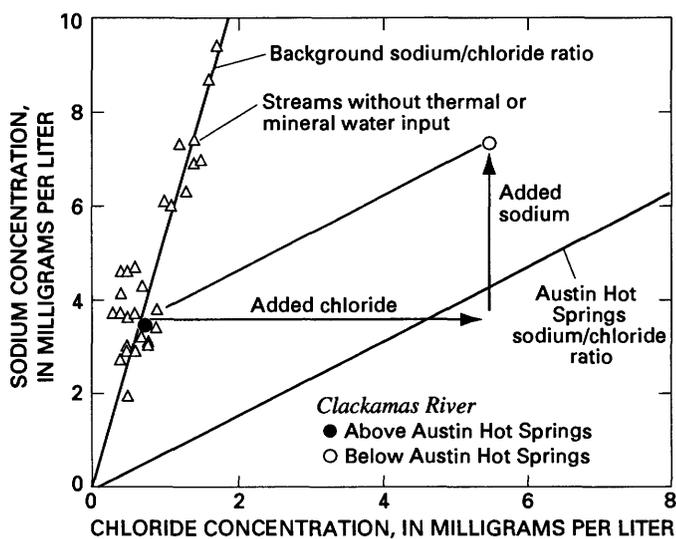
FIGURE 13.—Example showing how hot-spring discharge is calculated by solute-flux methods. Discharge of Clackamas River was 9,400 L/s; hot-spring discharge was determined to be 120 L/s by chloride-increase, sodium-increase, and mixing-model methods (table 7, Austin Hot Springs 8/15/85).

this seasonal variation to ground water-surface water interaction.

Total hot-spring discharge in the study area (220±20 L/s) amounts to less than 0.2 percent of the estimated ground-water recharge in the Quaternary arc (greater than 1×10^5 L/s, based on an estimated recharge rate greater than 26×10^{-9} m/s, listed in table 3, and about 4×10^9 m^2 of Quaternary rock exposed in the study area). No significant additional discharges of saline water were indicated by analyses of samples collected 15 to 40 km downstream from the hot-spring groups, with the exception of samples from the U.S. Geological Survey streamflow-gaging station on the McKenzie River east of Vida (table 7). At this site, located approximately 35 km downstream from Belknap Springs, the chloride flux appears to be greater than that attributable to the hot springs upstream. However, the low concentration of chloride in the Vida samples creates large uncertainties in the calculated chloride-flux values. Thermal-fluid occurrences in the McKenzie River drainage are discussed in greater detail in the section "Numerical Simulations."

HEAT TRANSPORT

The geochemical evidence summarized above indicates that the thermal waters are recharged in the Quaternary arc; therefore the hot-spring systems transfer heat from the Quaternary arc to the older rocks on the flanks of the Cascade Range. One measure of the heat transported advectively by a hot-spring system is given by the product $A = Q_t \rho c (T_g - 5)$, where Q_t is the hot-spring discharge (table 5), ρ is an appropriate fluid density, c is heat capacity of the fluid, T_g is a chemical geothermometer temperature (table 5), and 5°C is a reference temperature appropriate to the hot-spring recharge elevations inferred from the stable-isotope data. In this calculation it is appropriate to use T_g rather than the discharge temperature (table 5, T_d) because the hot-spring waters cool conductively from T_g to T_d, without gaining volume by mixing with nonthermal waters. The good agreement between SO_4-H_2O and anhydrite-saturation temperatures, low tritium levels in the hot-spring waters (Mariner and others, 1993), and a strong correlation between discharge rate and discharge temperature (table 5) rule out substantial near-surface mixing. The major sources of uncertainty in the heat-transport calculation are Q_t and T_g. The uncertainty in Q_t has been estimated from replicate measurements (table 5), and T_g may be ±10°C.

Hot-spring heat discharge is concentrated in the northern part of the study area (fig. 11). The Austin system (about 88 MW) accounts for more than half of the hot-spring heat transport in the study area. With the possible exception of hot springs that have developed on Mount St. Helens since the 1980 eruption (F.E. Goff, Los Alamos National Laboratory, written commun., 1989), Austin Hot Springs is the largest hot spring in the Cascade Range (Mariner and others, 1990). The Kahneeta Hot Springs system (about 27 MW) and the hot-spring system(s) in the McKenzie River drainage (about 24 MW) appear to transport roughly equal amounts of heat; there is considerable uncertainty in both of these heat-transport estimates due to the uncertainty in the thermal-fluid discharge values (table 7). The total heat transported by hot-spring systems in the McKenzie drainage, about 24 MW, was estimated to be 1.25 times the value obtained from individual spring groups (table 5), on the basis of diffuse input of thermal water into the surface drainage. The Breitenbush Hot Springs system (about 9 MW) transports an order of magnitude less heat than the Austin system, and the amount of heat transported by the Bagby Hot Springs system is negligible.

Considering the probable uncertainty, the total advective heat transport by hot-spring systems in the study area is in the range of 125–170 MW. The anhydrite-saturation temperatures listed in table 5 give a value of 148 MW (fig. 11); substituting SO_4-H_2O isotope temperatures (Mariner and others, 1993) gives a similar value of 147 MW. These values are large enough to represent a significant component of the regional heat budget, as discussed below in the "Heat Budget" section. For the actual heat-budget analysis, we calculate hot-spring heat discharge based on discharge temperatures (table 5, T_d) rather than geothermometer temperatures (T_g), assuming that the heat loss represented by the difference between T_g and T_d appears as conductive heat flow.

Advective heat transport by the hot-spring systems (about 148 MW) can be compared with the heat released by magmatic extrusion. The Quaternary magmatic extrusion rate of 3–6 km^3/km arc length/m.y. (Sherrod, 1986) represents an average heat release of 60 to 120 MW in the study area, assuming a basaltic magma with typical properties (initial temperature 1,200°C, latent heat of crystallization 420 J/g, specific heat 1.25 J/g/°C, and density 2.65 g/cm^3; these values for a basaltic melt are taken from Jaeger, 1964, and Harris and others, 1970). A more pertinent comparison would be with the heat provided by magmatic intrusion, but intrusion rates and subsolidus temperatures are unknown and can be inferred only within broad limits. In the "Heat Budget" section we derive a range of intrusion rates (9–33 km^3/km arc length/m.y.) that is consistent with a heat-budget analysis. There we invoke magmatic intrusion to explain a thermal input of 160 MW to the Quaternary arc.

CONDUCTIVE HEAT FLOW

Active ground-water flow can cause substantial variation in conductive heat flow with depth. Conductive heat flow generally increases with depth in ground-water recharge areas, where near-surface temperature gradients are depressed, and decreases with depth in ground-water discharge areas. It may increase, decrease, and even change sign with depth in areas with substantial lateral movement of ground water. This complicates the interpretation of near-surface conductive heat-flow data. (For a discussion of the thermal effects of regional ground-water flow see L. Smith and Chapman, 1983.)

Conductive heat-flow data indicate that the Quaternary arc and adjacent 2- to 7-Ma volcanic rocks constitute a large area of low-to-zero near-surface conductive heat flow resulting from downward and lateral flow of cold ground water. In contrast, near-surface conductive heat flow is high (100 mW/m^2 and greater) in rocks older than about 7 Ma exposed at lower elevations in parts of the Western Cascades. A similar pattern of low-to-zero conductive heat flow in permeable volcanic highlands and relatively high heat flow in older, less permeable rocks at lower elevations was observed by Mase and others (1982) in the Cascade Range of northern California. Mase and others (1982) concluded that the surficial (less than about 300 m depth) thermal regime of the California Cascades is dominated by advective heat transfer, and that the conductive heat flow from transition zones bounding the Cascade Range is masked by hydrothermal circulation.

The conductive heat-flow data set for the study area is presented in the appendix. We have augmented the extensive published data set (Blackwell and others, 1982a; Black and others, 1983; Steele and others, 1982; Blackwell and Baker, 1988b; Brown and others, 1980a) by logging open holes and by analyzing data collected by the State of Oregon and private companies that were previously unpublished or published only as temperature-depth profiles. Previously published heat-flow

interpretations are included in the appendix for the sake of comparison. All but four of the non-isothermal temperature-depth profiles described in the appendix were illustrated in Ingebritsen and others (1988, figs. 1–210); the exceptions are shown in figure 14. Table 8 shows the thermal-conductivity data used to estimate thermal conductivity where measurements from core or cuttings are lacking.

CONDUCTIVE HEAT-FLOW MAP

Conductive heat-flow data from the study area are plotted on plate 2. The heat-flow contours indicate estimated conductive heat flow at the depths of conventional heat-flow measurements (100–200 m). Thus in some instances (sites 39, 40, 61, 80, 87) changes in gradient found at depths greater than about 200 m were ignored (fig. 15). For example, site 87 was assigned a high heat flow on the basis of the high temperature gradient to about 205 m depth (appendix). The hydrologically controlled gradient disturbances observed in most of the deeper holes indicate that the actual crustal heat flow may be much different from the pattern defined by the shallow (less than about 200 m) measurements.

The data in the appendix were used to estimate values of a heat-flow surface at the nodal points of a 5-km by 5-km grid. Heat-flow values at each nodal point were estimated by calculating a constrained inverse-distance-squared weighted average of the nearest data points in each of four quad-

rants. Heat flow was contoured from the gridded values. In generating the grid, data from drill holes identified as nearly isothermal or advectively disturbed were omitted, as were data from a number of shallow (generally less than 50 m deep) holes that indicated very low heat flow (less than 25 mW/m^2 west of the Cascade Range crest or less than 40 mW/m^2 east of the Cascade Range crest). Heat-flow sites 41 and 102 (appendix) were also omitted.

The contours shown here are slightly revised from those of Ingebritsen and others (1991), on the basis of new information obtained in 1991–92. Heat-flow estimates from sites 13 and 85 were revised on the basis of new thermal-conductivity data and sites 38a and 79a were added.

Figure 16 allows comparison of our conductive heat-flow contours with those of Blackwell and others (1990a). The contours shown east of the Cascade Range crest are based on a limited amount of low-quality data (appendix), and both sets are highly speculative. West of the Cascade Range crest, where more data are available, our contours are generally similar to those of Blackwell and others (1990a). There are two significant differences: (1) we identify a heat-flow "trough" in the western part of the Western Cascades and (2) we close the 100 mW/m^2 contour against the Quaternary arc between hot-spring groups in the Western Cascades (between Austin and Breitenbush hot springs and between Breitenbush Hot Springs and the McKenzie River group). The heat-flow trough is suggested by data acquired by Ingebritsen and

FIGURE 14.—Temperature-depth profiles from heat-flow sites 13, 38a, 79a, and 85. See appendix for additional information about these sites.
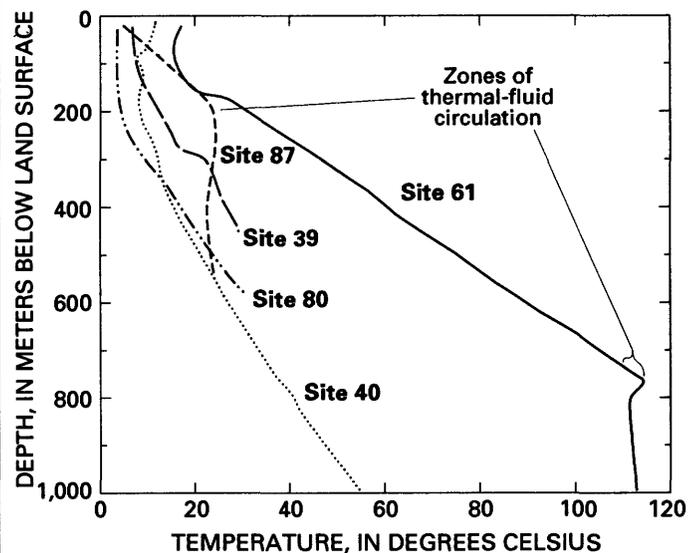
FIGURE 15.—Temperature-depth profiles from relatively deep drill holes (greater than 460 m depth) in study area. See appendix for additional information about these sites.

TABLE 8.—*Thermal conductivity measurements from Cascade Range and adjacent areas*

[Lithology and names are from the referenced publications. Summary statistics at the end of the table were used to estimate thermal conductivity from lithology at heat-flow sites (appendix) where measurements from core or cuttings were not available. Data from volcanic rocks in northern California and from depths greater than 1,000 m were omitted in calculating the summary statistics, but are listed for purposes of comparison. Location is by township, range, and section in Oregon; only generalized locations are given for sites in Washington (WA) and California (CA). >, greater than; <, less than; —, no data; nr, value not reported]

Location	Name	Depth interval (m)	Age (Ma)	Lithology	Number of measurements	Thermal condition (W/m·K)	Reference
				Basalt			
Rattlesnake, WA	RS-1	0	>7	basalt	6	1.71	Sass and Munroe, 1974
Rattlesnake, WA	RS-2	44-124	>7	basalt	14	1.71	Do.
Richland, WA	DH-3	175-1,041	>7	basalt	31	1.59	Do.
Richland, WA	DH-1	53-183	>7	basalt	19	1.71	Do.
2S-8E-15	OMF-7A	930-1250	>7	Columbia River Basalt Group	nr	1.83	Blackwell and others, 1982b
2S-8E-15	OMF-7A	1,375-1,415	>7	basalt	nr	2.04	Do.
7S-5E-22	CR-BHS	20-90	>7	basalt and claystone	7	1.46	Blackwell and others, 1982a
7S-7E-04	EWEB-TS	165-190	<7	basalt	10	1.62	Do.
7S-8E-05	EWEB-PC	70-185	<2	basalt	10	1.58	Do.
7S-8E-10	EWEB-CC	110-137	<2	basalt	10	1.45	Do.
14S-6E-32	WOLF MDW	42-155	>7	altered basalt and breccia	9	1.46	Do.
19S-5E-27	BRCK-CRK	135-154	>7	olivine basalt flow	nr	1.75	Black and others, 1983
19S-6E-25	N FORK	30-154	<7	olivine basalt	nr	1.35	Do.
Mt. Shasta area, CA	MP-32	150-274	—	basalt	nr	1.98	Mase and others, 1982
Mt. Shasta area, CA	MP-36	—	—	basalt	nr	1.82	Do.
				Andesite			
2S-8E-15	OMF-7A	410-650	>7	andesite	nr	1.65	Blackwell and others, 1982b
16S-6E-02	RDH-CRFP	100-150	>7	andesite	11	1.74	Blackwell and others, 1982a
17S-5E-20	RIDR-CRK	60-154	>7	andesite	nr	1.64	Black and others, 1983
17S-6E-25	RDH-MQCK	131-151	>7	basaltic andesite	5	1.55	Blackwell and others, 1982a
18S-5E-11	RDH-RBCK	55-78	>7	basaltic andesite	nr	1.55	Black and others, 1983
Lassen area, CA	LSND	0-105	—	andesite	9	1.88	Mase and others, 1982
Lassen area, CA	LSNE	46-168	—	andesite	15	2.00	Do.
Lassen area, CA	LSNF	30-224	—	andesite	19	2.51	Do.
Lassen area, CA	LSNG	0-165	—	andesite	12	1.64	Mase and others, 1982
Lassen area, CA	LSNG	165-172	—	andesite	1	1.64	Do.
Lassen area, CA	LSNH	0-185	—	andesite	17	1.81	Do.
Lassen area, CA	LSNI	0-186	—	andesite	15	2.15	Do.
Lassen area, CA	LSNL	0-93	—	andesite	8	2.36	Do.
				Dacite			
19S-4E-29	CHRS-CRK	70-154	>7	silicified plug	nr	1.75	Black and others, 1983
21S-13E-31	NEWBERRY 2	554-631	<2	dacite[a]	15	1.6[b]	R.J. Munroe, wrtn. comm., 1986
Lassen area, CA	LSNB	0-165	—	—	15	2.3	Mase and others, 1982
Lassen area, CA	LSNC	91-256	—	—	23	2.3	Do.
				Rhyolite			
21S-11E-25	BFZ-MB	28-35	<2	obsidian and rhyolite	2	1.51	Blackwell and others, 1982a
21S-13E-31	NEWBERRY 2	503-548	<2	rhyodacite[a]	8	1.9	R.J. Munroe, wrtn. comm., 1986
21S-17E-01	BFZ-BR	40-90	<7	rhyolite and rhyodacite	4	1.00	Blackwell and others, 1982a

TABLE 8.—*Thermal conductivity measurements from Cascade Range and adjacent areas*—Continued

Location	Name	Depth interval (m)	Age (Ma)	Lithology	Number of measurements	Thermal condition (W/m·K)	Reference
Tuff							
Indian Heaven, WA	DGER-2	102	>7	tuff, ash flow	2	1.44[b]	Schuster and others, 1978
9S-6E-23	RDH-BHSW	30–105	>7	crystal lithic tuff	7	1.61	Blackwell and others, 1982a
9S-7E-28	SUN NO.58	369–753	>7	welded to cemented tuff	nr	1.71[b]	Priest, 1987
9S-7E-28	SUN NO.58	936–1,366	>7	tuff	nr	2.10[b]	Do.
9S-7E-28	SUN NO.58	1,457–2,216	>7	welded to cemented tuff	nr	2.69[b]	Do.
16S-5E-30	ST DAM 2	25–61	>7	tuff	nr	1.32	Black and others, 1983
20S-4E-27	WALL-CRK	30–135	>7	tuff	nr	1.13	Do.
21S-13E-31	NEWBERRY 2	373–460	<2	rhy. pumice lapilli tuff and lithic breccia[a]	19	1.0[b]	R.J. Munroe, wrtn. comm., 1986
<7-Ma volcanic rocks, undifferentiated							
2S-8E-15	OMF-7A	90–335	<7	basalt and andesite	nr	1.60	Blackwell and others, 1982b
3S-8.5E-25	CR-SB	0–82	<7	volcanics	6	1.67	Steele and others, 1982
3S-9E-16	WHT RIVR	100–303	<7	debris	4	2.51	Do.
8S-8E-06	EWEB-SB	150–460	<7	basalt and andesite	20	1.49	Blackwell and others, 1982a
8S-8E-31	RHD-CBCK	70–98	<7	basalt and andesite	3	1.47	Do.
11S-7E-10	RDH-MTCK	30–109	<7	bs., andesite, and mudflows	nr	1.64	Black and others, 1983
12S-7E-09	EWEB-TM	300–600	<7	volcanics	20	1.36	Blackwell and others, 1982a
13S-7E-32	EWEB-CL	0–555	<7	andesite and volcanics	19	1.40	Do.
>7-Ma volcanic rocks, undifferentiated							
2S-8E-15	OMF-7A	725–850	>7	Columbia R. Basalt Group and andesite	nr	1.60	Blackwell and others, 1982b
2S-8E-15	OMF-7A	1,675–1,730	>7	volcaniclastic	nr	2.22	Do.
2S-8E-15	OMF-7A	1,745–1,790	>7	greenstone (Eocene)	nr	2.68	Do.
6S-7E-21	RDH-AHSE	10–40	>7	basalt, tuff, and andesite	4	1.47	Blackwell and others, 1982a
6S-7E-30	RDHCRAHS	90–135	>7	basalt, tuff and rhyolite	9	1.65	Do.
8S-5E-31	CDR CRK	35–345	>7	volcanics	4	1.80	Do.
10S-7E-11	RDH-DVCK	70–150	>7	volcanics	10	1.40	Do.
16S-4E-14	BH-3Z	12–45	>7	volcanics	3	1.80	Do.
16S-5E-30	DDH-15	15–85	>7	tuff and basalt	4	1.33	Do.
16S-6E-27	RDH-CRHC	30–150	>7	basalt and tuff	12	1.57	Do.
22S-5E-26	RDH-MHSW	30–150	>7	basalt and andesite	13	1.97	Do.
23S-5E-08	PNTO-CRK	40–154	>7	andesite and tuff	nr	1.52	Black and others, 1983
>2-Ma sedimentary rocks							
Indian Heaven, WA	DGER 2	109–126	>7	lahars	3	1.42[b]	Schuster and others, 1978
Indian Heaven, WA	DGER 2	138–152	>7	sandstone	3	1.41[b]	Do.
Indian Heaven, WA	DGER 3	104	>7	siltstone	1	1.1[b]	Do.
Indian Heaven, WA	DGER 3	110–130	>7	lahars	3	1.30[b]	Do.
Indian Heaven, WA	DGER 4	84–151	>7	siltst., mudst., and sandst.	6	1.18[b]	Do.
Indian Heaven, WA	DGER 5	106–116	>7	conglomerate	2	1.09[b]	Do.
Indian Heaven, WA	DGER 5	126–153	>7	lahar	4	1.32[b]	Do.

TABLE 8.—*Thermal conductivity measurements from Cascade Range and adjacent areas—Continued*

Location	Name	Depth interval (m)	Age (Ma)	Lithology	Number of measurements	Thermal condition (W/m·K)	Reference
				>2-Ma sedimentary rocks—Continued			
9S-3E-11	EV2-WW	48–85	>7	clay	1	1.34	Blackwell and others, 1982a
9S-3E-11	EV1-WW	25–60	>7	clay and sandstone	2	1.34	Do.
9S-7E-28	SUN NO. 58	305–314	<7	tuffaceous sediments	nr	1.50	Priest, 1987
11S-1W-14	BL-WW	30–125	>7	claystone	1	1.17	Blackwell and others, 1982a
11S-1E-07	RL-WW	40–58	>7	claystone	1	1.34	Blackwell and others, 1982a
11S-13E-24	SCHNDR-1	70–260	>7	pumiceous sandst. (Dalles Fm.)	1	1.44	Do.
12S-1W-04	B-9	30–65	>7	volcanic conglomerate	nr	1.34	Black and others, 1983
13S-1W-10	BJ-WW	28–62	>7	claystone and sediments	1	1.34	Blackwell and others, 1982a
22S-3E-10	PCCPG-WW	20–90	>7	clay, sands, and conglomerate	1	1.33	Do.
				<2-Ma sediments and sedimentary rocks			
19S-6E-08	RDHELKCK	40–140	<2	alluvial sand and gravel	nr	1.22	Black and others, 1983
21S-13E-31	NEWBERRY 2	313–319	<2	basaltic siltstone and mudst.[a]	3	.87[b]	R.J. Munroe, wrtn. comm., 1986
21S-13E-31	NEWBERRY 2	326–360	<2	pumiceous sand and gravel[a]	8	.80[b]	Do.
Klamath Falls area	LS	59–179	<2	lacustrine silty clay	19	.76	Sass and Sammel, 1976
Klamath Falls area	OC-1	53–176	<2	lacustrine silty clay	10	.77	Do.
				Granitic rocks			
Northern CA	CVN	60–235	—	granodiorite	13	2.77	Mase and others, 1982
Northern CA	GRP	91–189	—	quartz monzonite	21	2.74	Do.
Northern CA	IGO	76–145	—	granodiorite	11	2.79	Do.
Northern CA	IGO	145–229	—	granodiorite	16	3.06	Do.
Lassen area, CA	LSNM	0–122	—	quartz diorite	10	2.43	Do.
Lassen area, CA	LSNM	122–182	—	quartz diorite	5	2.43	Do.
Lassen area, CA	LSNO	76–187	—	granodiorite	10	2.97	Do.
Northern CA	RVN	160–229	—	granodiorite	10	2.41	Do.
Mt. Shasta area, CA	SHAS	64–216	—	quartz diorite	13	2.52	Do.
Northern CA	WC1	283–310	—	granodiorite	3	3.05	Do.

SUMMARY STATISTICS

Lithology	Number of sites	Thermal conductivity Mean (standard deviation)	Assigned value (standard deviation)	Corresponding map units (from table 1)
<7-Ma volcanic rocks	17	1.54 (0.33)	1.55 (0.35)	Qb(1–5), Qa(1–5), Qd(1–5), Qr(1–5), Tb(1), Ta(1), Td(1), Tr(1)
>7-Ma lava flows[c] (basalts and andesites)	14	1.65 (0.13)	1.65 (0.15)	Tb(2–5), Ta(5), Ta(2) unpatterned, Td(2–5), Tr(2–5)
>7-Ma tuffs and lahars	8	1.41 (0.17)	1.40 (0.20)	Ta(2) diamicton
>7-Ma rocks, undifferentiated	43	1.49 (0.21)	1.50 (0.25)	Ta(3–4)
>2 Ma sedimentary rocks	16	1.31 (0.11)	1.30 (0.15)	Ts(1–5)
Granitic rocks	10	2.72 (0.24)	2.70 (0.25)	some of unit Ti

[a]Lithology from MacLeod and Sammel (1982).
[b]Harmonic mean of individual measurements reported from specified depth interval.
[c]Following Blackwell and others (1982a), we have assigned a thermal conductivity value of approximately 1.60 to rocks of the Columbia River Basalt Group (map units Tcu and Tcl) in the appendix.

others (1988). Closing the 100-mW/m² contour is consistent with the limited data available in the area between hot-spring groups (pl. 2).

Blackwell and others (1982a, 1990a) and Blackwell and Steele (1983, 1985) explained the near-surface heat-flow data in terms of an extensive midcrustal heat source underlying both the Quaternary arc and adjacent older rocks. The edge of such a heat source would be below the inflection point in surficial heat flow, or approximately below the 80-mW/m² contour of Blackwell and others (1990a) (fig. 16B). The data also can be explained in terms of a narrower, spatially variable deep heat-flow anomaly that expands laterally at relatively shallow depths because of ground-water flow. This "lateral-flow" model attributes much of the

high heat flow observed in the older rocks to hydrothermal circulation, and thus predicts systematically lower heat-flow values between the two hot-spring groups. These alternative models are discussed more fully in the section "Conceptual Models."

AREA OF LOW-TO-ZERO NEAR-SURFACE HEAT FLOW

Available drill-hole data are insufficient to define the area of low-to-zero near-surface conductive heat flow directly. We have assumed that this area includes most of the area where 0- to 2-Ma rocks are exposed and those areas with 2- to 7-Ma rocks where temperature profiles indicate nearly isothermal conditions (pl. 2). Within the broad area of

EXPLANATION

QUATERNARY (0–2 Ma) DACITIC OR RHYOLITIC ROCKS

QUATERNARY (0–2 Ma) VOLCANIC ROCKS

AREA OF NEAR-ZERO NEAR-SURFACE HEAT FLOW

—80 — — LINE OF EQUAL HEAT FLOW (FIG. 16A)—Dashed where approximately located. Interval 20 milliwatts per square meter. Ticks on contours point toward areas of lower heat flow

····80···· LINE OF EQUAL HEAT FLOW (FIG. 16B)—From Blackwell and others (1990a). Interval 20 milliwatts per square meter

x   SITE OF HEAT-FLOW MEASUREMENT—Five sites with index number (see Appendix for additional information)

△   QUATERNARY VOLCANO

●   HOT SPRING

○   NONTHERMAL MINERAL SPRING

0   50 MILES
0   50 KILOMETERS

FIGURE 16.—Conductive heat-flow contours from (A) plate 2 of this report and (B) Blackwell and others (1990a).

low-to-zero near-surface heat flow, there may be local near-surface heat-flow highs due to lower permeability, favorable topographic configuration, and (or) hydrothermal circulation. Site 87 (fig. 15, appendix) is an example of such a local hydrothermal disturbance.

Our heat-flow map implies a stepwise transition in passing from low-to-zero to moderate-to-high near-surface conductive heat flow (pl. 2). Such a sharp boundary is physically unrealistic, but the available data do not define the actual geometry of the transition. The numerical experiments described in the section "Numerical Simulations" illustrate a number of physically reasonable transitions. Simulated transitions from near-zero values to relatively high values generally occur over distances of a few kilometers. Several hypothetical relations between fluid circulation patterns and near-surface heat flow were shown by Blackwell and others (1982a, fig. 10).

The thickness of the zone of low-to-zero conductive heat flow is poorly known and presumably highly variable. It may generally range from 150 to 1,000 m in thickness. In the study area, only two drill holes collared in Quaternary rocks are deep enough to measure conductive heat flow beneath the nearly isothermal zone (appendix, sites 40 and 80). The temperature log from heat-flow site 40 is nearly isothermal to depths in excess of 200 m and shows a linear conductive gradient below 650 m depth; the temperature log from site 80 is nearly isothermal to depths greater than 150 m and shows a linear conductive gradient below 240 m depth (fig. 15). Sites 40 and 80 are both in topographically low areas, and the nearly isothermal zone may be substantially thicker beneath topographic highs. Swanberg and others (1988) described two core holes on the flanks of Newberry volcano that are isothermal at mean annual air temperature to depths of 900–1,000 m (see pl. 2 for the location of Newberry volcano). The deepest water wells in the 2- to 7-Ma rocks of the High Lava Plains penetrate to about 250 m depth (appendix) and are nearly isothermal.

AREAS OF HIGH CONDUCTIVE HEAT FLOW

The heat-flow highs in the older rocks of the Austin and Breitenbush Hot Springs areas and in the McKenzie River drainage (pl. 2) are relatively well documented. The heat-flow high shown northwest of Kahneeta Hot Springs (pl. 2) is poorly documented and is considered speculative. The

density of conductive heat-flow data is greatest in the Breitenbush area, where temperature profiles (fig. 17) suggest that the high conductive heat flow measured in rocks older than 7 Ma is a relatively shallow phenomenon. Seventeen shallow drill holes (less than 500 m deep) had high gradients that generally correspond to heat flow greater than 110 mW/m^2. However, a similar gradient in the upper part of the deepest hole (appendix, site 61) changed abruptly below a zone of thermal fluid circulation at about 800 m depth. That such a change was observed in the deepest hole suggests that the gradients in the shallow holes are also controlled by ground-water flow.

HEAT BUDGET

The role of advective heat transfer in mountainous terrain is widely recognized, and the process has been illustrated in numerical modeling studies (for example, L. Smith and Chapman, 1983; Forster, 1987). The data set from this study area offers an opportunity to document the role of advective heat transfer in a specific system. We use a heat-budget approach to compare the heat deficit in rocks younger than about 7 Ma with the anomalous heat discharge in adjacent older rocks; we then estimate the magmatic heat input required
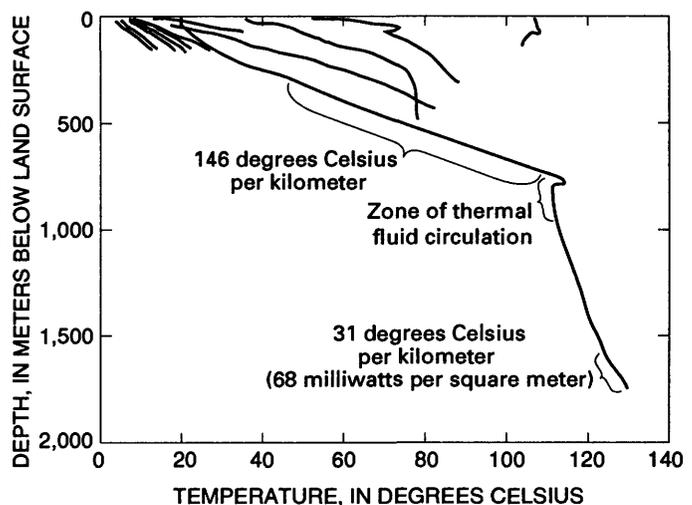
FIGURE 17.—Temperature-depth profiles from drill holes collared in rocks older than 7 Ma in Breitenbush Hot Springs area (Black and others, 1983; Blackwell and Baker, 1988b; Ingebritsen and others, 1988). Deepest hole (appendix, site 61) was completed to 2,457 m but was only logged to 1,715 m. Bottom-hole (2,457 m) temperature was at least 141°C (Priest, 1985). The gradient measured over the 1,465–1,715-m interval (31°C/km) projects to a bottom-hole temperature of 152°C.

to account for the total heat-flow anomaly. This analysis (table 9) is specific to the section of the volcanic arc between 44° and 45°15' N. The budget area is bounded on the west by the 60-mW/m^2 heat-flow contour and on the east by the Deschutes River (pl. 2); we assume that advective heat transport across these boundaries is negligible. The budget values (table 9) differ somewhat from those presented by Ingebritsen and others (1989) because the hot-spring discharge estimates (tables 5 and 7) and conductive heat-flow map (pl. 2) upon which they are based have been updated with new data.

The conductive components of the heat budget (table 9) are defined relative to assumed background heat-flow values and are obtained by measuring areas on plate 2 with a planimeter. In general, heat flow in a given area is taken as the average of adjacent contours (for example, 70 mW/m^2 between the 60-mW/m^2 and 80-mW/m^2 contours). We assign values of 140 mW/m^2 within the 120-mW/m^2 contours and 60 mW/m^2 outside the 80-mW/m^2 contours east of the Quaternary arc.

Important assumptions in the heat budget are as follows:

1. The background conductive heat flow beneath the nearly isothermal zone in the Quaternary arc is 100 mW/m^2. This value is typical for areas of Quaternary volcanism (for example, Hasabe and others, 1970) and is consistent with the data from two drill holes in the study area that are deep enough to penetrate the nearly isothermal zone (appendix, sites 40 and 80).

2. The background conductive heat flow in Tertiary terrane is 60 mW/m^2. Values greater than 60 mW/m^2 are the result of hydrologic sources.

3. The heat discharged by hot springs represents the anomalous advective heat discharge from rocks older than 7 Ma. This is a minimum value because it does not include lower-temperature advective discharge or allow for the possibility of yet-unidentified thermal fluids.

Assumptions 2 and 3 require some additional explanation. The global mean continental heat flow is about 60 mW/m^2 (Jessop and others, 1976). The mean heat flow for Tertiary tectonic provinces is higher than 60 mW/m^2, with a large scatter. The background heat flow for a given setting is determined by the competing effects of sinks (subducting slabs in this case) and sources (for example, radioactivity). One could as easily assume a background value of 50 or 70 mW/m^2 in Tertiary terrane (J.H. Sass, U.S. Geological Survey, written commun., 1988). Thus (as beneath the Quaternary arc) the appropriate background heat flow is subject to con-

siderable uncertainty. However, the results obtained in this study are not particularly sensitive to the exact value assumed. For example, a background value of 50 mW/m^2 in Tertiary terranes west of the Quaternary arc would increase the conductive anomaly from 127 (table 9) to 165 MW, which would not affect the results.

The values for hot-spring heat output used in the budget (assumption 3) are based on hot-spring discharge rates (table 5) and on discharge temperatures (T_d), rather than the geothermometer temperatures (T_g) used for figure 11. Two lines of evidence suggest that the difference between T_g and T_d is due to conductive cooling. First, there is a strong positive correlation between hot-spring discharge rates and discharge temperatures (table 5). This is an expected consequence of conductive cooling of upflowing thermal waters in sub-boiling systems, but would not be expected if cooling is due to mixing with relatively cold ground water. Second, tritium data (Mariner and others, 1993) indicate that the thermal waters do not mix with shallow, relatively tritium-rich ground water. Since the difference between T_g and T_d results primarily from conductive cooling, this increment of heat presumably appears as part of the conductive anomaly. In the Western Cascades, the thermal power represented by the difference between T_g and T_d (62 MW; compare the 121-MW value in fig. 11 and the 59-MW value in table 9) is equal to about half of the conductive anomaly (127 MW).

The area of near-zero near-surface conductive heat flow in this part of the Cascade Range (pl. 2) generally coincides with the areal extent of permeable volcanic rocks younger than 7 Ma. On the basis of our assumptions regarding background heat flow, about 470 MW of heat is swept out of these younger rocks between latitudes 44° and 45°15' N. by ground-water circulation. This amount is roughly balanced by 314 MW of anomalous heat discharge from rocks older than 7 Ma (table 9). Sufficient heat is removed advectively from the rocks younger than 7 Ma to explain the anomalous heat discharge measured on the flanks of the Cascade Range.

The difference between the heat deficit in the younger rocks and the anomaly in the older rocks (~470 MW – 314 MW = ~156 MW) is an estimate of lower-temperature advective discharge, which was not determined directly. "Lower-temperature advective discharge" refers to heat discharged by springs at temperatures within a few degrees of the local mean annual air temperature. Such springs presumably occur both in the Quaternary arc and in adjacent older rocks and may not be thermally or

TABLE 9.—*Components of heat budget for Cascade Range volcanic arc between lat 44° and 45°15' N.*

[MW, megawatts thermal]

Heat deficit represented by near-zero conductive heat discharge in <7-Ma rocks:		
Quaternary arc	-400 MW	
2- to 7-Ma rocks west of Quaternary arc	-19 MW	
2- to 7-Ma rocks east of Quaternary arc	-51 MW	
Total	-470 MW	
Anomalous heat discharge in >7-Ma rocks:		
Conductive anomaly in the Western Cascades	127 MW	(62 MW from cooling of thermal waters)
Heat discharged from hot springs in the Western Cascades[a]	59 MW[b]	
Conductive anomaly in the Deschutes basin	111 MW	(10 MW from cooling of thermal waters)
Heat discharged from hot springs in the Deschutes basin....	17 MW	
Total	314 MW	

[a]In calculating the heat discharged by hot springs in the McKenzie River drainage, we assumed that the total thermal-fluid discharge is 1.25 times that of the individual hot-spring groups, due to diffuse input of thermal water into the surface drainage. This approximate value is indicated by measurements made at the U.S. Geological Survey streamflow-gaging station on the McKenzie River near Vida (table 7).

[b]Based on hot-spring discharge temperatures. The difference between the geothermometer and discharge temperatures (table 5) is due primarily to conductive heat loss and, particularly in the Western Cascades, represents a significant fraction of the conductive anomaly.

chemically distinctive enough to be readily recognized. This quantity can only be estimated as the residual in the heat budget. The partitioning between discharge in the younger and older rocks is unknown.

Results presented in the section "Numerical Simulations" show that low-temperature advective heat discharge within the Quaternary arc is highly dependent on the permeability structure, which is poorly known. If only the Quaternary rocks are permeable, low-temperature advective heat discharge in the Quaternary arc will be significant. If the deeper, older rocks are also permeable, most of the background heat flow in the Quaternary arc will be removed at deeper levels, and low-temperature advective heat discharge within the arc itself will be relatively small.

Only about one-third of the heat removed from the younger rocks can be attributed to advective heat transfer by the hot-spring systems (148 MW/ 470 MW). The remainder must be removed by yet-unidentified thermal fluids or by lower-temperature ground water. In the context of our budget assumptions, conductive heat loss from such waters must be invoked to explain the fractions of the conductive anomalies that cannot be attributed to conductive cooling of the hot-spring waters (table 9).

Because the anomalous heat discharge in the older rocks (older than about 7 Ma) can be explained by advection from the younger rocks, we need invoke magmatic heat input only to explain an increment of about 40 mW/m^2 (100 mW/m^2 - 60 mW/m^2) in the background conductive heat flow beneath the Quaternary arc (an area of about 4,000 km^2). This requires an intrusion rate of 9 to 33 km^3/km arc length/m.y., again assuming a basaltic magma with an initial temperature of 1,200°C, a latent heat of crystallization of 420 J/g, specific heat of 1.25 J/g/°C, and a density of 2.65 g/cm^3. The lower intrusion rate assumes 900°C of magmatic cooling, whereas for the higher rate heat is supplied by latent heat only, with no cooling. For intermediate amounts of cooling, inferred intrusion rates scale nonlinearly between these values. Because the magmatic extrusion rate has been 3 to 6 km^3/km arc length/m.y. during the Quaternary (Sherrod and Smith, 1990), our analysis suggests an intrusion-to-extrusion ratio in the range of 1.5 to 11.

The intrusion rates calculated here are lower than those of Blackwell and others (1990b), who proposed an intrusion rate of about 55 km^3/km arc length/m.y. for central Oregon. This is partly because Blackwell and others (1990b) invoked a lower outer-arc background heat flow, but most of the discrepancy is due to their assumption that lateral heat transfer by ground water is negligible. Blackwell and others (1990a, b) argued that the high heat-flow values observed in rocks older than 7 Ma can be extrapolated to midcrustal depths.

The assumption of a uniform heat flow of 100 mW/m^2 below the isothermal zone in the Quaternary arc is certainly an oversimplification. The spatial distribution of anomalous heat discharge in

the Western Cascades relative to Quaternary dacitic and rhyolitic volcanoes (pl. 2) suggests that lateral flow of heated ground water into the Western Cascades may originate from heat sources localized near Quaternary silicic magmatic centers, as originally suggested by R.L. Smith and H.R. Shaw in the early 1970's. The areas of silicic volcanism are presumably areas with relatively high intrusion rates, high intrusion-to-extrusion ratios, and (by inference) relatively high background heat flow (Hildreth, 1981). A larger average heat flow beneath the Quaternary arc (greater than 100 mW/m^2) would reinforce our conclusion that sufficient heat is removed advectively from the Quaternary arc to support the heat-flow anomalies on its flanks.

The magnitude of lower-temperature advective heat discharge is another, more important source of uncertainty in the heat budget. If it is much larger or smaller than the value estimated by difference (157 MW), one or more of our assumptions must be in error. Results presented in the section "Numerical Simulation" show that both the magnitude and the areal distribution of lower-temperature advective heat discharge are highly dependent on the permeability structure.

CONCEPTUAL MODELS

Two competing conceptual models of the thermal structure of the north-central Oregon Cascades, shown in figure 18, have significant implications for magmatism and geothermal resource potential in the Cascades. One model invokes a relatively narrow, spatially variable deep heat-flow anomaly that expands laterally at shallow depths because of ground-water flow (fig. 18A). This "lateral-flow model" is similar to two of the models for the Western Cascade hot springs presented by Blackwell and others (1982a, fig. 10, models 2 and 3), except that we suggest significant spatial variability in the heat source. An alternative model invokes an extensive midcrustal heat source underlying both the Quaternary arc and adjacent older rocks (fig. 18B) (Blackwell and others, 1982a; Blackwell and Steele, 1983, 1985). As noted in the section "Conductive Heat Flow," the edge of such a heat source would lie approximately beneath the 80-mW/m^2 heat-flow contour, which is as far as 30 km west of the Quaternary arc (see fig. 16). More recently, Blackwell and Steele (1987), Blackwell and Baker (1988a, b) and Blackwell and others (1990a) have suggested that the thermal effects of hydrothermal circulation are locally superimposed on the effects of this extensive midcrustal heat source, which is envisioned as a long-lived zone of magma interception, storage, and crystallization with a time-averaged temperature of about 600°C (Blackwell and others, 1990a, p. 19,514). Though the actual thermal structure is probably more complex than either of the simple models shown in figure 18, the models provide useful end-members for discussion.

IMPLICATIONS OF REGIONAL GRAVITY, MAGNETIC, AND ELECTRICAL GEOPHYSICAL DATA

Regional geophysical data afford a possible means of discriminating between the alternative models for the deep thermal structure (fig. 18). For example, midcrustal, regional-scale geothermal phemonema may be expressed in regional gravity data, and we investigated this relationship in the study area in some detail.

Blackwell and others (1982a) preferred their model 1 (represented in our fig. 18B) because of the "close correspondence of the heat flow and [Bouguer] gravity anomalies" (Blackwell and others, 1982a, p. 8749; see also their fig. 8). Their preferred model "relates the gravity and heat flow data to a (large) zone of low-density (partially molten) material in the upper part of the crust (10±2 km) beneath the High Cascade Range and extending about 10 km west of the High Cascade Range boundary" (Blackwell and others, 1982a, p. 8750).

When we plotted the relation between gravity and heat-flow values from the study area (fig. 19), for every heat-flow datum we interpolated a corresponding gravity value from a gridded representation of regional gravity. This approach allows us to examine the nature and strength of any correlation between gravity and heat flow in this area, but it is limited by the nonuniform distribution of heat-flow data.

West of the Cascade Range crest there is a weak negative correlation between Bouguer gravity and heat flow, with a "step" change in Bouguer gravity values associated with a heat flow of approximately 60 mW/m^2 (fig. 19A). However, on a regional basis there is no correlation between wavelength-filtered residual gravity and heat flow (fig. 19B) or between isostatic residual gravity and heat flow (fig. 19C). Locally, a persistent negative correlation between gravity and heat flow in the vicinity of Mount Hood (figs. 19A–C) can be at least partly explained as a relict of strong correlations between elevation and heat flow and between elevation and gravity.

The wavelength-separated residual gravity was derived by spectral separation at a wavelength of approximately 90 km. Wavelength filtering at this threshold minimizes the effects of sources at depths greater than approximately 20 km (Couch and others, 1982a), although it will also eliminate anomalies that result from long-wavelength lateral density variations at shallow depth. The isostatic residual data have been processed to remove topographically induced regional trends and to enhance gravity anomalies related to crustal geologic features. As described by Simpson and others (1986), these data are produced using an Airy-Heiskanen model for isostatic compensation, by subtracting the calculated effect of a crust-mantle interface from the Bouguer values. Any correlation between gravity and heat flow that is due to a hot, partially molten body at shallow- or midcrustal levels should persist through, or even be enhanced by, the wavelength-filtering or isostatic-residual techniques. The fact that there is no significant correlation between heat flow and these forms of residual gravity suggests that the relation between heat flow and Bouguer gravity may be due to density contrasts at greater depths.

The negative correlation between heat flow and gravity reemerges when the isostatic residual gravity is continued upward (fig. 19D). Upward
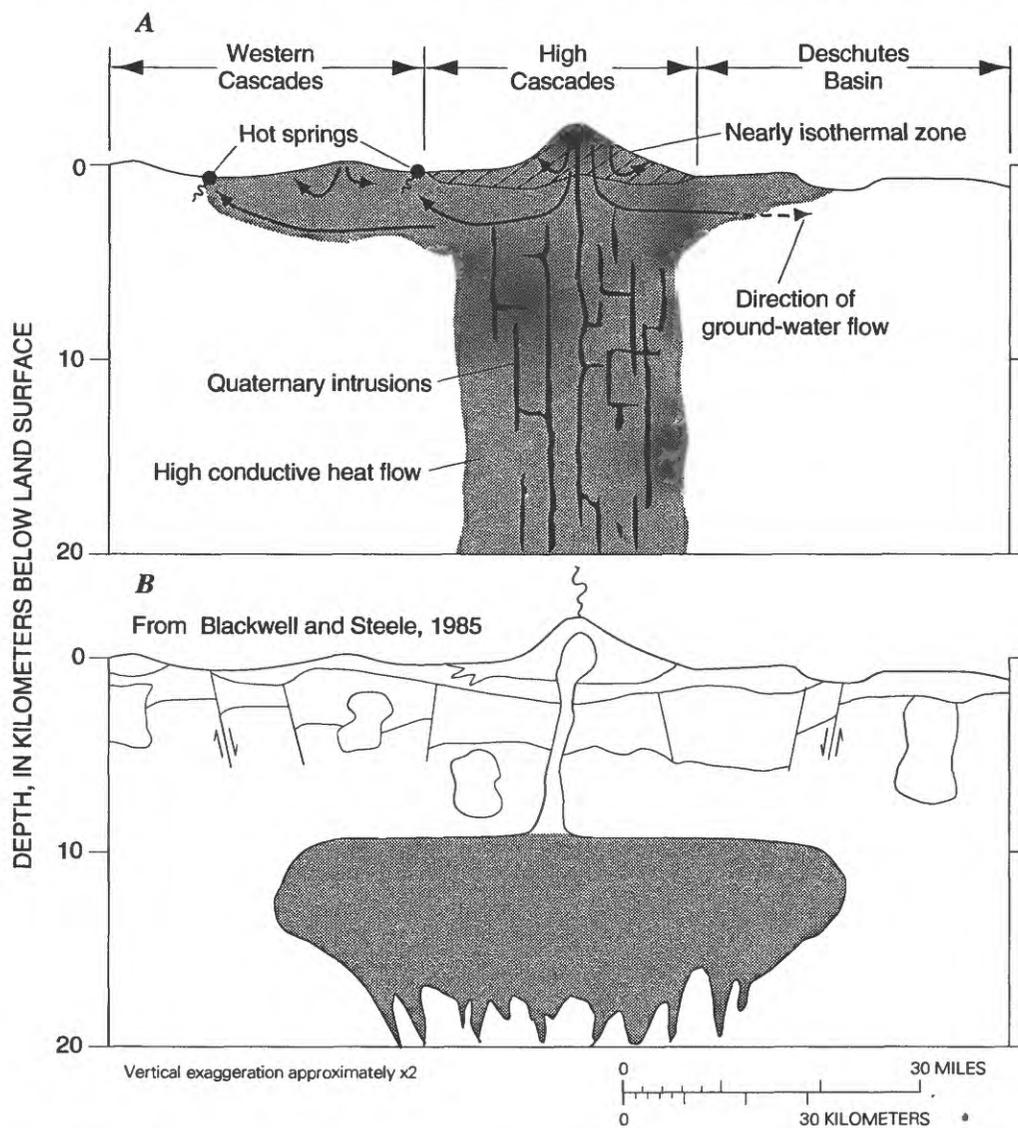
FIGURE 18.—Conceptual models of thermal structure of north-central Oregon Cascades, showing (A) magmatic heat sources beneath Quaternary arc and (B) extensive midcrustal heat source proposed in other studies (for example, Blackwell and others, 1982a, 1990a; Blackwell and Steele, 1983, 1985).
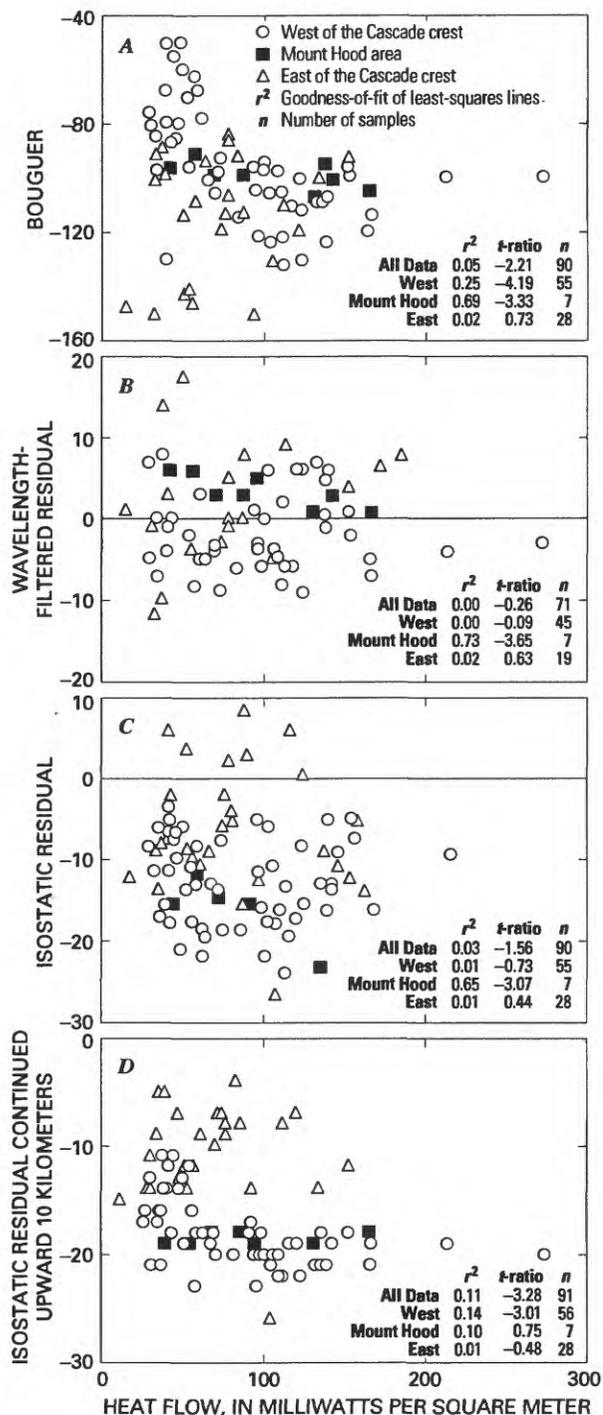
FIGURE 19.—Relation between heat-flow and gravity data. The r^2 and t-ratio values are for linear regressions of gravity on heat flow. Heat-flow data from study area are those compiled by Ingebritsen and others (1988). A, Bouguer gravity data from Godson and Scheibe (1982). B, Wavelength-filtered residual data from Couch and others (1982b). C, Isostatic residual data from Simpson and others (1986). D, Upward-continued isostatic residual data from R.J. Blakely (U.S. Geological Survey, written commun., 1988).

continuation of the isostatic residual emphasizes anomalies due to deep sources or broad shallow sources at the expense of shallower or narrower sources (Blakely and Jachens, 1990). The negative correlation between upward-continued isostatic residual gravity and heat flow is even weaker than that between Bouguer gravity and heat flow (note the change in scale between fig. 19A and D). However, the apparent relation has a similar form, with a "step" change in gravity at approximately 60 mW/m². The local negative correlation in the vicinity of Mount Hood, which persisted through the other forms of processing, is eliminated by upward continuation (fig. 19D). Blakely and Jachens (1990) applied a boundary-locating technique to upwardly continued isostatic residual gravity data from Washington, Oregon, and northern California. They identified a density boundary approximately 40 km west of the Three Sisters at lat 44° N., and noted that it approximately coincides with the heat-flow transition mapped by Blackwell and others (1982a). Blakely and Jachens (1990) also noted that the density boundary might reflect a geologic contact associated with a fault postulated by Sherrod (1986, his fig. 21), and not a thermal discontinuity.

Connard and others (1983) and Foote (1985) analyzed aeromagnetic measurements from the Cascade Range in central and northern Oregon to determine the depth extent of magnetic sources. They interpreted the basal source depth to represent the Curie-temperature isotherm, which is defined as the temperature at which rocks become essentially nonmagnetic. Connard and others (1983) noted that Curie-point temperatures in the crust may range from 300°C to 580°C.

Curie-depth estimates are susceptible to the problems of uniqueness inherent to all inverse methods (Blakely, 1988), and the basal depth of magnetic sources may not represent an isothermal surface as both the Curie temperature and other rock magnetic properties may vary from place to place. Despite these uncertainties, a high degree of spatial correlation between shallow Curie depths and high near-surface heat flow would be persuasive evidence for the extensive midcrustal heat source model (fig. 18B). An area of shallow Curie depths that is more closely confined to the Quaternary arc would be consistent with the lateral-flow model (fig. 18A).

The relation between near-surface heat flow, Curie-depth estimates, and the area of Quaternary vents can be studied by plotting them together (fig. 20). The precise locations of the Curie-depth boundaries are uncertain because the spatial

EXPLANATION

EXTENT OF QUATERNARY VOLCANIC ROCKS (0- 2 Ma)

——40—— LINE OF EQUAL HEAT FLOW—Interval 20 milliwatts per square meter, from plate 2. Dashed where approximately located

········80········ LINE OF EQUAL HEAT FLOW—In milliwatts per square meter, from figure 16B. Location approximates edge of inferred extensive midcrustal heat source of Blackwell and others [1990a]

6-9
━ ━ ━ ━ CURIE-DEPTH BOUNDARY—Dashed where approximately located. Numbers indicate inferred depth to Curie-point temperature, in kilometers below land surface

RISE IN DEEP CRUSTAL CONDUCTOR [Stanley and others, 1989]—Conductor is relatively shallow (12-20 kilometers) east of these locations but drops off steeply to west

• HOT SPRINGS

○ NONTHERMAL MINERAL SPRING

△ QUATERNARY VOLCANO

FIGURE 20.—Relation between near-surface heat flow, Curie-depth boundaries (Connard and others, 1983; Foote, 1985), and rise in Stanley and others' (1989, 1990) deep-crustal conductor. Blackwell and others' (1990a) 80-mW/m^2 contour represents inferred position of edge of Blackwell and others' (1982, 1990a) midcrustal heat source. Locations of rise in deep-crustal conductor are from Stanley and others' (1989) profiles BR2, BR1, DD', and EE' (see their figs. 1 and 5 for approximate locations).

resolution of the Curie-depth estimates is relatively poor. Connard and others (1983) resolved source depths for overlapping 77-km by 77-km or 155-km by 155-km areas, and Foote (1985) resolved source depths for 64-km by 64-km areas.

The lack of spatial resolution in the Curie-depth data makes it difficult to assess whether the Curie-depth boundaries correlate better with the areas of high near-surface heat flow or with the boundaries of the Quaternary arc. The speculative heat-flow high in the northeastern part of the study area is clearly not correlated with shallow Curie depths (fig. 20). The relative degree of correspondence on the west side of the Quaternary arc is variable: in the McKenzie River area, the Curie-depth boundary is nearly coincident with the edge of the Quaternary arc, but west of Mount Jefferson it is closer to the edge of the postulated midcrustal heat source. Connard and others (1983) and Foote (1985) invoked relatively recent intrusive activity to explain the shallow basal depths of magnetic sources beneath the High Cascades; they cited young volcanism and high heat flow as supporting evidence. Foote (1985) also interpreted the area of shallow basal source depth northwest of Austin Hot Springs (fig. 20) as being due to young intrusions. The latter interpretation is tenuous because the Austin Hot Springs area is not characterized by abundant young volcanism or by uniformly high heat flow. W.D. Stanley (U.S. Geological Survey, written commun., 1990) suggested that the shallow Curie depth northwest of Austin Hot Springs more likely results from nonmagnetic Tertiary intrusions.

Stanley and others (1989, 1990) mapped a deep-crustal electrical conductor at depths of 12 to 20 km in the Cascade Range. The upper boundary of this deep-crustal conductor rises near the Western Cascades-High Cascades boundary, where it becomes as shallow as about 6 km (see, for example, Stanley and others, 1989, their figs. 3 and 6). Stanley and others (1989, 1990) interpreted this rise in the conductor as being due to shallow magma or to rising magmatic fluids concentrated in fractures associated with graben-bounding faults. West of the rise the conductor drops off steeply, to depths greater than those mapped east of the rise. Figure 20 shows where the rise in the conductor has been mapped.

If the deep-crustal conductor has geothermal significance, as Stanley and others (1989, 1990) suggested, then a close correspondence between the shallowing of the conductor and high near-surface heat flow would support the midcrustal heat source model (fig. 18B), whereas a westward dropoff of the

conductor at the western edge of the Quaternary arc would be consistent with the lateral-flow model (fig. 18A). As with the Curie-depth interpretations, the relative degree of correspondence is variable. Four magnetotelluric profiles traverse the Cascade Range in the area shown in figure 20 (Stanley and others, 1989). Along the northernmost and southernmost profiles the westward dropoff of the conductor is relatively close to the edge of the Quaternary arc; west of Mount Jefferson it lies between the Quaternary arc and the near-surface heat-flow transition; and southwest of Mount Jefferson it more closely coincides with the heat-flow transition.

Stanley and others (1989, 1990) also evaluated seismic-refraction data from the Cascade Range. They noted that extensive magma accumulation in the midcrust is not compatible with seismic results, which show no extensive low-velocity high-attenuation regions below the Oregon Cascade Range.

The available regional gravity, magnetic, and electrical geophysical data thus fail to distinguish between the two conceptual models depicted in figure 18. The Bouguer and upward-continued isostatic residual gravity data show a weak negative correlation with heat flow. However, the gravity features responsible for these correlations can be explained in the study area without invoking thermal effects (Blakely and Jachens, 1990), and wavelength-filtered and unsmoothed isostatic residual gravity data show no correlation with heat flow. The magnetic and electrical boundaries have variable degrees of correspondence with the boundaries expected from the alternative conceptual models. The seismic-refraction data seemingly preclude extensive magma accumulations in the midcrust, but they do not rule out small pockets of magma in the region of the proposed midcrustal heat source (fig. 18B).

TESTING THE CONCEPTUAL MODELS

The heat-budget analysis in the previous section shows that a laterally extensive midcrustal heat source is not required to explain the high heat flow observed on the flanks of the Cascade Range. However, the heat-budget analysis cannot disprove the midcrustal heat-source model because of the uncertainty regarding the actual magnitude and distribution of lower-temperature advective heat discharge. Existing regional geophysical data sets also fail to clearly discriminate between the two conceptual models.

Deep drilling (3–4 km) in the areas of high heat flow in the older rocks would be the most conclu-

sive test because the lateral-flow model predicts reduced heat flow below zones of active fluid circulation, whereas the midcrustal heat source model predicts no change in heat flow with depth. The temperature profile from heat-flow site 61 (fig. 17) does show reduced heat flow below a zone of thermal-fluid circulation. However, the background heat flow beneath this thermal aquifer remains uncertain. As discussed further in the next section, the temperature profile can be interpreted in terms of either a long-lived (about 10^5 years) hydrothermal system and a relatively low (about 60–70 mW/m^2) background heat flow, or a shorter-lived (about 10^4 years) hydrothermal system superimposed on a relatively high (greater than 100 mW/m^2) background heat flow. The first interpretation is consistent with the lateral-flow model, the second with the midcrustal heat source model.

A much less expensive (and less conclusive) test of the alternative models would be to drill several shallow (150 m) heat-flow holes in the older rocks in areas where heating due to regional ground-water flow seems unlikely (Ingebritsen and others, 1993). The current heat-flow data set (appendix) is heavily biased toward hot-spring areas and other topographic lows that represent probable ground-water discharge areas.

NUMERICAL SIMULATIONS

Numerical simulation can be used to examine some of the thermal and hydrologic implications of the alternative conceptual models depicted in figure 18. We simulated ground-water flow and heat transport through two generalized geologic cross sections west of the Cascade Range crest: one in the Breitenbush area, where there is no evidence for major arc-parallel down-to-the-east faulting, and one in the McKenzie River drainage, where major graben-bounding faults exist (see fig. 3 for fault locations). The simulation results provide some constraints on the regional permeability structure and also show that either model for the deep thermal structure can satisfy the near-surface heat-flow observations.

The numerical code used for the simulations, PT (Bodvarsson, 1982), employs an integrated-finite-difference method to solve coupled equations of heat and energy transport:

$$\int_v \frac{\partial}{\partial_t} (\phi\rho) \, dV = -\int_A \rho \mathbf{v_d} \cdot \mathbf{n} \, dA + \int_v G_f \, dV$$

and

$$\int_v \frac{\partial}{\partial_t} (\rho_m e) \, dV =$$

$$-\int_A \lambda \nabla T \cdot \mathbf{n} \, dA - \int_A \rho c_f \delta T \mathbf{v_d} \cdot \mathbf{n} \, dA + \int_v G_h \, dV$$

respectively, where t is time, ϕ is effective porosity, ρ and ρ_m are density of the fluid and the medium, respectively, V is volume, $\mathbf{v_d}$ is volumetric flow rate (Darcy velocity), $\mathbf{n}$ is a unit vector normal to an interface, A is area, e is internal energy of the medium, λ is medium thermal conductivity, T is temperature and δT denotes a volume-interface temperature, c_f is the heat capacity of the fluid, and G_f and G_h are mass and heat source/sink terms, respectively. The volumetric flow rate $(\mathbf{v_d})$ is calculated using Darcy's Law. The mass and energy balance equations are coupled through pressure- and temperature-dependent parameters, as well as the source and sink terms.

The land surface defines the upper boundary of each cross section. We assumed that the water table is coincident with the land surface. This may be a poor approximation in some mountainous areas (see Forster and Smith, 1988), but in our particular cases the presence of abundant perennial streams and springs, generally shallow static water levels in wells (appendix), and high rates of ground-water recharge (table 3) combine to suggest a relatively shallow water table. Simulated land-surface temperatures (12.8°C–5.5°C per km above sea level) were derived from the observed relation between spring temperature and elevation (fig. 21).
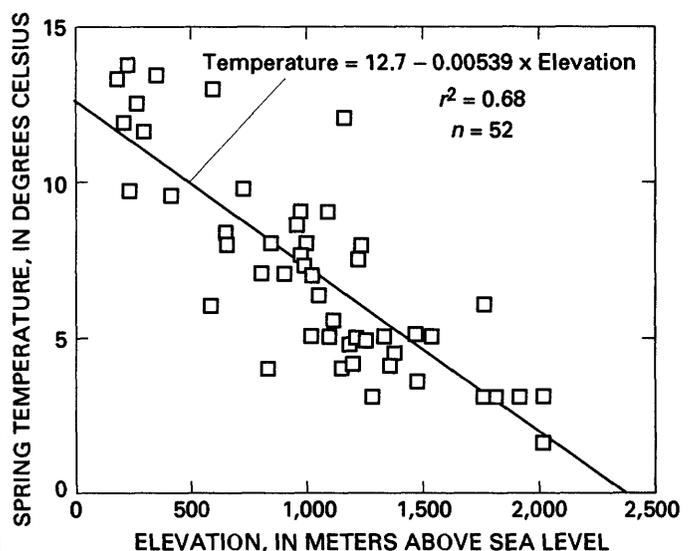
FIGURE 21.—Relation between spring temperature and elevation. Line is linear-least-squares fit to data.

For each cross section we present selected steady-state results that were obtained through long-term transient simulations. Initial conditions were a hydrostatic pressure distribution and temperature gradients of 50°C/km in the Quaternary arc and 30°C/km in the Western Cascades. The systems approached a steady state over simulation times of 10^5 years or more. At simulation times of 10^5 years, maximum rates of temperature change were typically less than 0.5°C/1,000 yr. At simulation times of 10^6 years, rates of temperature change were less than 0.02°C/1,000 yr.

The lithologic units used in the numerical simulations are somewhat different from those of Sherrod and Smith (1989; see our table 1) because the geology of the cross sections is based in part on detailed mapping by Priest and others (1987, 1988). Table 10 describes lithologic units and the values of permeability, porosity, and thermal conductivity assigned to those units. The values of porosity and thermal conductivity shown in table 10 were used for all of the simulations, but permeabilities were varied about the listed values. Porosity is assumed to be inversely correlated with the age of the rock, and thermal-conductivity values are based on the data of table 8.

PERMEABILITY STRUCTURE

Few permeability data are available for the study area, but two lines of evidence indicate that the older rocks are generally less permeable than the younger rocks. First, the ground-water recharge estimates discussed in the section "Hydrologic Setting" show an inverse correlation between recharge rates and bedrock age. Second, as discussed in the section "Conductive Heat Flow," most 100- to 200-m-deep wells in rocks younger than about 7 Ma show pervasive advective disturbance, whereas wells of that depth in older rocks have dominantly conductive temperature profiles. We can assume on this basis that the bulk permeability of the older rocks is relatively low, but the existence of hot springs and of localized advective disturbances (for example, fig. 17) in the older rocks are direct evidence for discrete zones of high permeability.

The older rocks have lost primary permeability through hydrothermal alteration. Alteration of volcanic glass to clays and zeolites severely reduces permeability, as does recrystallization of glass to higher-temperature minerals. The extent of alteration depends largely on the primary permeability, glass content, and time-temperature history of the rock. We can correlate loss of permeability with age because, in the study area, rocks of a given age are lithologically similar and share similar time-temperature histories. The abundance of ash-rich sequences such as the Breitenbush Tuff in the 17- to 25-Ma age interval is an example of lithology influencing alteration patterns on a regional scale.

Keith (1988) noted that tuffaceous volcanic rocks affected by high-temperature (greater than 200°C) alteration consist mostly of anhydrous minerals and are more easily fractured than rocks affected by lower-temperature alteration, so that secondary permeability may be relatively high. She suggested that a thermal aquifer in rocks affected by high-temperature alteration might consist of interconnected fractures at the same general stratigraphic horizon.

The simulations described herein allow us to place some limits on regional-scale permeabilities. Bulk permeabilities greater than about 10^{-17} m^2 in the oldest rocks (table 10, unit Tv_3) allow widespread advective heat transport; this is inconsistent with the heat-flow data, which suggest that significant advective transport in these rocks is only very localized. Permeabilities less than about 10^{-14} m^2 in the youngest rocks (unit QTv) lead to near-surface conductive heat-flow values that are consistently higher than observed values from these rocks. For the intermediate-age units we assumed an inverse correlation between permeability and age.

A pronounced permeability-depth relation within each unit can also be inferred from the results of our simulations. Although the range of permeability values shown in table 10 allows us to match the conductive heat-flow observations, higher near-surface permeabilities are required to match the ground-water recharge estimates. Well-test data from shallow (less than 50 m) domestic wells in the Western Cascades also indicate relatively high permeabilities, in the range of 10^{-14} to 10^{-12} m^2 (McFarland, 1982).

BREITENBUSH SECTION

The 22-km-long Breitenbush cross section extends west-northwest from the Cascade Range crest through Breitenbush Hot Springs (figs. 22 and 23). There are several dacite and rhyolite domes of 0.25 to 0.7 Ma age in the eastern part of the section (fig. 22), and the underlying silicic magmatic system is a possible heat source for the hydrothermal system (R.L. Smith and Shaw, 1975).

TABLE 10.— *Description of rock units and values of permeability, porosity, and thermal conductivity assigned in numerical simulations*

Symbol used on cross section[a]	Description	Permeability (m^2)	Porosity	Thermal conductivity (W/m•K)
QTv	Chiefly lava flows and domes younger than 2.3 Ma	1.0×10^{-14}	0.15	1.55
Tv$_1$	Lava flows and minor pyroclastic rocks from 4 to 8 Ma in age	5.0×10^{-16}	.10	1.55
Tv$_2$	Lava flows from 8 to 17 Ma in age (8–13 Ma in Breitenbush area)	1.0×10^{-16}	.05	1.65
Tv$_3$	Chiefly volcanic and volcaniclastic strata from 18 to 25 Ma in age (divided into Tv$_3$u and Tv$_3$l in Breitenbush area)	1.0×10^{-17} (Tv$_3$u: 5.0×10^{-17})	.05	2.00 (Tv$_3$u: 1.50)
Tv$_3$q	Quartz-bearing ash-flow tuff in Breitenbush area (Priest and others, 1987)	2.5×10^{-14}	.02	2.00

[a]"Q" and "T" denote rocks of Quaternary (less than 2 Ma) and Tertiary age, respectively, and "v" denotes volcanic rocks. The subscripts indicate subdivisions of the Tertiary that are roughly analogous to those of Sherrod and Smith (1989) (table 1). As noted in the text, the lithologic units used in the numerical simulations are somewhat different from those of Sherrod and Smith (1989), because our geologic cross sections are partly based on the detailed mapping of Priest and others (1987, 1988).

Temperature-depth data from the Breitenbush area define a broad area of elevated temperatures extending south of Breitenbush Hot Springs. The elevation of the 100°C isotherm (fig. 22) is estimated from the elevation of the hot springs, temperature-depth data from heat-flow site 61 (fig. 17), and projection of terrain-corrected gradients from 15 other drill holes. The drill hole at site 61 intercepted a thermal aquifer at about 800 m depth, in or near a quartz-bearing ash-flow tuff (Priest and others, 1987). The spring orifices at Breitenbush Hot Springs are in the same stratigraphic unit (Priest and others, 1987), which suggests the presence of a stratigraphically controlled thermal aquifer, as does the broad upwarp in the 100°C isotherm. We treated the quartz-bearing tuff as a 30-m-thick zone of relatively high permeability (fig. 23, unit Tv$_3$q). This unit is too thin to be shown as other than a heavy line in figure 23 and succeeding figures.

Breitenbush Hot Springs includes a number of orifices on both sides of the Breitenbush River. The hot springs lie within an electrically conductive zone identified from telluric data by H. Pierce and others (U.S. Geological Survey, written commun., 1989). These data indicate either two linear, electrically conductive structures (as shown in fig. 22) or curvilinear intertwined structures that splay and converge along a broadly northeast-southwest trend. In addition to the hot springs, the conductive zone encompasses two unusual low-discharge Na-HCO$_3$ mineral springs (table 4, analyses 11, 13). The 100°C isotherm deepens abruptly northwest of the conductive zone (fig. 22). The conductive zone

may represent fractures that channel thermal water to the surface or a relatively impermeable barrier that blocks lateral movement of thermal water.

A 6- to 7-km-deep integrated-finite-difference grid (fig. 23) was used to simulate ground-water flow and heat transport in the Breitenbush section; pressure and temperature solutions were calculated at 790 nodal points. The lateral boundaries were treated as no-flow (symmetry) boundaries; the lower boundary as a controlled-flux boundary (impermeable to fluid flow, with a specified conductive heat flow); and the upper boundary as a constant pressure-temperature boundary (pressure = 1 bar, temperature = 12.8°C–5.5°C per km above sea level). We simulated the thermal input for the alternative conceptual models depicted in figure 18 by varying the conductive heat flow at the base of the cross section (the "basal heat flow") and, in some cases, by introducing a shallow heat source beneath the Quaternary arc.

Figures 24 through 28 show selected steady-state results from numerical simulations of the Breitenbush section. Simulated near-surface conductive heat flows were calculated using the temperature differences between the top two nodes in each column of nodes (fig. 23). The heat-flow values thus represent depths ranging from a few tens of meters to about 200 meters, depths similar to those at which most of the conductive heat-flow data were collected. The simulated recharge and discharge rates are the volumetric flow rates (Darcy velocities) between the top two nodes in each column. The labeled arrows on figure 24 and succeeding figures show how the heat supplied to

and discharged from the system is partitioned between the Quaternary arc and the Western Cascades. These values, in joules per second, are calculated by assigning the two-dimensional section an arbitrary thickness of 1 km.

The simulated results are compared with near-surface heat-flow data projected onto the line of section, with ground-water recharge estimates (table 3), and with temperature profiles from the deep (>1 km) drill holes at heat-flow sites 40 and

61. Results from a conduction-only simulation with uniform basal heat flow (fig. 24A) were used to correct for topographic distortion of simulated heat-flow values. The minor transfer of heat (0.61×10^5 J/s) from the Quaternary arc to the Western Cascades in this simulation owes to topography and the relatively low thermal conductivity of the wedge of younger rocks.

Conduction-only simulations with narrow (fig. 24B) or wide (fig. 24C) basal heat-flow anomalies

EXPLANATION

QUATERNARY AND RHYOLITIC DACITIC ROCKS

OTHER QUATERNARY VOLCANIC ROCKS

PLIOCENE TO OLIGOCENE VOLCANIC AND VOLCANICLASTIC ROCKS

—-200— TEMPERATURE CONTOUR—Shows estimated altitude of the 100 degree Celsius contour. Contour interval 200 meters. Datum is sea level

61 o SITE OF HEAT-FLOW MEASUREMENT—Two sites with index number. See appendix for additional information

NONTHERMAL MINERAL SPRING

FIGURE 22.—Breitenbush Hot Springs area showing line of section used in numerical simulations, locations of thermal and nonthermal mineral springs, Quaternary volcanic rocks, electrically conductive zones identified by H. Pierce and others (U.S. Geological Survey, written commun., 1989), and estimated elevation of 100°C contour. Geologic data are from Priest and others (1987) and from D.R. Sherrod and R.M. Conrey (U.S. Geological Survey, unpublished data, 1988).

failed to reproduce either the low near-surface conductive heat flow in the Quaternary arc or the elevated heat flow between Breitenbush Hot Springs and the Quaternary arc; some permeability is required. A simulation using a narrow heat-flow anomaly and incorporating the permeability values listed in table 10 (fig. 24D) provided a better match to the observed heat-flow values, although simulated heat-flow values between Breitenbush Hot Springs and the Quaternary arc are still mostly below the range of observed values.

In the simulation summarized in figure 24D, most of the ground water recharged in the Quaternary arc (303 kg/s) discharges locally in topographic lows (301 kg/s), but carries little heat. Simulated discharge in the Breitenbush Hot Springs area (about 1 kg/s) is a small fraction of total recharge in the Quaternary arc, but this relatively small mass flux transports substantial amounts of heat from the Quaternary arc to the Western Cascades. In this particular simulation the ratio of hot-spring discharge to recharge in the Quaternary arc (0.003) is similar to the ratio (0.002) that we estimated from measured ground-water recharge (table 3) and hot-spring discharge rates (table 5).

The simulated results are highly sensitive to permeability (figs. 25 and 26). Isotropic permeabilities one-tenth of those listed in table 10 (fig. 25A) lead to near-surface heat-flow values in the Western Cascades that are not significantly different from the conduction-only case of figure 24B. Increasing permeability tenfold (fig. 25B) provides a better match to the ground-water recharge estimates, but decreases heat flow between Breitenbush Hot Springs and the Quaternary arc markedly, to
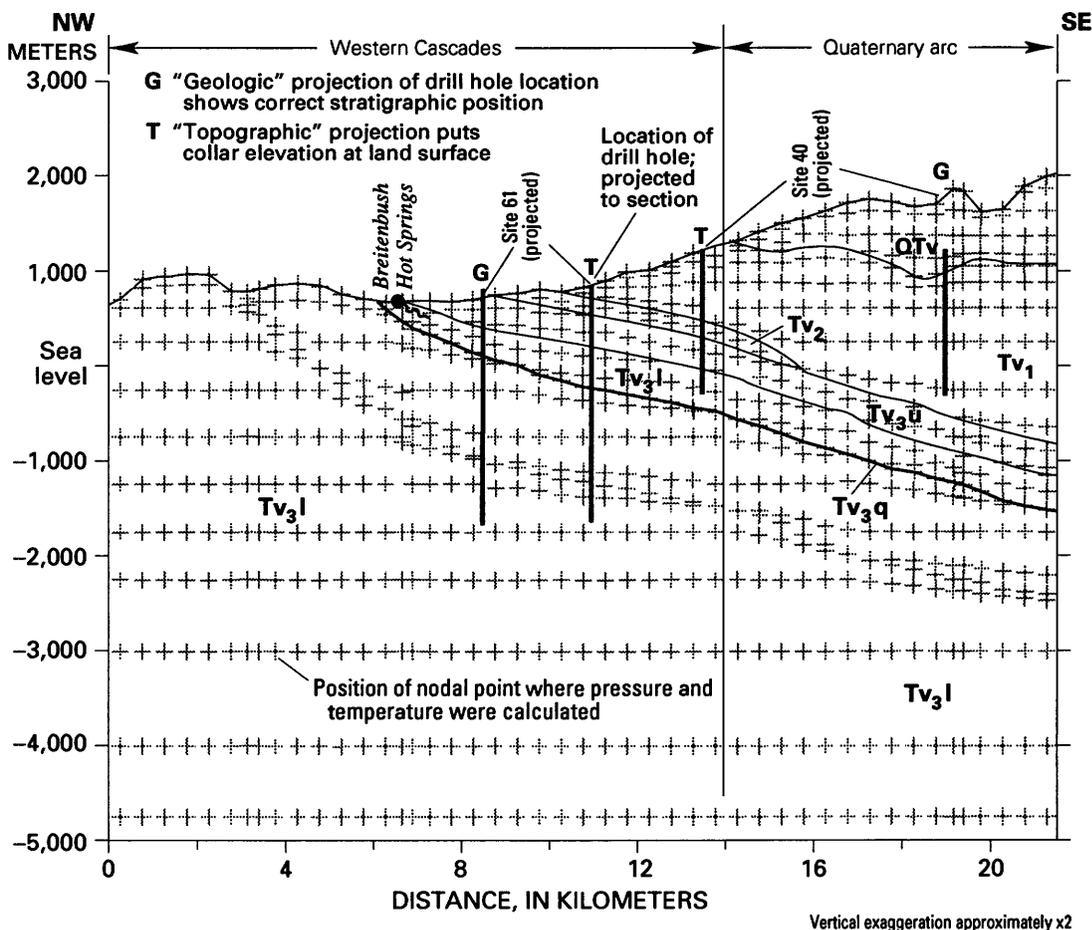
FIGURE 23.—Generalized lithologic section used for numerical simulation of Breitenbush Hot Springs system. Lithologic units, which are lava flows or other volcanic and volcaniclastic strata, are described in table 10. Heat-flow sites 40 and 61, which lie off section (fig. 22), are projected onto section in two different ways to indicate possible range of appropriate geologic and topographic contexts. Geologic projection (G) locates drill hole correctly relative to stratigraphic contacts, and topographic projection (T) puts collar elevation at land surface.

values well below those observed. Figures 25C and 25D illustrate the effects of moderate hydraulic anisotropy within each lithologic unit. In the simu-lation summarized in figure 25C, horizontal permeabilities (k_x) are those listed in table 10, whereas vertical permeabilities (k_y) are reduced by
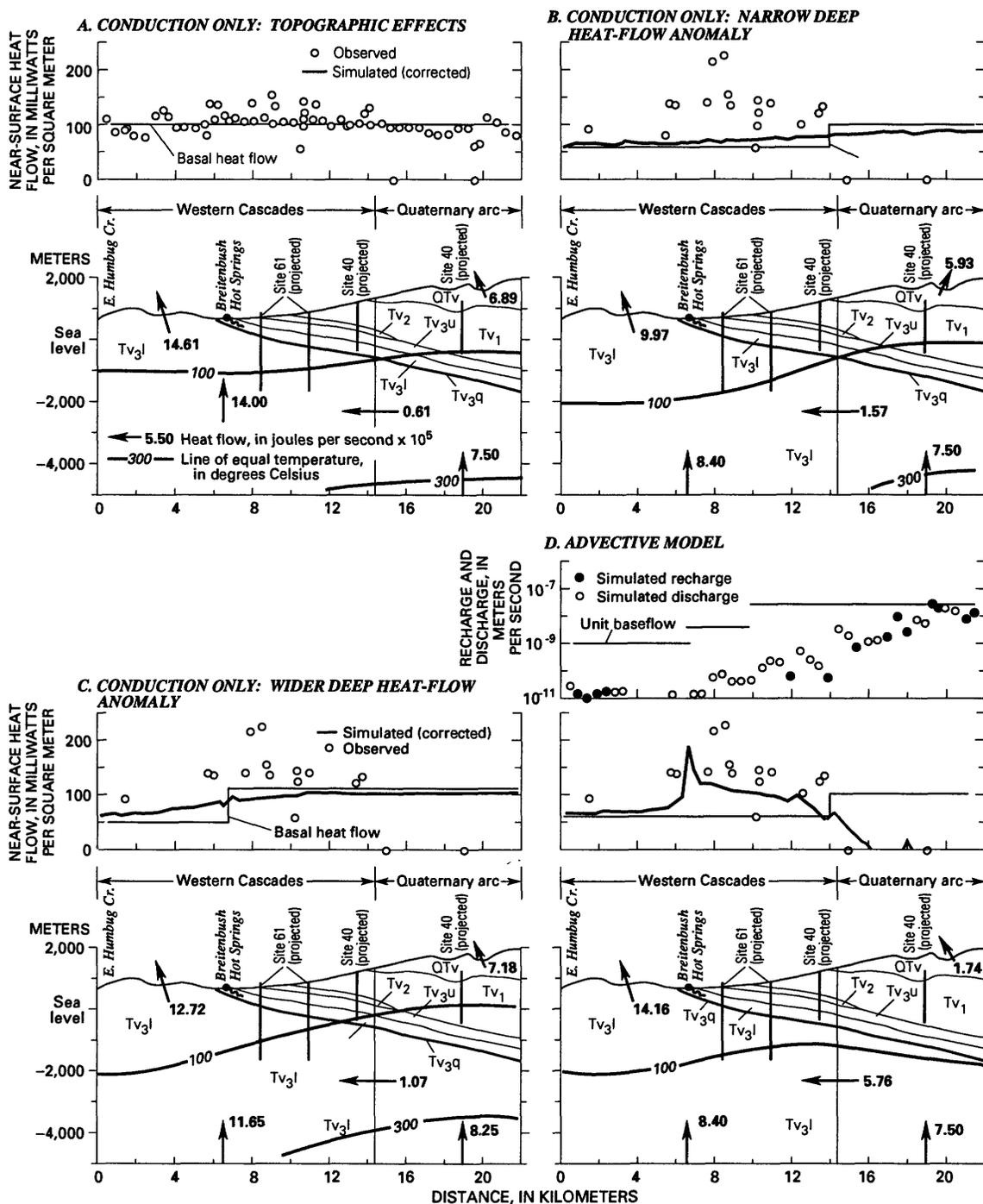
FIGURE 24.—Selected steady-state results from numerical simulation of Breitenbush section. Conduction-only case of (A) was used to correct simulated near-surface conductive heat flows from other simulations. In B, C, and D simulated heat-flow values are compared with measured values and, in D, simulated hydro-logic recharge and discharge rates are compared with minimum recharge rates (unit baseflow) that were estimated for rocks of similar ages (table 3). Labeled arrows indicate how heat supplied to system is partitioned. For example, in D basal heat flow beneath Quaternary arc totals 7.50×10^5 J/s. Of this quantity, 5.76×10^5 J/s flows laterally into Western Cascades and 1.74×10^5 J/s flows across land surface within Quaternary arc. Line of section shown in figure 22; lithologic units described in table 10.

a factor of 10. In figure 25D, k_y is 10 times higher than the k_x values listed in table 10. Enhanced horizontal permeability might be explained by the layering of volcanic units; enhanced vertical permeability might be explained by pervasive vertical fractures. Evidence from New Zealand geothermal
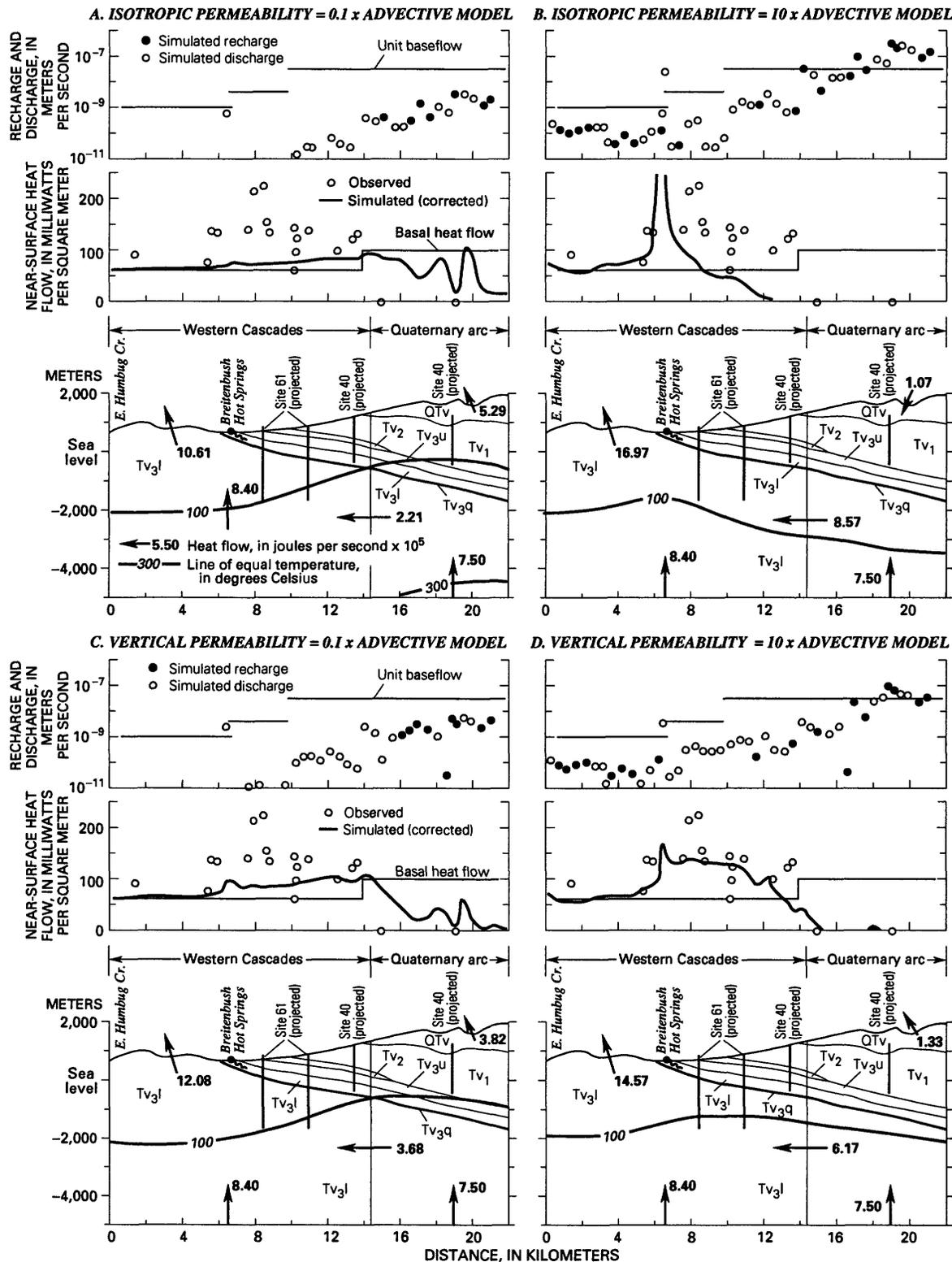
FIGURE 25.—Selected steady-state results from numerical simulation of Breitenbush section, showing sensitivity to permeability. Line of section shown in figure 22; lithologic units described in table 10.

fields in volcanic rocks suggests that k_x/k_y is approximately 10 (P.R.L. Browne, oral commun., 1990), the case represented in figure 25C.

The heat-flow observations are best matched with the permeability values of table 10 (fig. 24D). However, for the full range of permeability values illustrated (figs. 24D and 25), simulated hydrologic fluxes at the land surface are generally less than the minimum ground-water recharge calculated for rocks of similar ages (table 3). Permeabilities higher than those of figure 25B would be required to match the recharge estimates and would clearly cause excessive cooling. To match both the heat-flow observations and the recharge estimates would require a strong permeability-to-depth relation within each unit, with near-surface (less than about 50 m) permeabilities significantly higher than those used in our simulations. As noted above, well-test data from domestic wells in the Western Cascades (McFarland, 1982), support the inference of much higher permeabilities at relatively shallow depths.

The limited sensitivity analysis discussed above provides some constraints on the regional permeability structure but does not constrain the permeability of the thermal aquifer (unit Tv_3q), which was treated as a 30-m-thick zone of relatively high permeability. Figure 26 shows some effects of varying the permeability of the thermal aquifer independently within the overall permeability structures of figures 24D (table 10: $k = 1.0\times$), 25A ($k = 0.1\times$) and 25B ($k = 10\times$). The results are summarized in terms of flow rates and temperatures in the thermal aquifer at the edge of the Quaternary arc. If the other units are assigned permeability values from table 10 ($k = 1.0\times$), assigning permeabilities less than about 10^{-14} m^2 to the thermal aquifer restricts the volumetric flow rate and thus limits advective heat transfer. Assigning permeabilities greater than about 10^{-14} m^2 to the thermal aquifer leads to significant cooling and thus reduces conductive heat flow between Breitenbush Hot Springs and the Quaternary arc. Permeabilities on the order of 10^{-14} m^2 seem to be required for lithologic unit Tv_3q to function as an effective thermal aquifer, given its assumed thickness and the constraints on the permeabilities of other units.

Although the simulation involving a narrow basal heat-flow anomaly and the permeability values listed in table 10 reproduced the near-surface heat-flow values reasonably well, the temperature-depth profiles from the deep drill holes at heat-flow sites 40 and 61 were matched poorly; simulated

temperatures and temperature gradients were generally less than the measured values (fig. 27A). A conduction-dominated simulation with a wide heat source and fluid flow confined to rocks younger than about 2.3 Ma (table 10, unit QTv) matched the data from site 40 fairly well, but failed to reproduce the high heat flow between Breitenbush Hot Springs and the Quaternary arc or the elevated gradient measured to depths of about 800 m at site 61 (fig. 27B). When fluid flow is confined to unit QTv, most of the heat supplied to the Quaternary arc discharges advectively there.
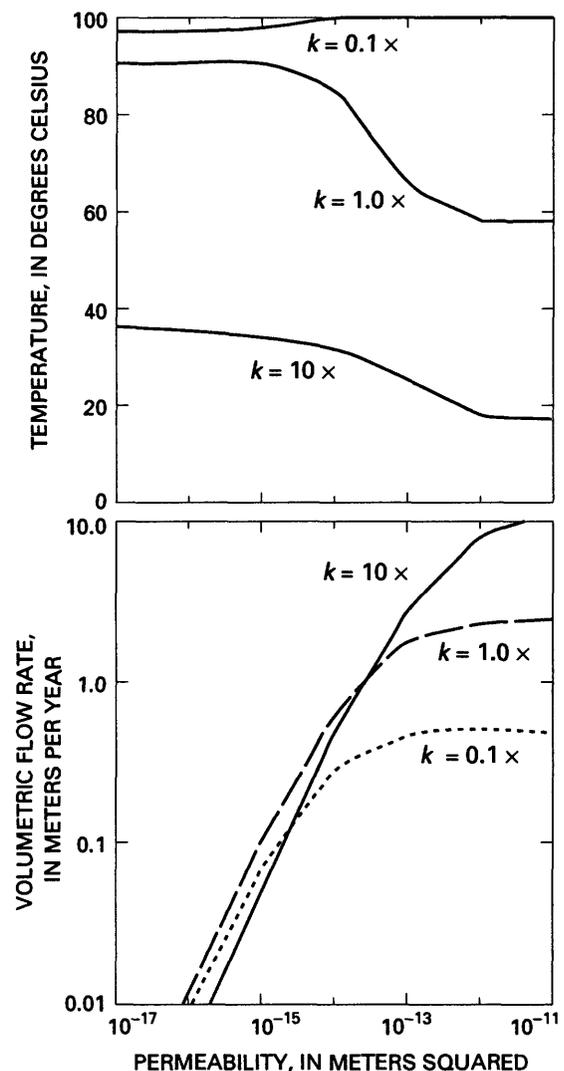
FIGURE 26.—Relation between permeability of thermal aquifer (lithologic unit Tv_3q [see table 10]) and temperature and volumetric flow rate (Darcy velocity) in thermal aquifer at edge of Quaternary arc. Overall permeability structures (k) are those of figures 24D ($k = 1.0\times$), 25A ($k = 0.1\times$), and 25B ($k = 10\times$).

Both the near-surface heat-flow data and the temperature-depth profiles from sites 40 and 61 can be reproduced reasonably well using two very different deep thermal structures, again using the permeability values listed in table 10 (fig. 28). The simulation summarized in figure 28A involved uniform basal heat flow of 60 mW/m^2 and an intense local heat source beneath the Quaternary arc, a situation analogous to the lateral-flow model (fig.

18A); the simulation in figure 28B involved a wide basal heat-flow anomaly of 130 mW/m^2, analogous to the midcrustal heat source (fig. 18B). The local heat source in figure 28A represents the thermal input of an upper-crustal magma body. The total heat supplied to the system in these two simulations (fig. 18) is identical. Both simulations match the observations reasonably well, and the rates of advective heat transfer from the Quaternary arc to
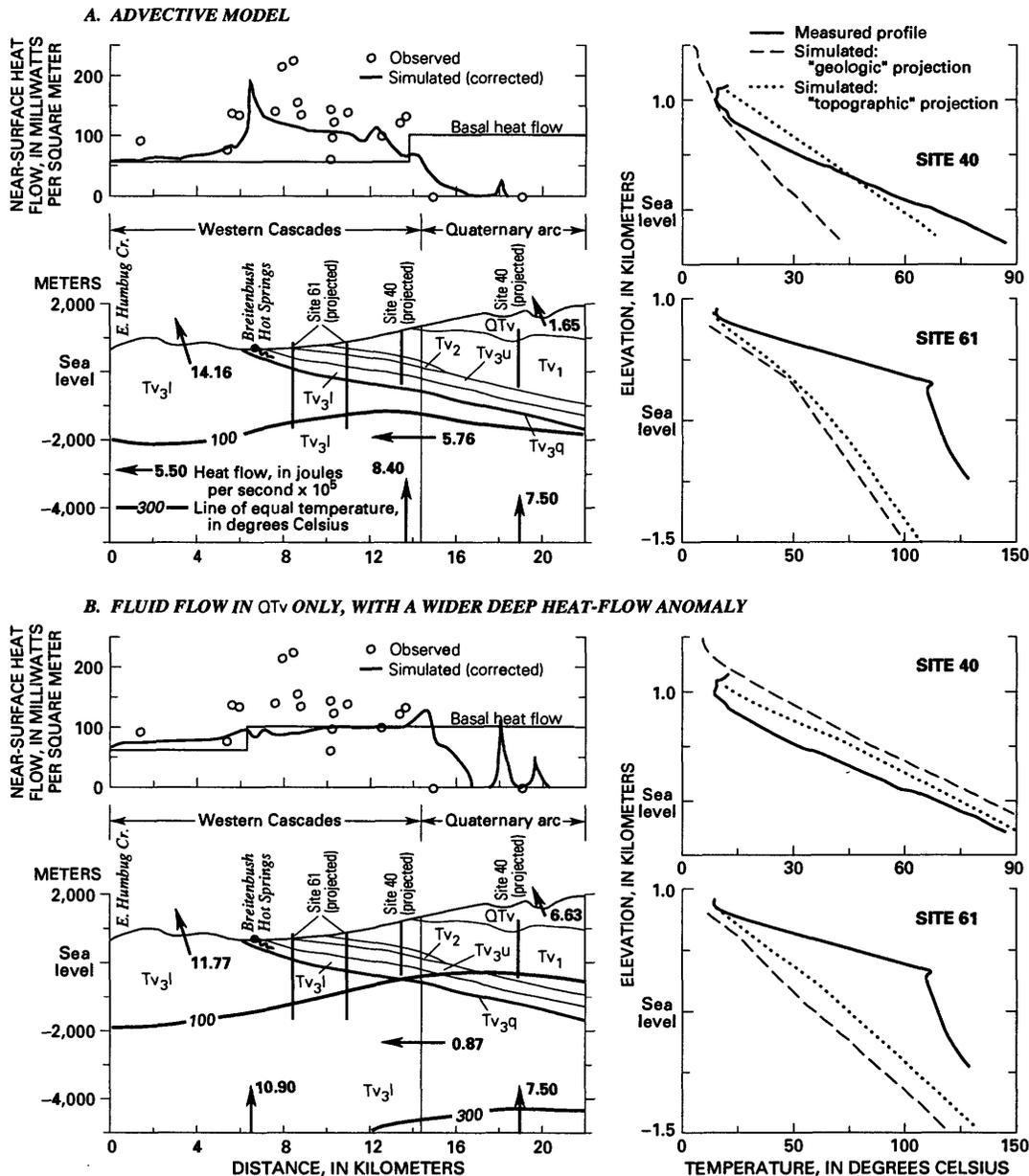
FIGURE 27.—Selected steady-state results from numerical simulation of Breitenbush section, showing poor match between simulated temperature profiles and those measured at heat-flow sites 40 and 61. Heat-flow sites 40 and 61 are off section (fig. 22) and cannot be projected to section in a way that reflects both their geologic and topographic contexts. Thus we compare data from each hole with simulated temperature profiles representing geologic and topographic projections (see fig. 23 for additional information). Lithologic units described in table 10.

the Western Cascades (0.7–1.2 MW) are similar to the length-normalized rate of heat transfer by the hot-spring systems (121 MW ÷ 135 km arc length = 0.9 MW/km arc length; see fig. 11 for measured values).

Our simulations cannot simultaneously match the temperature profile from site 61 and the near-surface heat-flow data. If the simulated temperature at the depth of the thermal aquifer (about 800 m) matched the measured temperature exactly, near-surface conductive heat flow between

Breitenbush Hot Springs and the Quaternary arc would greatly exceed the observed values (see, for example, figure 28, where simulated heat flows are higher than most observed values despite thermal-aquifer temperatures that are lower than those observed). This implies that the actual fluid-flow geometry is probably more complex than in the system we simulated. For example, the geometry of unit Tv_3q (the quartz-bearing ash-flow tuff) may be different, and focusing of flow in the third
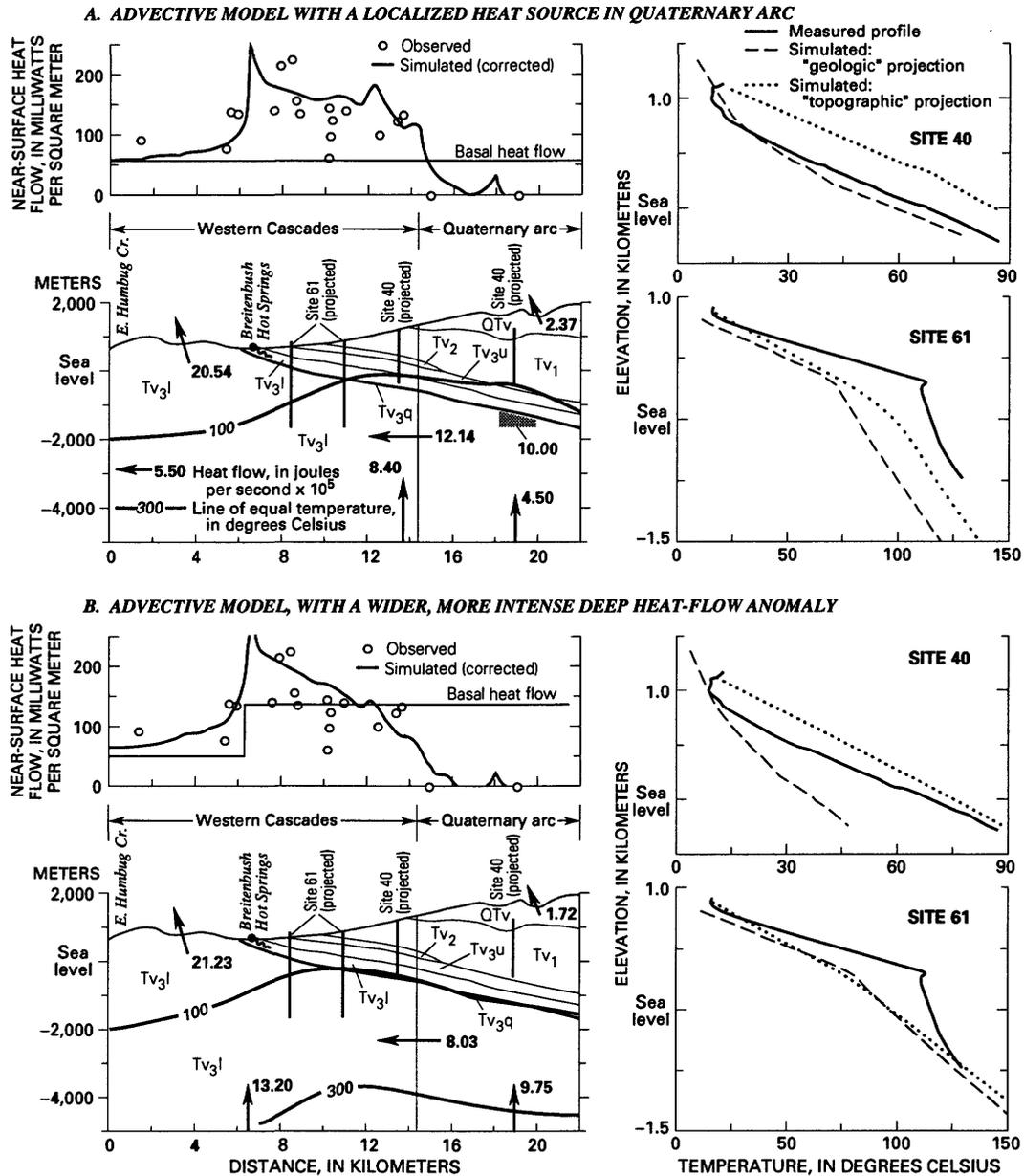
FIGURE 28.—Selected results from numerical simulation of Breitenbush section, showing that thermal observations can be reproduced reasonably well with two very different deep thermal structures. In A, the dark polygon in unit Tv_3l indicates location of heat source producing 10.0×10^5 J/s. See captions to figures 23 and 27 for explanation of geologic and topographic projections of heat-flow sites 40 and 61. Lithologic units described in table 10.

(unsimulated) dimension may be important. Three-dimensional effects are certainly responsible for some of the scatter in the observed heat-flow data that are projected to the section, and the nonuniform distribution of hot-spring heat transport (fig. 11) indicates significant three-dimensional focusing of fluid flow.

Different ways of matching the temperature profile from heat-flow site 61 carry distinct implications about the age of the hydrothermal system. Under near-steady-state conditions (time scales greater than about 10^5 years), the low temperature gradient below 800 m depth is best matched with a relatively low basal heat flow. As noted in figure 17, the temperature gradient measured across the 1,465- to 1,715-m interval is 31°C/km and predicts a bottom-hole (2,457 m) temperature of 152°C, which is consistent with the measured bottom-hole temperature of at least 141°C (Priest, 1985). This gradient corresponds to a heat flow of about 68 mW/m^2 (appendix). If flow in the thermal aquifer has been relatively short-lived (about 10^4 years), the observed profile can be matched well with a much higher basal heat flow. For example, Blackwell and Baker (1988a; Blackwell and others, 1990a) used a heat flow of 124 mW/m^2 and a time of 2.5×10^4 years to obtain a good match. If the hydrothermal system is driven by a long-lived silicic magmatic system such as fed the 0.25- to 0.7-Ma dacite domes in the eastern part of the cross section, the near-steady-state match is more appropriate. In either case, volumetric flow rates (Darcy velocities) on the order of 1 m per year are required to maintain elevated aquifer temperatures.

In conclusion, regardless of the conceptual model invoked for the deep thermal structure, significant advective heat transport is required to reproduce several of the observations from the Breitenbush area, including the near-zero near-surface heat flow in the Quaternary arc, elevated heat flow between Breitenbush Hot Springs and the Quaternary arc, and the major decrease in the temperature gradient below 800 m depth at heat-flow site 61. Because of the strong advective effects, the deep thermal structure cannot be uniquely inferred from the available temperature-depth observations.

MCKENZIE RIVER SECTION

The 44-km-long McKenzie River cross section extends west from the Cascade Range crest through Terwilliger Hot Spring (fig. 29). Silicic volcanic rocks exposed near the eastern end of the section in the South Sister area (fig. 29) include Pleistocene and Holocene rhyolite and dacite (Taylor and others, 1987); thus the underlying silicic magmatic systems may drive hydrothermal activity.

Temperature-depth data are sparser in the McKenzie River area than in the Breitenbush area, and deep (greater than 1 km) drill-hole data are lacking. In the Breitenbush area, there is evidence for a zone of relatively high permeability at the approximate stratigraphic position of unit Tv$_3$q, as summarized above. In the McKenzie River cross section we have experimented with simulation of analogous 30-m-thick stratigraphically controlled aquifers at three different depths (fig. 30), although there is no direct evidence for such aquifers. The hypothetical dikes shown on the cross section (fig. 30) underlie silicic vents near South Sister; zones of relatively high vertical permeability associated with such dikes could enhance deep recharge in the Quaternary arc.

The hot springs in the McKenzie River drainage lie near two major down-to-the-east normal fault zones, the Horse Creek fault zone and the Cougar Reservoir fault zone (figs. 3 and 29). Relatively chloride-rich waters sampled at several other localities suggest a "leaky" thermal system in the area. Dilute Na-Cl water from a 62-m-deep well at White Branch Youth Camp (table 4, analysis 30) could contain approximately 5 percent thermal water, and the Bigelow thermal well (table 2) discharges thermal water compositionally similar to that from Belknap Springs (see fig. 29 for well locations). The unnamed spring between Foley Springs and White Branch Youth Camp (fig. 29) is anomalously high in chloride (table 4, analysis 29), as are Separation Creek (table 7) and the White Branch of McKenzie River (Ingebritsen and others, 1988). The anomalous chloride flux in Separation Creek (about 10 g/s) is larger than the fluxes from some of the hot springs in the study area (table 5). This widespread evidence for diffuse discharge of thermal water is consistent with data from the U.S. Geological Survey stream-gaging station near Vida (table 7), which suggest that the total discharge of high-chloride water in the McKenzie drainage is somewhat greater than the sum of the individual hot springs.

Pressure and temperature solutions for the McKenzie River section were calculated at 921 nodal points within a 5.5- to 7.5-km-deep integrated-finite-difference grid (fig. 30). The boundary conditions were the same as those used in simulations of the Breitenbush section: the lateral boundaries were no-flow boundaries, the lower boundary

a controlled-flux boundary, and the upper boundary a constant pressure-temperature boundary. We again simulated the thermal input for the alternative thermal structures (fig. 18) by varying the distribution of deep heat sources. Except where otherwise noted, lithologic units and rock properties are those listed in table 10.

We treated the faults (fig. 30) as 30-m-wide zones of relatively high permeability. The presence of several fault zones and the major topographic divide between Horse Creek and Cougar Reservoir make the McKenzie River section significantly different from the Breitenbush section; the degree of continuity of regional ground-water flow across these barriers is one of the major issues of interest.

In selected results from numerical simulation of the McKenzie River section (figs. 31–33), simulated near-surface heat-flow values are compared with data projected onto the line of section, and volumetric flow rates (Darcy velocities) in the hypothetical aquifer units are shown for some cases. Results from a conduction-only simulation with uniform basal heat flow (fig. 31A) were used to

correct for topographic distortion of simulated heat-flow values.

As was the case with the Breitenbush section, conduction-only simulations with narrow (fig. 31B) or wider (fig. 31C) basal heat-flow anomalies failed to reproduce the near-surface heat-flow observations. However, the heat-flow data are concentrated near the Horse Creek and Cougar Reservoir fault zones (fig. 29). The elevated heat flow in those areas (fig. 31) could be explained in terms of convective (density-driven) circulation within the fault zones themselves, with insignificant advective heat transport in the two dimensions that we simulated, although such relatively local circulation would be inconsistent with some of the geochemical evidence discussed in the section "Thermal Waters."

Figure 31D summarizes the results of three simulations in which aquifer depth was varied. The 30-m-wide fault zones and the aquifer were assigned permeabilities of 2.5×10^{-14} m^2. These simulations resulted in pronounced conductive heat-flow anomalies at the Horse Creek and Cougar Reservoir fault zones and in the Separation

EXPLANATION

	QUATERNARY DACITIC AND RHYOLITIC ROCKS
	OTHER QUATERNARY VOLCANIC ROCKS
	PLIOCENE TO OLIGOCENE VOLCANIC AND VOLCANICLASTIC ROCKS

———⸽——— FAULT—Bar and ball on downthrown side. Dashed where inferred; dotted where concealed

o   SITE OF HEAT-FLOW MEASUREMENT

⤳●   THERMAL SPRING

⤳○   NONTHERMAL MINERAL SPRING

●   WELL

0   10 MILES

0   10 KILOMETERS
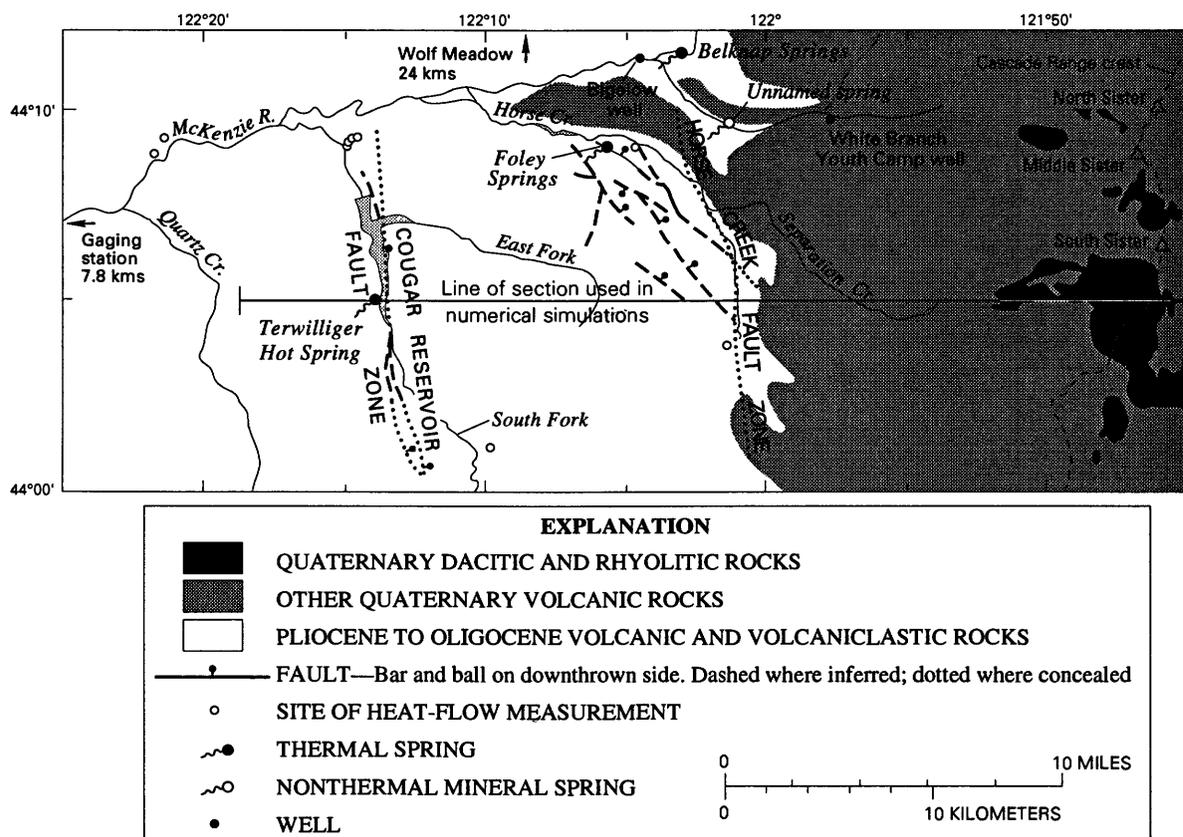
FIGURE 29.—McKenzie River area showing line of section used in numerical simulations (figs. 30–33), locations of thermal springs and other springs and wells discussed in text, faults, and Quaternary volcanic rocks. Geologic data are from Priest and others (1988) and from authors' unpublished compilation map.

Creek area but resulted in very low heat flow between the two fault zones. In each of these simulations, advective heat transfer between the Quaternary arc and the Western Cascades is small, amounting to less than 10 percent of the heat supplied to the Quaternary arc; most of the heat supplied to the Quaternary arc discharges in the Separation Creek area or at the Horse Creek fault zone. Only for the deepest aquifer configuration is there continuous regional ground-water flow and a net transfer of heat from the Quaternary arc to the Western Cascades (see the volumetric flow rates and labeled arrows in fig. 31D). For the shallower aquifer configurations there is actually net heat transfer from the Western Cascades to the Quaternary arc, because some ground water recharged in the Western Cascades discharges in the Horse Creek area.

Simulated heat transfer between the Quaternary arc and the Western Cascades is sensitive to the permeability structure. Net heat transfer is increased by reducing the permeability of the upper (dashed) part of the Horse Creek fault zone to values similar to those assigned to the rocks surrounding the fault zone (fig. 32A); incorporating 30-m-wide high-permeability (2.5×10^{-14}) conduits (dikes, fig. 30) for deep recharge within the Quaternary arc (fig. 32B); and lowering the permeability of the 8- to 17-Ma lava flows (table 10, Tv_2) to 2×10^{-17} m^2 (fig. 32C). If these relatively minor modifications to the poorly constrained permeability structure are combined (fig. 32D), the net heat transfer is significant, and near-surface conductive heat flow between the Horse Creek and Cougar Reservoir fault zones is greater than the basal heat flow.
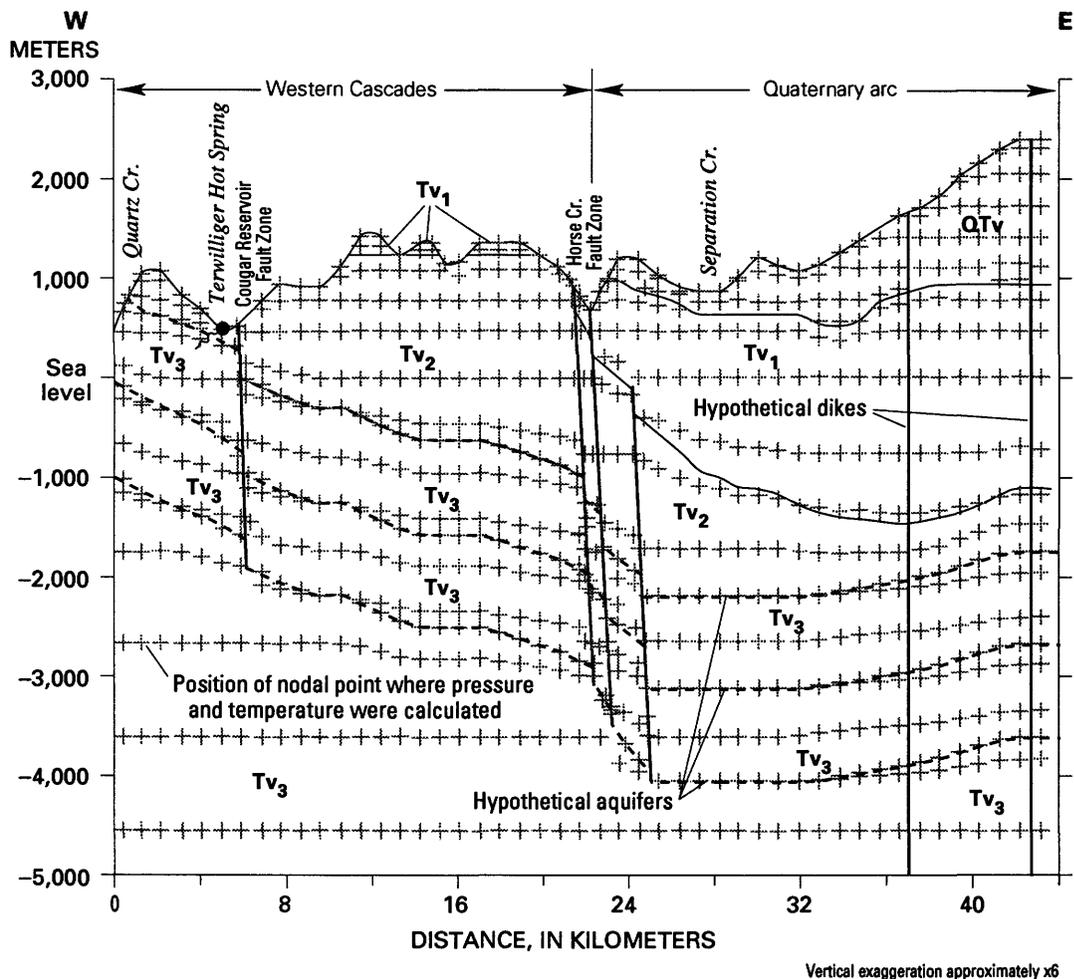
FIGURE 30.—Generalized lithologic section (see fig. 29) used for numerical simulation of McKenzie River area. Lithologic units, which are lava flows or other volcanic and volcaniclastic strata, are described in table 10.

Reduced permeability in the upper part of the Horse Creek fault zone (fig. 32A) might be explained by hydrothermal alteration and (or) silica deposition. Note that if the permeabilities of the Horse Creek and Cougar Reservoir fault zones are equal (for example, fig. 31D), discharge of heated ground water is concentrated at Horse Creek, with relatively minor hydrothermal effects at Cougar Reservoir. Over time, focused discharge at Horse Creek could lead to decreased permeability. Silica
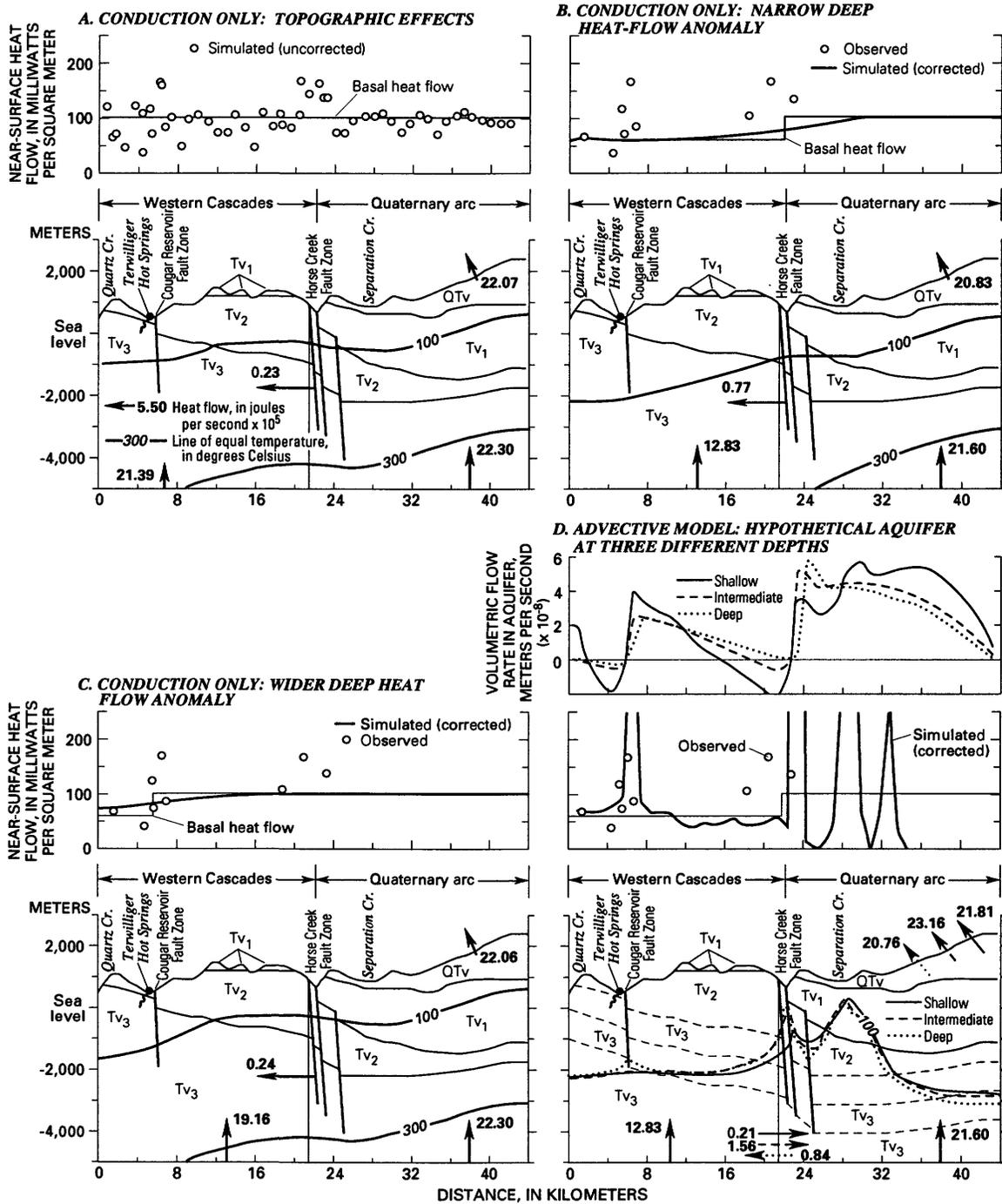
FIGURE 31.—Selected steady-state results from numerical simulation of McKenzie River section. Simulated heat-flow values are compared with measured values and, in D, simulated volumetric flow rates (Darcy velocities) in deep "aquifer" unit are shown. Labeled arrows indicate how heat supplied to the system is partitioned. In D, the solid, dashed, and dotted lines and arrows indicate results for shallowest, intermediate, and deepest aquifer configurations, respectively. Line of section shown in figure 29; lithologic units described in table 10.
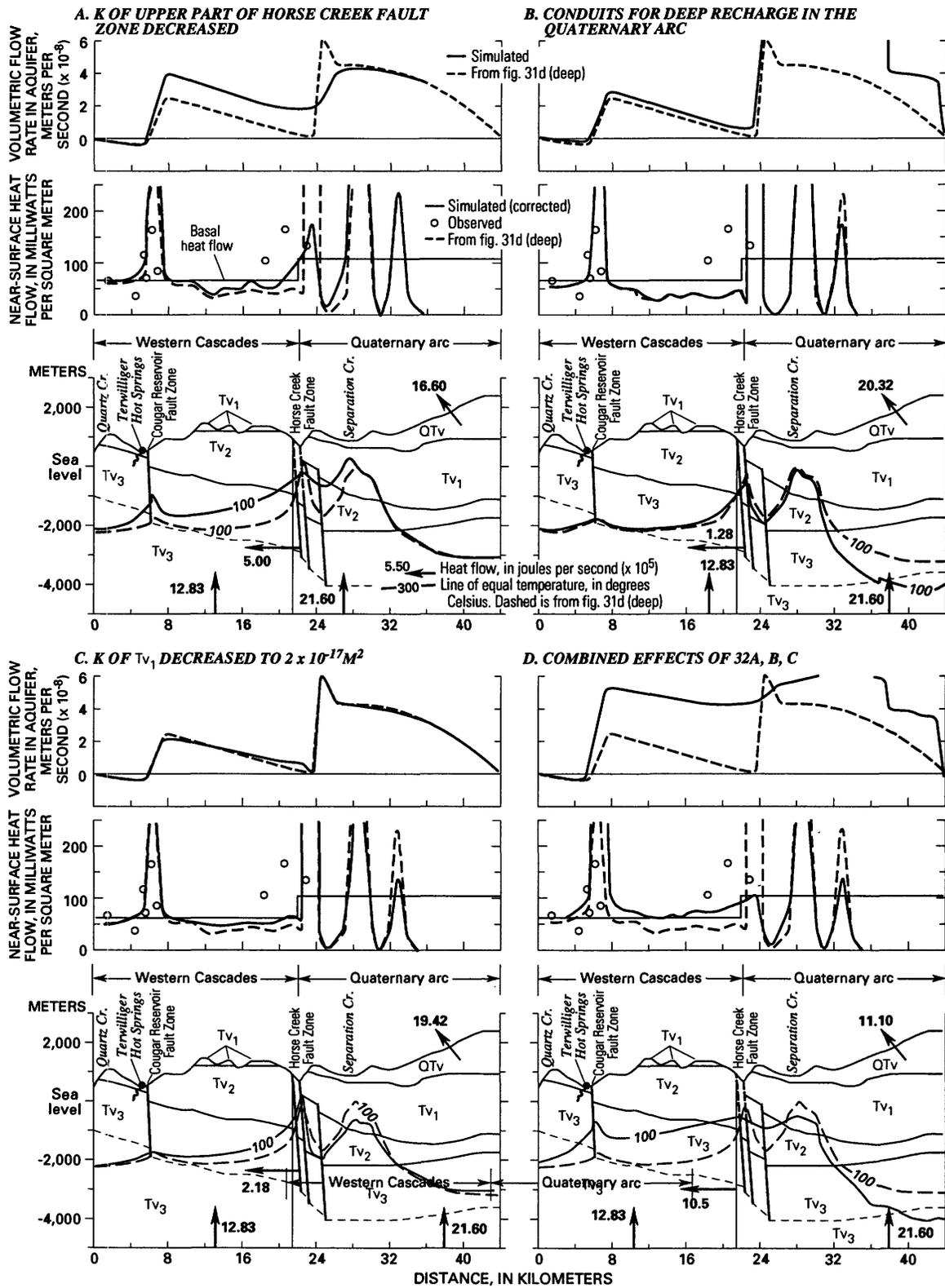
FIGURE 32.—Selected steady-state results from numerical simulation of McKenzie River section, showing sensitivity to permeability. Dashed lines indicate results from deepest aquifer configuration of figure 31D. Vertical dashed lines in B and D indicate dikes treated as high-permeability conduits. Line of section shown in figure 29; lithologic units described in table 10.

deposition might be concentrated in the upper part of the fault zone, where temperature gradients are relatively steep.

As with the Breitenbush section, very different distributions of deep heat sources can produce similar matches to the available data. However, unlike the Breitenbush case, one of the matches that we consider reasonable for the McKenzie River section is conduction-dominated. A conduction-dominated simulation with a wide basal heat-flow anomaly and fluid flow confined to unit QTv (fig. 33A) is analogous to the midcrustal heat source model (fig. 18B) and provides a reasonable match to the available data; elevated heat flow near the Horse Creek and Cougar Reservoir fault zones can be explained in terms of circulation in a third (unsimulated) dimension, as noted above. Simulations involving localized heat sources, which are analogous to the lateral-flow model (fig. 18A), can also match the thermal data (for example, fig. 33B); they involve advective heat-transfer rates (0.9–1.8 MW) that are roughly comparable to the measured rates of heat transfer by hot-spring systems (0.9 MW/km arc length).

In conclusion, the shallow, sparser thermal observations in the McKenzie River area allow conduction- or advection-dominated numerical simulations. Advection-dominated models lead to elevated heat flow in the highlands between the Horse Creek and Cougar Reservoir fault zones only if there is a thermal aquifer at depths of several kilometers. At shallower depths, regional ground-water flow may be interrupted by the Horse Creek fault zone and the topographic divide between the fault zones. Blackwell and others (1990a, p. 19,484) argued against the lateral-flow model (fig. 18A) on the basis of a high conductive gradient measured in the "Wolf Meadow hole," which is located north of the McKenzie River in a topographic position analogous to the highlands between Horse Creek and Cougar Reservoir (fig. 29). Our results show that regional ground-water flow could influence heat flow at such locations and explain the observed gradient.
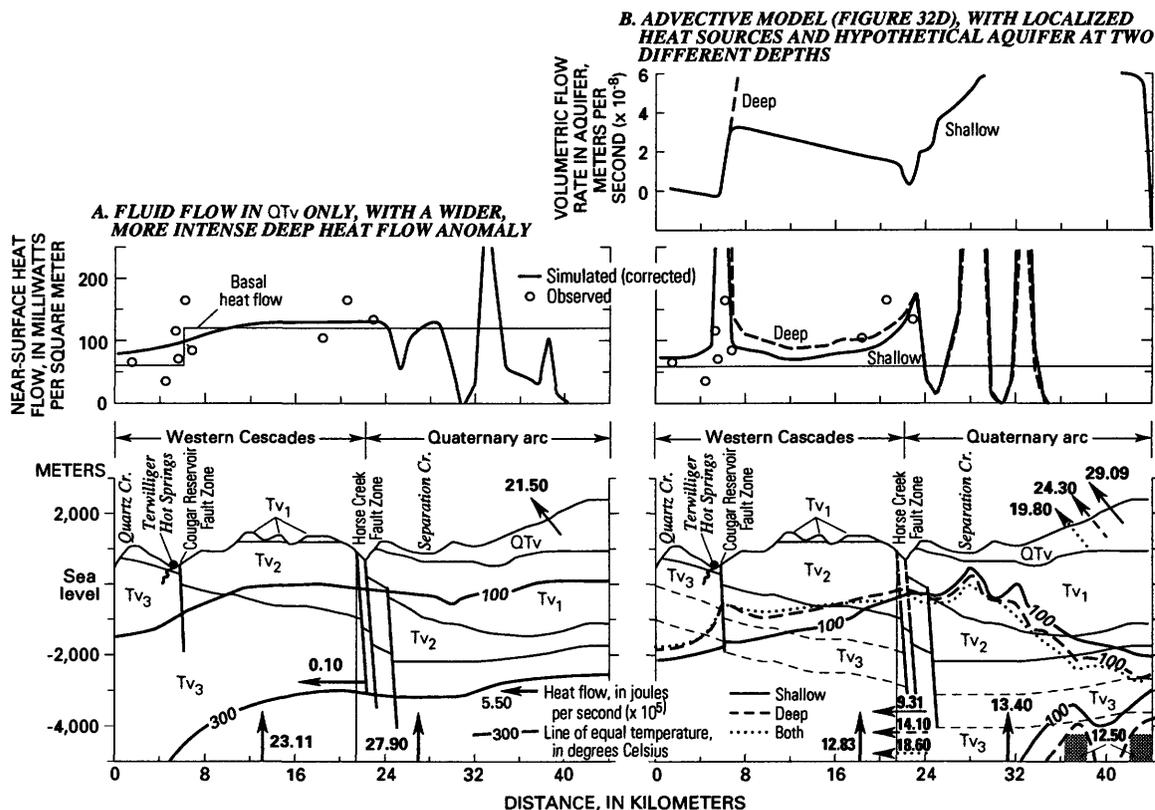
FIGURE 33.—Selected results from numerical simulation of McKenzie River section, showing that sparse near-surface heat-flow observations can be matched using (A) conduction-dominated model involving fluid flow only in unit QTv or (B) advection-dominated model with localized heat sources. Solid and dashed lines and arrow in B indicate results for shallower and deeper aquifer configurations, respectively; the dotted lines and arrow indicate results from simulation in which both aquifers were present. Labeled dark rectangles in B indicate localized heat sources each producing 12.5 × 10⁵ J/s; permeability structure is that of figure 32D. Line of section shown in figure 29; lithologic units described in table 10.

HEAT TRANSFER RATES AND RESIDENCE TIMES

Actual patterns of fluid circulation are certainly more complex than the representations in our two-dimensional sections. For example, topographic variations in the unsimulated (north-south) dimension presumably act to focus thermal-fluid discharge in the deeply incised valleys of the Western Cascades. Nevertheless, comparison of simulated and measured heat-transfer rates is a useful test of the simulated results.

In advection-dominated simulations that match the observations reasonably well (figs. 28 and 33B), rates of advective heat transfer from the Quaternary arc to the Western Cascades range from 0.7 to 1.8 MW per kilometer of arc length. These values encompass the length-normalized measured value of 0.9 MW/km arc length. Our cross sections include hot-spring areas, and these simulated heat-transfer rates allow us to match observed conductive heat-flow values that are considerably in excess of 100 mW/m^2. A lower rate of about 0.5 MW/km arc length is sufficient to support conductive heat-flow of about 100 mW/m^2 between Breitenbush Hot Springs and the Quaternary arc (fig. 24D). Such relatively low advective heat-transfer rates might be more typical of the areas between hot-spring groups.

As discussed in the section "Thermal Waters," thermal-fluid residence times are only weakly constrained by the available data. Sulfate-water isotopic equilibrium implies minimum residence times of 40 to 2,000 years, and our interpretation of the stable-isotope data implies maximum residence times of less than 10,000 years. Simulated volumetric flow rates (v_d) in the thermal aquifers are on the order of one meter per year (for example, fig. 33B), and similar rates are required to maintain the elevated thermal-aquifer temperature observed at heat-flow site 61 (fig. 17). Fluid particle velocities are approximated by v_d/ϕ, where ϕ is effective porosity. Thus for ϕ equal to 0.02 (table 10), fluid velocities in the thermal aquifer are about 50 m/year, and thermal-aquifer residence times are a few hundred years. Rates of vertical recharge through the less permeable layers that confine the thermal aquifer are much lower, so that simulated particle velocities are as low as 0.1 m per year, and total residence times exceed 10,000 years. The addition of localized conduits for deep recharge (figs. 32B, D; 33B) reduces total residence times to less than 1,000 years. If our interpretation of the stable-isotope data is correct, recharge to thermal aquifers must occur through discrete zones with relatively high vertical permeability. Such vertical conduits might be created by intrusions or by normal faulting.

COMPARISON WITH OTHER VOLCANIC-ARC AREAS

Both in central Oregon and in southern British Columbia (Lewis and others, 1988), abrupt increases in near-surface conductive heat flow are located well seaward (west) of the active volcanic zone. A common explanation seems likely. In each case, other workers (Blackwell and others, 1982a, 1990a; Lewis and others, 1988) have proposed a magmatic origin for the increase in heat flow. However, in each case the heat-flow increase coincides with the major discharge area for regional ground-water flow. In Oregon, the heat-flow transition coincides with a belt of hot springs in the Western Cascades (for example, Blackwell and others, 1982a, fig. 8), and in British Columbia it is located at the heads of fjords (Lewis and others, 1988, figs. 2 and 4) that represent the base level for ground-water flow. Systematic collection of water-chemistry data in British Columbia would help to determine whether a variant of the lateral-flow model (fig. 18A) can explain the Canadian observations.

Comparison with better-explored arcs provides some perspective on geothermal resource estimates for the central Oregon Cascade Range. The Taupo volcanic zone (TVZ) of New Zealand is petrologically and geomorphically very different from the Cascade Range: the dominantly rhyolitic eruptive products fill a broad structural and topographic depression. However, it is perhaps the only volcanic-arc segment where heat-discharge rates are as well known as in central Oregon. Table 11 compares length-normalized heat-discharge rates and resource estimates for the TVZ and central Oregon. Rates of volcanic production, volcanic heat discharge, and hydrothermal heat discharge are approximately an order of magnitude higher in the TVZ; the ratio of hydrothermal to volcanic heat discharge is larger. The New Zealand Department of Scientific and Industrial Research has estimated that the geothermal power potential of the TVZ (6 MW$_e$/km; Lawless and others, 1981) amounts to about one-third of the natural heat discharge (20 MW$_t$/km; Hedenquist, 1986). In contrast, the power estimates of Black and others (1983) for central Oregon (6 to 900 MW$_e$/km) are 4 to 500 times the natural heat discharge (about 2 MW$_t$/km). The relatively conservative New Zealand estimate is

TABLE 11.— *Heat discharge and geothermal resource estimates for central Oregon Cascade Range and Taupo volcanic zone*

[All rates are length-normalized. Production and heat-discharge rates for the TVZ were summarized by Hedenquist (1986). Estimates of geothermal potential are from Black and others (1983) and Lawless and others (1981). m.y., million years; MW, megawatts thermal; MWe, megawatts electrical]

	Cascade Range (length = 135 km)	Taupo volcanic zone (length = 250 km)
Volcanic production	3–6 km^3/m.y. (basaltic andesite)	33 km^3/m.y. (rhyolite)
Volcanic heat discharge	0.6 MW	4 MW
Hydrothermal heat discharge	1.1 MW	16 MW
Hydrothermal:volcanic heat discharge (ratio)	2	4
Estimated geothermal potential	6–900 MWe	6 MWe
Estimated geothermal potential : natural heat discharge (ratio)	4–500	0.3
Current geothermal power production	0 MWe	1 MWe

based on extensive research drilling and ongoing exploitation of three geothermal fields. Perhaps the published resource estimates for central Oregon are overly optimistic.

SUMMARY

The Cascade Range in central Oregon is characterized by relatively high Quaternary volcanic extrusion rates and hot-spring discharge rates and by high conductive heat flow. Extrusion rates and hot-spring discharge rates decrease both to the north and south, and conductive heat flow decreases to the north and possibly to the south.

All hot springs in the study area (between lat 44° and 45°15' N.) discharge from Miocene or Oligocene rocks at elevations of 440 to 680 m; there are no hot springs in the Quaternary arc. The hot springs are in the deeply incised valleys of major streams that originate in the Quaternary arc. The presence of hot springs within a relatively narrow elevation range implies that topography is a major control on their location; most of the hot springs are also located near the surface exposures of permeable structurally or stratigraphically controlled conduits.

The isotopic composition of thermal waters in the Western Cascades is similar to that of meteoric waters at elevations of 1,350 to 1,850 m. Recharge at elevations of 1,350 to 1,850 m implies recharge within the Quaternary arc, because only small areas outside the Quaternary arc reach such elevations. The isotopic composition of the Western Cascade thermal waters can also be explained in terms of local recharge under colder (Pleistocene) climatic conditions. Because the Western Cascade hot springs are located at sites that would tend to capture regional ground-water flow from the

Quaternary arc, we prefer to explain their isotopic composition in terms of recharge at higher elevations during the Holocene.

Commonly used geothermometers (silica, Na-K-Ca, and SO_4-H_2O) give disparate results when applied to the Na-Cl and Na-Ca-Cl waters of the Western Cascades. However, the SO_4-H_2O isotope equilibrium and anhydrite-saturation temperatures for these waters are similar, suggesting that the SO_4-H_2O temperatures (117–181°C) are the best indicators of thermal-fluid temperatures at depth.

Determinations of hot-spring discharge by a chloride-flux method indicate discharge rates that are generally higher than those reported previously. The product of hot-spring discharge, density, heat capacity, and the difference between a chemical geothermometer temperature and a reference temperature is a measure of advective heat transport by a hot-spring system. The total heat discharge for the hot-spring systems in the study area is about 148 MW, which represents a significant fraction of the regional heat budget.

These isotopic data and heat-discharge measurements indicate that gravitationally driven thermal-fluid circulation transports significant amounts of heat from the Quaternary arc into older Western Cascade rocks. This pattern of regional ground-water flow profoundly affects near-surface conductive heat flow. The Quaternary arc and adjacent 2- to 7-Ma volcanic rocks constitute a large area of low-to-zero near-surface conductive heat flow that results from downward and lateral flow of cold ground water. In contrast, near-surface conductive heat flow is anomalously high where rocks older than about 7 Ma are exposed in the eastern part of the Western Cascades physiographic subprovince. The thickness of the zone of low-to-zero conductive heat flow is poorly known and presumably highly

variable; it may thicken significantly beneath topographic highs. The relatively well documented heat-flow high in the Breitenbush Hot Springs area may be largely attributable to hydrothermal circulation.

A heat-budget analysis shows that sufficient heat is removed advectively from rocks younger than about 7 Ma to explain the anomalously high heat discharge measured on the flanks of the Cascade Range. The magnitude of relatively low-temperature advective heat discharge, the greatest source of uncertainty in the heat budget, is estimated by difference. The total heat-flow anomaly can be explained in terms of magmatic intrusion at rates of 9 to 33 cubic kilometers per kilometer of arc length per million years; the required intrusion rate varies depending on the degree of cooling assumed. These intrusion rates imply an intrusion-to-extrusion ratio in the range of 1.5 to 11.

Two alternative conceptual models have been proposed to explain the near-surface heat-flow observations. The models involve (1) an extensive midcrustal magmatic heat source underlying both the Quaternary arc and adjacent older rocks or (2) a relatively narrow, deep heat-flow anomaly that expands laterally at shallow depths due to ground-water flow (the lateral-flow model). Relative to the midcrustal heat source model, the lateral-flow model suggests a more limited geothermal resource base, but a better defined exploration target. Regional gravity, magnetic, and electrical geophysical data fail to distinguish between these alternative models.

Deep drilling in the areas of high heat flow in the older rocks could indicate which model is more appropriate for the near-surface heat-flow data. In such areas, uniformly high conductive heat flow would be consistent with the midcrustal heat source model, and reduced heat flow below zones of active ground-water circulation would be consistent with the lateral-flow model. The data from heat-flow site 61 (fig. 17) show reduced heat flow below a thermal aquifer, but the temperature profile can be matched with either a high (greater than 100 mW/m^2) or low (60–70 mW/m^2) background heat flow, depending on the longevity of the hydrothermal system.

We simulated ground-water flow and heat transport through two generalized geologic cross sections west of the Cascade Range crest: one in the Breitenbush area, where there is no evidence for major arc-parallel normal faulting, and one in the McKenzie River drainage, where major graben-bounding faults exist. The alternative conceptual models were simulated by varying the distribution

of deep heat sources. The results show that either model for the deep thermal structure can satisfy the near-surface thermal observations, and they also provide some constraints on the regional permeability structure: the bulk permeability of the youngest (less than 2.3 Ma) rock unit simulated is estimated to be about 10^{-14} m^2; that of the oldest (greater than 18 Ma) to be about 10^{-17} m^2. The near-surface heat-flow observations in the Breitenbush area are most readily explained in terms of lateral heat transport by regional ground-water flow. Given significant advective heat transport, the deep thermal structure cannot be uniquely inferred from the available data. The sparser thermal data set from the McKenzie River area can be explained either by deep regional ground-water flow or by a conduction-dominated system, with most ground-water flow confined to Quaternary rocks and fault zones.

The actual thermal structure of the Oregon Cascade Range is probably more complex than that represented by either of the models considered here. A fuller understanding of hydrothermal activity would require additional drill-hole data. Quantitative data regarding the deep permeability structure, which are critical to an understanding of hydrothermal circulation, are virtually nonexistent. Sets of permeability tests in wells with changing temperature gradients, like that observed at heat-flow site 61, would be particularly useful. Careful comparison with other, better-explored arcs may also prove productive. A comparison of length-normalized heat-discharge rates and resource estimates for the Taupo volcanic zone of New Zealand and central Oregon suggests that published resource estimates for central Oregon are optimistic.

REFERENCES CITED

Andrews, J.N., 1983, Dissolved radioelements and inert gases in geothermal investigations: Geothermics, v. 12, p. 21–23.

Armstrong, R.L., Taylor, E.M., Hales, P.O., and Parker, D.J., 1975, K-Ar dates for volcanic rocks, central Cascade Range of Oregon: Isochron/West, no. 13, p. 5–10.

Baldwin, E.M., 1976, Geology of Oregon (revised ed.): Dubuque, Iowa, Kendall/Hunt, 147 p.

Bentley, H.W., Phillips, F.M., Davis, S.N., Habermehl, M.A., Airey, P.L., Calf, G.E., Elmore, David, Gove, H.E., and Torgerson, Thomas, 1986, Chlorine 36 dating of very old groundwater 1. The Great Artesian Basin, Australia: Water Resources Research, v. 22, p. 1991–2001.

Black, G.L., 1983, Newberry hydrology, in Priest, G.R., Vogt, B.F., and Black, G.L., eds., Survey of potential geothermal exploration sites at Newberry volcano, Deschutes County, Oregon: Oregon Department of Geology and Mineral Industries Open-File Report O-83-3, p. 28–36.

Black, G.L., Blackwell, D.D., and Steele, J.L., 1983, Heat flow in the Oregon Cascades, in Priest, G.R., and Vogt, B.F., eds., Geology and geothermal resources of the central Oregon Cascade Range: Oregon Department of Geology and Mineral Industries Special Paper 15, p. 69–76.

Black, G.L., Woller, N.M., and Ferns, M.L., 1987, Geologic map of the Crescent Mountain area, Linn County, Oregon: Oregon Department of Geology and Mineral Industries Geological Map Series GMS-47, scale 1:62,500.

Blackwell, D.D., and Baker, S.L., 1988a, Thermal analysis of the Breitenbush geothermal system: Geothermal Resources Council Transactions, v. 12, p. 221–227.

———1988b, Thermal analysis of the Austin and Breitenbush geothermal systems, Western Cascades, Oregon, in Sherrod, D.R., ed., Geology and geothermal resources of the Breitenbush-Austin Hot Springs area, Clackamas and Marion Counties, Oregon: Oregon Department of Geology and Mineral Industries Open-File Report O-88-5, p. 47–62.

Blackwell, D.D., Bowen, R.G., Hull, D.A., Riccio, Joseph, and Steele, J.L., 1982a, Heat flow, arc volcanism, and subduction in northern Oregon: Journal of Geophysical Research, v. 87, p. 8735–8754.

Blackwell, D.D., Hull, D.A., Bowen, R.G., and Steele, J.L., 1978, Heat flow of Oregon: Oregon Department of Geology and Mineral Industries Special Paper 4, 42 p.

Blackwell, D.D., Murphey, C.F., and Steele, J.L., 1982b, Heat flow and geophysical log analysis for OMF-7A geothermal test well, in Priest, G.R., and Vogt, B.F., eds., Geology and geothermal resources of the Mt. Hood area, Oregon: Oregon Department of Geology and Mineral Industries Special Paper 14, p. 47–56.

Blackwell, D.D., and Steele, J.L., 1983, A summary of heat flow studies in the Cascade Range: Geothermal Resources Council Transactions, v. 7, p. 233-236.

———1985, Heat flow of the Cascade Range, in Guffanti, Marianne, and Muffler, L.J.P., eds., Proceedings of the workshop on geothermal resources of the Cascade Range, U.S. Geological Survey Open-File Report 85-521, p. 20–23.

———1987, Geothermal data from deep holes in the Oregon Cascade Range: Geothermal Resources Council Transactions, v. 11, p. 317–322.

Blackwell, D.D., Steele, J.L., Frohme, M.K., Murphy, C.F., Priest, G.R., and Black, G.L., 1990a, Heat flow in the Oregon Cascade Range and its correlation with regional gravity, Curie point depths, and geology: Journal of Geophysical Research, v. 95, p. 19,475–19,494.

Blackwell, D.D., Steele, J.L., Kelley, Shari, and Korosec, M.A., 1990b, Heat flow in the State of Washington and Cascade thermal conditions: Journal of Geophysical Research, v. 95, p. 19,495–19,516.

Blakely, R.J., 1988, Curie temperature isotherm analysis and tectonic implications of aeromagnetic data from Nevada: Journal of Geophysical Research, v. 93, p. 11,817–11,832.

Blakely, R.J., and Jachens, R.C., 1990, Volcanism, isostatic residual gravity, and regional tectonic setting of the Cascade volcanic province: Journal of Geophysical Research, v. 95, p. 19,439–19,452.

Blattner, P., 1985, Isotope shift data and the natural evolution of geothermal systems: Chemical Geology, v. 49, p. 187–203.

Bloomquist, R.G., Black, G.L., Parker, D.S., Sifford, A., Simpson, S.J., and Street, L.V., 1985, Evaluation and ranking of geothermal resources for electrical generation or electrical offset in Idaho, Montana, Oregon and Washington: U.S. Department of Energy, Bonneville Power Administration, DOE/BP-13609-1, v. 1, 504 p.

Bodvarsson, G.S., 1982, Mathematical modeling of geothermal systems: Berkeley, University of California, Ph.D. dissertation, published as Lawrence Berkeley Laboratory report LBL-13937, 348 p.

Bolke, E.L., and Laenan, Antonius, 1989, Ground-water inflow to the Deschutes River near the Warm Springs Indian Reservation, Oregon, August 1985: U.S. Geological Survey Water-Resources Investigations Report 88-4184, 18 p.

Brehler, B., and Fuge, R., 1978, Bromine, in Wedepohl, K.H., ed., Handbook of geochemistry, v. 2, no. 3: New York, Springer, variously paginated.

Brook, C.A., Mariner, R.H., Mabey, D.R., Swanson, J.R., Guffanti, Marianne, and Muffler, L.J.P., 1979, Hydrothermal convection systems with reservoir temperatures >90°C, in Muffler, L.J.P., ed., Assessment of geothermal resources of the United States-1978: U.S. Geological Survey Circular 790, p. 18–85.

Brown, D.E., Black, G.L., McLean, G.D., and Petros, J.R., 1980a, Preliminary geology and geothermal resource potential of the Powell Buttes area, Oregon: Oregon Department of Geology and Mineral Industries Open-File Report O-80-8, 117 p.

Brown, D.E., McLean, G.D., Priest, G.R., Woller, N.M., and Black, G.L., 1980b, Preliminary geology and geothermal resource potential of the Belknap-Foley area, Oregon: Oregon Department of Geology and Mineral Industries Open-File Report O-80-2, 58 p.

Buchanan, T.J., and Somers, W.P., 1969, Discharge measurements at gaging stations: Techniques of Water-Resources Investigations of the U.S. Geological Survey, Book 3, Chapter A8, 65 p.

Burnham, C.W., 1979, Magmas and hydrothermal fluids, in Barnes, H.L., ed., Geochemistry of hydothermal ore deposits: New York, Wiley, p. 71-136.

Callaghan, Eugene, 1933, Some features of the volcanic sequence in the Cascade Range in Oregon: Transactions American Geophysical Union, 14th Annual Meeting, p. 243–249.

Callaghan, Eugene, and Buddington, A.F., 1938, Metalliferous mineral deposits of the Cascade Range in Oregon: U.S. Geological Survey Bulletin 893, 141 p.

Connard, Gerald, Couch, R.W., and Gemperle, Michael, 1983, Analysis of aeromagnetic measurements from the Cascade Range in central Oregon: Geophysics, v. 48, p. 376–390.

Conrey, R.M., and Sherrod, D.R., 1988, Stratigraphy of drill holes and geochemistry of surface rocks, Breitenbush Hot Springs 15-minute quadrangle, Cascade Range, Oregon, in Sherrod, D.R., ed., Geology and geothermal resources of the Breitenbush-Austin Hot Springs area, Clackamas and Marion Counties, Oregon: Oregon Department of Geology and Mineral Industries Open-File Report O-88-5, p. 15–29.

Couch, R.W., Pitts, G.S., Gemperle, Michael, Braman, D.E., and Veen, C.A., 1982a, Gravity anomalies in the Cascade Range in Oregon: Structural and thermal implications: Oregon Department of Geology and Mineral Industries Open-File Report O-82-9, 66 p.

Couch, R.W., Pitts, G.S., Gemperle, Michael, Veen, C.A., and Braman, D.E., 1982b, Residual gravity maps, northern, central, and southern Oregon Cascade Range: Oregon Department of Geology and Mineral Industries Geological Map Series GMS-26, scale 1:250,000.

Craig, Harmon, 1961a, Isotopic variations in meteoric waters: Science, v. 133, p. 1702–1703.

———1961b, Standard for reporting concentrations of deuterium and oxygen-18 in natural waters: Science, v. 133, p. 1833–1834.

————1963, The isotopic geochemistry of water and carbon in geothermal areas, in Nuclear geology on geothermal areas: Pisa, Consiglio Nazionale delle Ricerche Laboratorio di Geologia Nucleare, p. 17–53.

Craig, H., Lupton, J.E., and Horie, Yoshio, 1978, A mantle component in circum-Pacific volcanic gases: Hakone, the Marianas, and Mt. Lassen, in Alexander, E.C., Jr., and Ozima, M., eds., Terrestrial rare gases: Tokyo, Center for Academic Publications Japan, p. 3–16.

Dansgaard, W., 1964, Stable isotopes in precipitation: Tellus, v. 16, p. 436–468.

Ellis, A.J., and Mahon, W.A.J., 1977, Chemistry and geothermal systems: New York, Academic Press, 392 p.

Ellis, A.J., and Wilson, S.H., 1955, The heat from the Wairakei-Taupo thermal region calculated from the chloride output: New Zealand Journal of Science and Technology, v. 36, p. 622–631.

Faure, Gunter, 1986, Principles of isotope geology (second ed.): New York, Wiley, 589 p.

Ferronsky, V.I., Vlasova, L.S., Esikov, A.D., Polyakov, V.A., Seletsky, Yu.B., Punning, Ya.-M.K., and Vajkmyaeh, R.A., 1983, Relationships between climatic changes and variations in isotopic composition of groundwater, precipitation, and organic soil matter in the Quaternary Period, in Palaeoclimates and palaeowaters: A collection of environmental isotope studies: Vienna, International Atomic Energy Agency, p. 13–35.

Flaherty, G.M., 1981, The Western Cascade-High Cascade transition in the McKenzie Bridge area, central Oregon Cascade Range: Eugene, University of Oregon, M.S. thesis, 178 p.

Foote, R.W., 1985, Curie-point isotherm mapping and interpretation from aeromagnetic measurements in the northern Oregon Cascades: Corvallis, Oregon State University, M.S. thesis, 115 p.

Forster, C.B., 1987, Interaction of groundwater flow systems and thermal regimes in mountainous terrain: A numerical study: Vancouver, University of British Columbia, Ph.D. thesis, 202 p.

Forster, C.B., and Smith, Leslie, 1988, Groundwater flow in mountainous terrain 2. Controlling factors: Water Resources Research, v. 24, p. 1011–1023.

Fournier, R.O., 1981, Application of water chemistry to geothermal exploration and reservoir engineering, in Rybach, L., and Muffler, L.J.P., eds., Geothermal systems: Principles and case histories: Chichester, Wiley, p. 109–143.

Fournier, R.O., and Rowe, J.J., 1966, Estimation of underground temperatures from the silica content of water from hot springs and wet-steam wells: American Journal of Science, v. 264, p. 685–697.

Fournier, R.O., and Truesdell, A.H., 1973, An empirical Na-K-Ca geothermometer for natural waters: Geochimica et Cosmochimica Acta, v. 37, p. 1255–1275.

Frank, F.J., 1979, Ground water in the Myrtle Creek-Glendale area, Douglas County, Oregon: U.S. Geological Survey Water-Resources Investigations 79-8, scale 1:62,500.

Friedman, Irving, and Smith, G.I., 1970, Deuterium content of snow cores from Sierra Nevada area: Science, v. 169, p. 467–470.

Gat, J.R., 1980, The isotopes of hydrogen and oxygen in precipitation, in Fritz, P., and Fontes, J.Ch., eds., Handbook of environmental isotope geochemistry, vol. 1: Amsterdam, Elsevier, p. 21–47.

Giggenbach, W.F., 1986, Graphical techniques for the evaluation of water/rock equilibrium conditions by use of Na, K, Mg, and Ca contents of discharge waters: Proceedings of the Eighth New Zealand Geothermal Workshop, Auckland, New Zealand, p. 37–43.

Godson, R.H., and Scheibe, D.M., 1982, Description of magnetic tape containing conterminous U.S. gravity data in gridded format: National Technical Information Service Report PB-254798, 5 p.

Hamilton, Warren, and Myers, W.B., 1966, Cenozoic tectonics of the western United States: Reviews of Geophysics, v. 4, p. 509–549.

Hardie, L.A., 1983, Origin of $CaCl_2$ brines by basalt-seawater interaction: Insights provided by some simple mass balance calculations: Contributions to Mineralogy and Petrology, v. 82, p. 205–213.

Harris, P.G., Kennedy, W.Q., and Scarfe, C.M., 1970, Volcanism versus plutonism-The effect of chemical composition, in Newall, G., and Rast, N., eds., Mechanism of igneous intrusion: Geological Journal Special Issue 2, p. 187–200.

Hasabe, K., Fujii, N., and Uyeda, S., 1970, Thermal processes under island arcs: Tectonophysics, v. 10, p. 335–355.

Hedenquist, J.W., 1986, Geothermal systems in the Taupo volcanic zone: Their characteristics and relation to volcanism and mineralisation, in Smith, I.E.M., ed., Late Cenozoic volcanism in New Zealand: Royal Society of New Zealand Bulletin 23, p. 134–168.

Hem, J.D., 1985, Study and interpretation of the chemical characteristics of natural water: U.S. Geological Survey Water-Supply Paper 2254, 263 p.

Hildreth, Wes, 1981, Gradients in silicic magma chambers: Implications for lithospheric magmatism: Journal of Geophysical Research, v. 86, p. 10,153–10,192.

Ingebritsen, S.E., Mariner, R.H., Cassidy, D.E., Shepherd, L.D., Presser, T.S., Pringle, M.K.W., and White, L.D., 1988, Heat-flow and water-chemistry data from the Cascade Range and adjacent areas in north-central Oregon: U.S. Geological Survey Open-File Report 88-702, 205 p.

Ingebritsen, S.E., Mariner, R.H., and Sherrod, D.R., 1991, Hydrothermal systems of the Cascade Range, north-central Oregon: U.S. Geological Survey Open-File Report 91-69, 217 p.

Ingebritsen, S.E., Scholl, M.A., and Sherrod, D.R., 1993, Heat flow from four new research drill holes in the Western Cascades, Oregon, U.S.A.: Geothermics, v. 22, p. 151–163.

Ingebritsen, S.E., Sherrod, D.R., and Mariner, R.H., 1989, Heat flow and hydrothermal circulation in the Cascade Range, north-central Oregon: Science, v. 243, p. 1458–1462.

Ingebritsen, S.E., and Sorey, M.L., 1985, A quantitative analysis of the Lassen hydrothermal system, north central California: Water Resources Research, v. 21, p. 853–868.

Jaeger, J.C., 1964, Thermal effects of intrusions: Reviews of Geophysics, v. 2, p. 443–466.

Jessop, A.M., Hobart, M.A., and Schlater, J.G., 1976, The world heat flow data collection-1975: Geothermal Service of Canada Geothermal Series Number 5, 125 p.

Junge, C.E., and Werby, R.T., 1958, The concentration of chloride, sodium, potassium, calcium, and sulfate in rain water over the United States: Journal of Meteorology, v. 15, p. 417–425.

Keach, R.W., II, Oliver, J.E., Brown, L.D., and Kaufman, S., 1989, Cenozoic active margin and shallow Cascades structure: COCORP results from western Oregon: Geological Society of America Bulletin, v. 101, p. 783–794.

Keith, T.E.C., 1988, Hydrothermal alteration patterns in the Breitenbush Hot Springs area, Cascade Range, Oregon: Geothermal Resources Council Transactions, v. 12, p. 299–304.

Kharaka, Y.K., Gunter, W.D., Aggarwal, P.K., Perkins, E.H., and DeBraal, J.D., 1988, SOLMINEQ.88: A computer program for geochemical modeling of water-rock interactions: U.S. Geological Survey Water-Resources Investigations Report 88-4227, 420 p.

Larson, P.B., and Taylor, H.P., Jr., 1986, An oxygen isotope study of hydrothermal alteration in the Lake City caldera, San Juan Mountains, Colorado: Journal of Volcanology and Geothermal Research, v. 30, p. 47–82.

Lawless, J.V., Lumb, J.T., Clelland, L., Kear, D., and Drew, S.R., 1981, Geothermal energy for New Zealand's future: New Zealand Department of Scientific and Industrial Research Bulletin 229, 40 p.

Lewis, T.J., Bentkowski, W.H., Davis, E.E., Hyndman, R.D., Souther, J.G., and Wright, J.A., 1988, Subduction of the Juan de Fuca plate: Thermal consequences: Journal of Geophysical Research, v. 93, p. 15,207–15,225.

MacLeod, N.S., and Sammel, E.A., 1982, Newberry Volcano, Oregon: A Cascade Range geothermal prospect: California Geology, v. 35, p. 235–244.

MacLeod, N.S., and Sherrod, D.R., 1988, Geologic evidence for a magma chamber beneath Newberry volcano, Oregon: Journal of Geophysical Research, v. 93, p. 10,067–10,079.

Mariner, R.H., Presser, T.S., and Evans, W.C., 1977, Hot springs of the central Sierra Nevada, California: U.S. Geological Survey Open-File Report 77-559, 27 p.

———1993, Geothermometry and water-rock interaction in selected thermal systems in the Cascade Range and Modoc Plateau, western United States: Geothermics, v. 22, p. 1–15.

Mariner, R.H., Presser, T.S., Evans, W.C., and Pringle, M.K.W., 1989, Discharge rates of thermal fluids in the Cascade Range of Oregon and Washington and their relationship to the geologic environment, in Muffler, L.J.P., Weaver, C.S., and Blackwell, D.D., eds., Proceedings of workshop XLIV: Geological, geophysical, and tectonic setting of the Cascade Range: U.S. Geological Survey Open-File Report 89-178, p. 663–694.

———1990, Discharge rates of fluid and heat by thermal springs of the Cascade Range, Washington, Oregon, and northern California: Journal of Geophysical Research, 95, p. 19,517–19,532.

Mariner, R.H., Swanson, J.R., Orris, G.J., Presser, T.S., and Evans, W.C., 1980, Chemical and isotopic data for water from thermal springs and wells of Oregon: U.S. Geological Survey Open-File Report 80-737, 50 p.

Mase, C.W., Sass, J.H., Lachenbruch, A.H., and Munroe, R.J., 1982, Preliminary heat-flow investigations of the California Cascades: U.S. Geological Survey Open-File Report 82-150, 240 p.

McFarland, W.D., 1982, A description of aquifer units in western Oregon: U.S. Geological Survey Open-File Report 82-165, 35 p.

McKenzie, W.F., and Truesdell, A.H., 1977, Geothermal reservoir temperatures estimated from the oxygen isotope compositions of dissolved sulfate and water from hot springs and shallow drillholes: Geothermics, v. 5, p. 51–61.

Miller, P.R., and Orr, W.N., 1984a, Geologic map of the Wilhoit quadrangle, Oregon: Oregon Department of Geology and Mineral Industries Geological Map Series GMS-32, scale 1:24,000.

———1984b, Geologic map of the Scotts Mill quadrangle, Oregon: Oregon Department of Geology and Mineral Industries Geological Map Series GMS-33, scale 1:24,000.

Mizutani, Y., and Rafter, T.A., 1969, Oxygen isotopic composition of sulphates—Part 3. Oxygen isotopic fractionation in the bisulfate ion-water system: New Zealand Journal of Science, v. 12, p. 54–59.

Muffler, L.J.P., Bacon, C.R., and Duffield, W.A., 1982, Geothermal systems of the Cascade Range: Proceedings of the Pacific Geothermal Conference, Auckland, New Zealand, p. 337–343.

National Oceanic and Atmospheric Administration, 1985, Climates of the states (two volumes): Detroit, Gale Research Company, 1572 p.

Orr, W.N., and Miller, P.R., 1984, Geologic map of the Stayton quadrangle, Oregon: Oregon Department of Geology and Mineral Industries Geological Map Series GMS-34, scale 1:24,000.

———1986a, Geologic map of the Drake Crossing quadrangle, Marion County, Oregon: Oregon Department of Geology and Mineral Industries Geological Map Series GMS-50, scale 1:24,000.

———1986b, Geologic map of the Elk Prairie quadrangle, Marion and Clackamas Counties, Oregon: Oregon Department of Geology and Mineral Industries Geological Map Series GMS-51, scale 1:24,000.

Peck, D.L., Griggs, A.B., Schlicker, H.G., Wells, F.G., and Dole, H.M., 1964, Geology of the central and northern parts of the Western Cascade Range in Oregon: U.S. Geological Survey Professional Paper 449, 56 p.

Priest, G.R., 1985, Geothermal exploration in Oregon, 1984: Oregon Geology, v. 47, p. 63–66.

———ed., 1987, Investigation of the thermal regime and geologic history of the Cascade volcanic arc: First phase of a program for scientific drilling in the Cascade Range: Oregon Department of Geology and Mineral Industries Open-File Report O-86-3, 120 p.

———1990, Volcanic and tectonic evolution of the Cascade volcanic arc, central Oregon: Journal of Geophysical Research, v. 95, p. 19,583–19,600.

Priest, G.R., Black, G.L., Woller, N.M., and Taylor, E.M., 1988, Geologic map of the McKenzie Bridge quadrangle, Lane County, Oregon: Oregon Department of Geology and Mineral Industries Geological Map Series GMS-48, scale 1:62,500.

Priest, G.R., Mattinson, J.M., and Damon, P.E., 1989, Implications of new isotopic ages from drill holes in the Oregon Cascades [abs.]: Eos, Transactions American Geophysical Union, v. 70, p. 1299.

Priest, G.R., Woller, N.M., Black, G.L., and Evans, S.H., 1983, Overview of the central Oregon Cascade Range, in Priest, G.R., and Vogt, B.F., eds., Geology and geothermal resources of the central Oregon Cascade Range: Oregon Department of Geology and Mineral Industries Special Paper 15, p. 3–28.

Priest, G.R., Woller, N.M., and Ferns, M.L., 1987, Geologic map of the Breitenbush River area, Linn and Marion Counties, Oregon: Oregon Department of Geology and Mineral Industries Geological Map Series GMS-46, scale 1:62,500.

Riddihough, R.P., Finn, Carol, and Couch, R.W., 1986, The Klamath-Blue Mountain lineament: Geology, v. 14, p. 528–531.

Robison, J.H., 1974, Availability and quality of ground water in the Sutherlin area, Douglas County, Oregon: U.S. Geological Survey Water-Resources Investigations 74-32, scale 1:62,500.

Robison, J.H., and Collins, C.A., 1977, Availability and quality of ground water in the Drain-Yoncalla area, Douglas County, Oregon: U.S. Geological Survey Water-Resources Investigations 76-105, scale 1:62,500.

Robison, J.H., and Laenan, Antonius, 1976, Water resources of the Warm Springs Indian Reservation, Oregon: U.S. Geological Survey Water Resources Investigations 76-26, 85 p.

Sass, J.H., and Munroe, R.J., 1974, Basic heat-flow data from the United States: U.S. Geological Survey Open-File Report 74-9, 451 p.

Sass, J.H., and Sammel, E.A., 1976, Heat flow data and their relation to observed geothermal phenomena near Klamath Falls, Oregon: Journal of Geophysical Research, v. 81, p. 4863–4868.

Schuster, J.E., Blackwell, D.D., Hammond, P.E., and Hunting, M.T., 1978, Heat flow studies in the Steamboat Mountain-Lemei Rock area, Skamania County, Washington: State of Washington Department of Natural Resources, Division of Geology and Earth Resources Information Circular 62, 56 p.

Sherrod, D.R., 1986, Geology, petrology, and volcanic history of a portion of the Cascade Range between latitudes 43°–44° N, central Oregon, U.S.A.: Santa Barbara, University of California, Ph.D. thesis, 320 p.

Sherrod, D.R., and Conrey, R.M., 1988, Geologic setting of the Breitenbush-Austin Hot Springs area, Cascade Range, north-central Oregon, in Sherrod, D.R., ed., Geology and geothermal resources of the Breitenbush-Austin Hot Springs area, Clackamas and Marion Counties, Oregon: Oregon Department of Geology and Mineral Industries Open-File Report O-88-5, p. 1–14.

Sherrod, D.R., and Pickthorn, L.G., 1989, Some notes on the structural evolution of the Cascade Range in Oregon, in Muffler, L.J.P., Weaver, C.S., and Blackwell, D.D., eds., Proceedings of Workshop XLIV: Geological, geophysical, and tectonic setting of the Cascade Range: U.S. Geological Survey Open-File Report 89-178, p. 451–468.

Sherrod, D.R., and Smith, J.G., 1989, Preliminary map of upper Eocene to Holocene volcanic and related rocks of the Cascade Range, Oregon: U.S. Geological Survey Open-File Report 89-14, scale 1:500,000.

——1990, Quaternary extrusion rates of the Cascade Range, northwestern United States and southern British Columbia: Journal of Geophysical Research, v. 95, p. 19,465–19,474.

Simpson, R.W., Jachens, R.C., Blakely, R.J., and Saltus, R.W., 1986, A new isostatic residual gravity map of the conterminous United States with a discussion of the significance of isostatic residual anomalies: Journal of Geophysical Research, v. 91, p. 8348–8372.

Smith, G.A., Snee, L.W., and Taylor, E.M., 1987, Stratigraphic, sedimentologic, and petrologic record of late Miocene subsidence of the central Oregon High Cascades: Geology, v. 15, p. 389–392.

Smith, G.A., and Taylor, E.M., 1983, The central Oregon High Cascade graben: What? When? Where?: Geothermal Resources Council Transactions, v. 7, p. 275–279.

Smith, G.A., Vincent, K.R., and Snee, L.W., 1989, An isostatic model for basin formation in and adjacent to the central Oregon High Cascade Range, in Muffler, L.J.P., Weaver, C.S., and Blackwell, D.D., eds., Proceedings of Workshop XLIV: Geological, geophysical, and tectonic setting of the Cascade Range: U.S. Geological Survey Open-File Report 89-178, p. 411–429.

Smith, J.G., 1989, Geologic map of upper Eocene to Holocene volcanic and related rocks in the Cascade Range, Washington: U.S. Geological Survey Open-File Report 89-311, scale 1:500,000.

Smith, Leslie, and Chapman, D.S., 1983, On the thermal effects of groundwater flow, 1. Regional scale systems: Journal of Geophysical Research, v. 88, p. 593–608.

Smith, R.L., and Shaw, H.R., 1975, Igneous-related geothermal systems, in White, D.E., and Williams, D.L., eds., Assessment of geothermal resources of the United States-1975: U.S. Geological Survey Circular 726, p. 58–83.

——1979, Igneous-related geothermal systems, in Muffler, L.J.P., ed., Assessment of geothermal resources of the United States—1978: U.S. Geological Survey Circular 790, p. 12–17.

Stanley, W.D., Fuis, G.S., and Mooney, W.D., 1989, Details of crustal structure in the Cascade Range and surrounding regions from seismic and magnetotelluric data, in Muffler, L.J.P., Weaver, C.S., and Blackwell, D.D., eds., Proceedings of workshop XLIV: Geological, geophysical, and tectonic setting of the Cascade Range: U.S. Geological Survey Open-File Report 89-178, p. 31–73.

Stanley, W.D., Mooney, W.D., and Fuis, G.S., 1990, Deep crustal structure of the Cascade Range and surrounding regions from seismic refraction and magnetotelluric data: Journal of Geophysical Research, v. 95, p. 19,419–19,438.

Steele, J.L., Blackwell, D.D., and Robison, J.H., 1982, Heat flow in the vicinity of the Mount Hood volcano, Oregon, in Priest, G.R., and Vogt, B.F., eds., Geology and geothermal resources of the Mt. Hood area, Oregon: Oregon Department of Geology and Mineral Industries Special Paper 14, p. 31–42.

Swanberg, C.A., Walkey, W.C., and Combs, Jim, 1988, Core hole drilling and the "rain curtain" phenomenon at Newberry Volcano, Oregon: Journal of Geophysical Research, v. 93, p. 10,163–10,173.

Taylor, E.M., 1981, Central Oregon High Cascade roadside geology: Bend, Sisters, McKenzie Pass, and Santiam Pass, Oregon, in Johnston, D.A., and Donnelly-Nolan, Julie, eds., Guides to some volcanic terranes in Washington, Idaho, Oregon, and northern California: U.S. Geological Survey Circular 838, p. 55–83.

Taylor, E.M., MacLeod, N.S., Sherrod, D.R., and Walker, G.W., 1987, Geologic map of the Three Sisters Wilderness, Deschutes, Lane, and Linn Counties, Oregon: U.S. Geological Survey Miscellaneous Field Studies Map MF-1952, scale 1:63,360.

Taylor, H.P., Jr., 1971, Oxygen isotope evidence for large-scale interaction between meteoric ground waters and Tertiary granodioritic intrusions, Western Cascade Range, Oregon: Journal of Geophysical Research, v. 76, p. 7855–7874.

Thayer, T.P., 1936, Structure of the North Santiam River section of the Cascade Mountains in Oregon: Journal of Geology, v. 44, p. 701–716.

Tolstikhin, I.N., 1978, A review: Some recent advances in isotope geochemistry of light rare gases, in Alexander, E.C., Jr., and Ozima, M., eds., Terrestial rare gases: Tokyo, Center for Academic Publications Japan, p. 33–62.

U.S. Department of Agriculture, Soil Conservation Service, 1964, State of Oregon normal annual precipitation 1930-1957: Portland, U.S. Department of Agriculture, Soil Conservation Service, scale 1:2,000,000.

U.S. Geological Survey, 1983a, Water resources data for Oregon water year 1981: Volume 2. Western Oregon: U.S. Geological Survey Water-Data Report OR-81-2, 522 p.

——1983b, Water resources data for Oregon water year 1982: Volume 2. Western Oregon: U.S. Geological Survey Water-Data Report OR-82-2, 432 p.

——1984, Water resources data for Oregon water year 1983: Volume 1. Western Oregon: U.S. Geological Survey Water-Data Report OR-83-2, 424 p.

——1986a, Water resources data for Oregon water year 1984: Volume 1. Eastern Oregon: U.S. Geological Survey Water-Data Report OR-84-1, 238 p.

——1986b, Water resources data for Oregon water year 1984: Volume 2. Western Oregon: U.S. Geological Survey Water-Data Report OR-84-2, 481 p.

——1987a, Water resources data for Oregon water year 1985: Volume 1. Eastern Oregon: U.S. Geological Survey Water-Data Report OR-85-1, 218 p.

——1987b, Water resources data for Oregon water year 1985: Volume 2. Western Oregon: U.S. Geological Survey Water-Data Report OR-85-2, 396 p.

——1988a, Water resources data for Oregon water year 1986: Volume 1. Eastern Oregon: U.S. Geological Survey Water-Data Report OR-86-1, 244 p.

——1988b, Water resources data for Oregon water year 1986: Volume 2. Western Oregon: U.S. Geological Survey Water-Data Report OR-86-2, 410 p.

Wadge, G., 1984, Comparison of volcanic production rates and subduction rates in the Lesser Antilles and Central America: Geology, v. 12, p. 555–558.

Walker, G.W., and Duncan, R.A., 1989, Geologic map of the Salem 1° by 2° quadrangle, Oregon: U.S. Geological Survey Miscellaneous Investigations Map I-1893, scale 1:250,000.

Walker, G.W., MacLeod, N.S., and Blakely, R.J., 1985, Mineral resource potential of the Bull of the Woods Wilderness, Clackamas and Marion Counties, Oregon: U.S. Geological Survey Open-File Report 85-247, 28 p.

Wareham, S.I., 1986, Geology and petroleum potential of the Hay Creek anticline, north-central Oregon: Loma Linda, Calif., Loma Linda University, M.S. thesis, 65 p.

Waring, G.A., 1965, Thermal springs of the United States and other countries of the world—A summary: U.S. Geological Survey Professional Paper 492, 383 p.

Weaver, C.S., and Smith, S.W., 1983, Regional tectonic and earthquake hazard implications of a crustal fault zone in southwestern Washington: Journal of Geophysical Research, v. 88, p. 10,371–10,383.

Wells, F.G., and Peck, D.L., 1961, Geologic map of Oregon west of the 121st meridian: U.S. Geological Survey Miscellaneous Investigations Map I-325, scale 1:500,000.

White, A.F., and Peterson, M.L., 1991, Chemical equilibrium and mass balance relationships associated with the Long Valley hydrothermal system, California, U.S.A.: Journal of Volcanology and Geothermal Research, v. 48, p. 283–302.

White, C.M., 1980, Geology of the Breitenbush Hot Springs quadrangle, Oregon: Oregon Department of Geology and Mineral Industries Special Paper 9, 26 p.

Ziagos, J.P., and Blackwell, D.D., 1986, A model for the transient temperature effects of horizontal fluid flow in geothermal systems: Journal of Volcanology and Geothermal Research, v. 27, p. 371–397.

APPENDIX.—*Conductive heat-flow data from the Cascade Range and adjacent areas in north-central Oregon*

[Some of these data have been published and analyzed previously. Where available, previously published information is shown below our analysis for the sake of comparison: (1) indicates information from Blackwell and others, 1982a; (2) = Black and others, 1983; (3) = Steele and others, 1982; (4) = Blackwell and Baker, 1988; and (5) = Brown and others, 1980a. Names are from the referenced publications or from well logs on file with the Oregon Department of Water Resources. Dashes indicate the absence of data. Values followed by "e" are approximate. Sites are ordered by township, range, and section, in parentheses where unsurveyed. Codes: OR, Oregon Department of Geology and Mineral Industries files; US, U.S. Geological Survey files; SU, Sunoco Energy Development Company; UT, University of Utah Research Institute. Static water level is reported in meters below land surface. Interval is the depth interval over which the reported gradient was measured. Previously published measured thermal conductivity values are used when available. Square brackets signify previously published estimated values. Values followed by "e" are estimated from the drill hole lithology based on the summary statistics of table 8. The standard error is shown in parentheses. In cases where the measured values were published without any measure of error, or where we rely on published estimates, we have no basis for assigning uncertainties. In general, the previously published measured thermal conductivity values are ±5–10 percent, and the summary statistics of table 8 suggest that the estimated values are ±20 percent or better, depending on the lithology. Nearly isothermal temperature profiles are indicated by "iso." Nonisothermal advectively disturbed profiles are indicated by "adv." The standard deviation of the uncorrected gradient is shown in parentheses. Most of the terrain corrections were done with a two-dimensional numerical heat-conduction model (T.C. Lee, University of California–Riverside, written commun., 1987). Where the topography could not readily be represented in two dimensions, the maximum possible two-dimensional correction was used, in order to bracket the actual corrected gradient. In these cases the corrected gradients (and heat flow values) are modified by greater than (>) or less than (<) signs. Where the two-dimensional correction is a very poor approximation the corrected gradient is followed by an "e". The corrected gradient for site 87 is a "background" value from Ziagos and Blackwell (1986). Heat flow is the product of thermal conductivity and the corrected gradient. Square brackets indicate poorer quality estimates. The approximate reliability of the heat-flow estimates can be calculated from the standard deviation of the uncorrected gradient and some statistical measure of the standard error of the thermal conductivity (shown below); the inexact terrain correction is an additional source of error that is difficult to quantify. Abbreviations: U.S.D.A., U.S. Department of Agriculture; U.S.F.S., U.S. Forest Service; CG., Campground; L., Lake; R., River]

	T-R-Sec. 1/4	Longitude	Latitude	Name	Code	Date logged (mo/d/yr)	Elev. (m)	Depth (m)	Static water level (m)	Bottom-hole temp. (°C)	Interval (m)	Therm. cond. (W/m·K)	Gradient (°C/km) Uncorr.	Gradient (°C/km) Corr.	Heat flow (mW/m²)
									West of the Cascade crest						
1.	3S-4E-03 NE	122°17'30"	45°20'25"	—	OR	07/27/77	287	92	10–13	12.2	75–90	1.35e (0.20)	55.6 (1.52) adv.	>51.0	[>69]
2.	3S-4E-18 NW	122°22'13"	45°18'56"	—	US	08/07/85	111	65	39.6	11.0	—	—	adv.	—	—
3.	3S-4E-23 SE	122°16'46"	45°17'22"	—	US	08/04/86	337	49	32	11.8	39–49	1.40e (0.20)	32.8 (4.69)	32.8	[46]
4.	3S-4E-27 SW	122°18'25"	45°16'29"	—	US	06/07/85	256	50	—	11.5	38–50	1.40e (0.20)	49.1 (4.16)	52.0	[73]
5.	3S-4E-28 NW	122°19'48"	45°16'53"	Short	OR	07/07/81	129	63	10–15	11.7	50–63	1.40e (0.20)	26.8 (2.71)	>25.7	[>36]
6.	3S-4E-29 NW	122°20'31"	45°17'08"	—	OR	07/08/81	131	205	20	16.5	21–205	1.51e (0.20)	39.9 (1.48)	>36.6	>55
7.	3S-4E-33 NE	122°19'41"	45°15'31"	—	US	07/19/86	154	114	58.8	15.6	—	—	adv.	—	—
8.	3S-4E-35 SW	122°16'58"	45°15'34"	—	US	11/11/88	341	60	27	11.5	34–60	1.40e (0.20)	18.7 (0.33)	>20.1	>28
9.	3S-5E-20 NE	122°12'37"	45°17'51"	Elliot	OR	07/10/81	451	61	10–15	9.8	15–61	1.40e (0.20)	7.8 (0.43)	8.7	[12]
10.	3S-5E-28 SW	122°12'10"	45°16'36"	—	US	08/04/86	280	98	66	13.6	—	—	iso.	—	—
11.	4S-5E-29 NE	122°12'55"	45°11'45"	U.S.D.A.	US	08/13/85	207	20	4.3	10.2	15–20	1.60e (0.15)	47.4 (8.60)	34.1	[55]
12.	5S-5E-02 SE	122°09'05"	45°09'43"	U.S.D.A.	US	08/13/85	280	25	6.0	9.3	15–25	1.60e (0.15)	55.3 (2.06)	>42.2	[>68]
13.	5S-5E-23 SE	122°09'22"	45°07'04"	Fish Creek	US	04/17/92	488	150	—	16.6	43–150	1.42 (0.12)	66.7 (0.3)	51.4	73
14.	5S-6E-06 SE	122°06'49"	45°09'32"	— (Roaring R. CG.)	US	08/08/85	311	40	4.5	10.6	23–40	1.60e (0.15)	56.7 (1.50)	>43.6	>70
15.	5S-6E-36 SE	122°00'56"	45°05'28"	— (Oak Grove Work Center)	US	10/17/88	607	67	15	7.6	—	—	adv.	—	—

APPENDIX.—*Conductive heat-flow data from the Cascade Range and adjacent areas in north-central Oregon*—Continued

West of the Cascade crest—Continued

No.	T-R-Sec. 1/4	Longitude	Latitude	Name	Code	Date logged (mo/d/yr)	Elev. (m)	Depth (m)	Static water level (m)	Bottom-hole temp. (°C)	Interval (m)	Therm. cond. (W/m·K)	Gradient Uncorr. (°C/km)	Gradient Corr. (°C/km)	Heat flow (mW/m²)
16.	6S-1E-13 SE	122°37'11"	45°02'51"	TWW	OR	10/06/76	326	140	—	14.9	95–140	1.38	34.8 (0.67)	37.8	44
17.	6S-1E-35 SW	122°39'26"	45°00'20"	MC-WW	OR	10/06/76	285	195	—	(1,2): 15.2	35–95	1.59	26.2	28.6	45
											95–140	[1.17]	34.7	37.7	44
											110–195	[1.17]	31.4 (0.20)	34.8	41
18.	6S-2E-18 NW	122°36'42"	45°03'18"	QWW	OR	10/06/76	259	92	7–10	(1,2): 11.7	95–195	[1.17]	30.9	34.3	40
											55–92	1.30e (0.15)	28.9 (0.41)	28.8	37
19.	6S-6E-23 SW	122°02'42"	45°01'48"	DH-5000	OR	11/04/75	(2): 487	90	—	—	55–90	—	29.1	29.0	[84]
								24	<13	8.7	15–24	1.50e (0.25)	69.6 (2.80)	56.1	
20.	6S-6E-23 SW	122°02'42"	45°01'49"	—	OR	11/04/75	(2): 498	22	—	—	15–22	—	70.0	—	—
								27	<8e	8.3	22–27	—	adv.	—	—
21.	6S-6E-34 SW	122°03'46"	44°59'57"	RDHCRCDR	OR	09/30/76	487	150	—	20.9	15–150	1.64 (0.04)	90.5e / 81.4 (0.29)	64.7	106
22.	6S-7E-04 SE	121°57'36"	45°04'18"	RDHCRLKH	OR	07/25/77	666	38	—	(1,2,4): 7.6	10–150	1.64	81.8	65.0	106
											—		iso.	—	—
23.	6S-7E-04 SE	121°57'25"	45°04'21"	— (L. Harriet CG.)	US	(1,2): 09/22/85	686	40	—	—	0–38	—	—	—	—
							625	22	15.3	15.9	—	—	adv.	—	—
24.	6S-7E-21 SW	121°57'44"	45°01'46"	RDH-AHSE	OR	06/29/77	603	40	—	17.9	28–40	1.47 (0.07)	155. (6.71)	109.	[160]
25.	6S-7E-30 NW	122°00'32"	45°01'20"	RDHCRAHS	OR	09/30/76	512	135	4–5	(1,2,4): 55.3	10–40	1.47	231.6	162.8	240
											95–135	1.65 (0.08)	236 (3.36)	166	274
26.	6S-7E-30 NW	122°00'20"	45°01'24"	—	US	08/03/86	(1,2,4): 509	132	—	—	95–130	1.65	240.7	169.5	279
								293	<15	82.1	146–293	1.50e (0.25)	83.4 (0.71)	62.7	94
27.	7S-1E-11 NE	122°38'47"	44°58'46"	OW W1	OR	07/—/62	214	2379	—	—	—	—	—	—	—
28.	7S-5E-14 SE	122°09'51"	44°57'47"	U.S.F.S.	US	08/15/85	616	18	6.1	(1,2): 5.5	0–2379	[1.59]	26.0	26.0	41
											15–18	—	adv. / 70.7e	—	—
29.	7S-5E-22 NE	122°10'23"	44°57'07"	CR-BHS	OR	09/30/76	655	90	—	13.5	20–90	1.46 (0.05)	84.3 (0.96)	66.8	97
30.	7S-5E-23 NE	122°09'53"	44°57'09"	— (Bagby H.S. trailhead)	US	08/20/85	646	21	—	(1,2,4): 5.8	20–90	1.46	84.3	66.8	97
											15–22	—	adv. / 43.8e / adv. / 11.0e	—	—
31.	(7S-7E-04) SE	121°57'01"	44°58'59"	EWEB-TS	OR	05/28/80	1273	194	50–55	5.3	25–194	—	—	—	—
				(1,4):	OR	11/13/79	1273	—	—	—	165–190	1.62	—	—	—
				(2): EWEB-PC	OR	05/28/80	1273	194	—	—	165–190	1.62	—	—	—
					OR	05/28/80	975	187	10–15	6.4	—	—	iso.	—	—
32.	(7S-8E-05) SE	121°50'50"	44°59'00"	(1,4):	OR	10/30/79	975	—	—	—	70–185	1.58	4.5	—	—
				(2):	OR	05/28/80	975	187	—	—	70–185	1.58	—	—	—

APPENDIX.—Conductive heat-flow data from the Cascade Range and adjacent areas in north-central Oregon—Continued

No.	T-R-Sec. 1/4	Longitude	Latitude	Name	Code	Date logged (mo/d/yr)	Elev. (m)	Depth (m)	Static water level (m)	Bottom-hole temp. (°C)	Interval (m)	Therm. cond. (W/m·K)	Gradient (°C/km) Uncorr.	Corr.	Heat flow (mW/m²)
							West of the Cascade crest—Continued								
33.	(7S-8E-10) NE	121°48'26"	44°58'32"	EWEB-CC	OR	05/30/80	1140	137	45°	4.5	115–137	—	adv. 9.4e	—	—
34.	8S-1E-08 SE	122°42'32"	44°53'19"	(1,4):	OR	10/18/79	1140	—	—	—	110–137	1.45	—	—	—
				(2):	OR	05/30/80	1140	137	—	—	110–137	1.45	—	—	—
				H-1-WW	OR	10/08/76	303	218	15–20	15.8	95–215	1.72	27.6 (0.14)	27.6	47
35.	8S-1E-09 NW	122°41'38"	44°53'28"	WOLFF	OR	04/30/80	338	103	—	(1,2): 12.1	95–215	1.72	27.6	27.6	47
											30–100	1.60e (0.15)	38.3 (2.89)	38.3	[61]
36.	8S-1E-17 SE	122°42'18"	44°52'18"	SM-WW	OR	10/06/76	315	112	60–65	(2): 13.3	30–100	—	34.9	—	—
											65–110	1.60e (0.15)	45.7 (2.03)	45.7	[73]
37.	8S-5E-31 SW	122°14'47"	44°49'52"	CDR CK	OR	10/26/77	705	345	<5	(2): 17.2	10–110	1.80 [1.59]	28.5	27.0	43
											25–345	1.80 (0.33)	32.3 (0.10)	28.6	51
38.	8S-6E-01 SE	122°00'51"	44°54'19"	—	US	10/20/88 (42 days after completion)	914	62	56	(1,2,4): 7.1	35–345	1.80	32.3	28.6	51
											—	—	adv.	—	—
38a.	8S-7E-07 NW	122°00'21"	44°53'51"	Upper Collawash	US	07/08/92	707	89	—	10.8	52–89	3.03 (0.28)	36.1 (0.1)	23.4	71
39.	(8S-8E-06) SE	121°52'53"	44°54'21"	EWEB-SB	OR	04/29/80	860	460	<5	29.8	335–460	1.50e (0.25)	50.1 (0.93)	44.7	67
40.	(8S-8E-28) SE	121°49'54"	44°51'02"	(1):	OR	11/13/79	860	—	—	—	150–460	1.49	71.5	63.3	95
				(2,4):	OR	04/29/80	860	460	—	—	150–460	1.49	71.5	63.3	94
				CTGH-1	UT	09/05/86	1170	1465	—	87	655–1448	1.50e (0.25)	72.9 (0.29)	72.9	109
41.	(8S-8E-31) SW	(4):	44°51'06"	RDH-CBCK	—	08/06/87	1146	—	—	—	500–1465	[1.38]	81.7	79.8	110
		121°52'52"	44°50'01"		OR	07/31/80	1072	98	30	6.9	85–97	1.47 (0.08)	28.9 (2.44)	26.0	[38]
42.	9S-1E-25 SE	122°37'19"	44°45'11"	(1,2,4):	OR	09/28/79	1072	98	—	—	70–98	1.47	37.8	34.0	50
				—	US	08/11/86	463	100e	70	11.4	73–99	1.60e (0.15)	20.7 (1.96)	22.8	[37]
43.	9S-2E-16 NW	122°34'25"	44°47'24"	—	US	08/05/86	216	110	5e	14.1	88–107	1.30e (0.15)	35.4 (1.42)	33.1	43
44.	9S-2E-21 SE	122°33'35"	44°46'11"	GI-WW	OR	10/07/76	213	49	12–15	10.9	20–48	1.26	51.9 (2.13)	46.3	58
45.	9S-2E-29 NW	122°35'08"	44°45'40"	—	US	07/14/86	218	76	6e	(1,2): 13.6	22–48	1.26	53.2	47.5	59
											—	—	adv.	—	—
46.	9S-3E-11 NW	122°24'31"	44°48'28"	EV2-WW	OR	10/14/76	317	85	—	11.4	60–85	1.34	29.9 (0.99)	26.3	35
47.	9S-3E-11 SW	122°24'49"	44°48'06"	EV1-WW	OR	10/07/76	333	65	10–13	(1,2): 10.5	48–85	1.34	27.3	24.0	32
											25–60	1.34	26.5 (0.14)	23.6	31
48.	9S-3E-28 SW	122°27'06"	44°45'24"	GR-WW	US	08/05/86	268	54	10	(1,2): 12.5	25–60	1.34	26.5	23.6	31
											30–52	1.30e (0.15)	32.9 (1.46)	30.7	[40]
				(2):	OR	10/14/76	268	55	—	—	25–52	—	30.0	28.0	—

APPENDIX.—Conductive heat-flow data from the Cascade Range and adjacent areas in north-central Oregon—Continued

No.	T-R-Sec. 1/4	Longitude	Latitude	Name	Code	Date logged (mo/d/yr)	Elev. (m)	Depth (m)	Static water level (m)	Bottom-hole temp. (°C)	Interval (m)	Therm. cond. (W/m·K)	Gradient (°C/km) Uncorr.	Gradient (°C/km) Corr.	Heat flow (mW/m²)
						West of the Cascade crest—Continued									
49.	9S-3E-36 NW	122°23'31"	44°44'59"	—	US	08/05/86	317	73	4.6	11.9	30–73	1.30e (0.15)	22.0 (0.97)	20.0	26
50.	9S-6E-21 SE	122°04'37"	44°46'25"	Willamette National Forest	US	09/24/85	597	45	9.6	8.3	—	—	adv.	—	—
51.	9S-6E-23 NW	122°02'25"	44°46'59"	RDH-BHSW	OR	09/30/76	594	108	—	14.7	40–105	1.61 (0.11)	68.4 (0.30)	56.4	91
52.	(9S-7E-03) SW	121°56'03"	44°49'08"	SUN-BRA1	SU	(1,2): 09/30/81	550 1220	150 138	artesian	12.1	30–105 40–138	1.61 1.50e (0.25)	67.6 69.4 (0.53)	55.7 65.6	90 98
53.	(4): (9S-7E-07) SE	121°56'06" 121°59'30"	44°49'06" 44°48'06"	SUN-BR5	SU	09/30/81 09/30/81	1219 957	— 149	— —	— 11.7	30–138 35–149	1.38 1.50e (0.25)	63.5 55.4 (0.23)	67.5 53.3e	92 [80]
54.	9S-7E-20 NE	121°58'37"	44°47'02"	Breitenbush Hot Springs Resort	US	09/01/85, 08/06/86	688	482	artesian	(4): 77.9	50–150	[1.38]	55.4 (0.23) adv.	61.7	84
55.	9S-7E-20 NE	121°58'15"	44°46'48"	BEAMER 2	US	09/24/85	679	87	4.4	35.2	58–87	1.40e (0.20)	299 (7.78)	253	355
56.	(1,2,4): 9S-7E-20 NE	121°58'16" 121°58'20"	44°46'50" 44°47'04"	—	OR US	04/29/80 08/02/86	680 725	74 433	— <60	— 83.7	6–74 378–433	1.27 1.50e (0.25)	407.3 105 (2.60)	339.4 101	430 151
57.	9S-7E-20 NE	121°58'22"	44°46'55"	BEAMER 3	OR	04/29/80	677	310	artesian	89.2	255–310	1.50e (0.25)	49.8 (0.31)	44.1	[66]
58.	9S-7E-20 NE	121°58'33"	44°46'52"	BEAMER 1	OR	02/06/78	686	150	artesian	(1,2): — (4): — (1,2,4): 104.8	5–35 5–35 0–310	1.27 1.27 1.55	1300 1097 <277.2 adv.	1100 1097 <261.0	1393 1393 <404
59.	(1,2,4): (9S-7E-21) NE	121°58'37" 121°57'07"	44°46'52" 44°46'44"	RDH-BHSE	OR OR	02/06/78 05/06/77	682 725	150 155	— —	— 22.5	0–150 70–155	[1.46] 1.65 (0.15)	600 91.9 (0.71)	521.7 81.7	763 135
60.	(9S-7E-28) SW	121°57'50"	44°45'30"	(1,2,4): SUN-BR11	OR SU	09/30/76 09/16/80	725 878	155 152	— —	— 27.2	90–150 110–152	1.65 1.50e (0.25)	92.9 156. (3.26)	82.6 >142	136 >213
61.	(4): (9S-7E-28) SE	121°57'51" 121°57'26"	44°45'30" 44°45'32"	SUNEDCO 58-28	SU	09/16/80 08/12/82	878 881	— 2457	— —	— >141	120–153 1465–1715	[1.38] 2.2 (0.10)	146 30.7 (0.35)	130 30.7	180 68
62.	(4): (9S-7E-28) SE	121°57'33" 121°57'09"	44°45'33" 44°45'48"	SUN-BR10	SU	08/12/82 09/30/81	823 945	— 152	— —	— 19.0	250–856 0–2457 90–152	1.51 1.88 1.50e (0.25)	148.0 56.0 101 (0.41)	148.0 56.0 101	222 105 152
63.	(4): (9S-7E-29) SW	121°55'42" 121°59'12"	44°45'59" 44°45'36"	SUN-BR2	SU	09/30/81 09/30/81	828 927	— 84	— —	— 7.9	30–153 75–84	[1.38] 1.50e (0.25)	94.9 90.5 (0.40)	67.3 90.9	93 [136]
64.	(4): (9S-7E-34) SE	121°56'06"	44°44'53"	SUN-BRA4	SU	(4): 09/30/81	939 942	— 151	— —	— 20.1	70–84 20–150	1.65e (0.15) [1.38]	83.4 104 (0.20)	78.0 85.2	109 141
65.	(4): (9S-7E-36) NW	121°56'12" 121°53'48" (4): 121°53'36"	44°44'57" 44°45'16" 44°44'48"	SUN-BR12	SU	09/30/81 10/02/81 10/02/81	939 1049 895	— 154 —	— — —	— 17.6 —	20–150 75–150 50–154	[1.38] 1.50e (0.25) [1.38]	103.6 89.0 (0.40) 86.7	96.2 79.5 77.3	130 120 107

APPENDIX.—Conductive heat-flow data from the Cascade Range and adjacent areas in north-central Oregon—Continued

West of the Cascade crest—Continued

No.	T-R-Sec. 1/4	Longitude	Latitude	Name	Code	Date logged (mo/d/yr)	Elev. (m)	Depth (m)	Static water level (m)	Bottom-hole temp. (°C)	Interval (m)	Therm. cond. (W/m·K)	Gradient (°C/km) Uncorr.	Gradient (°C/km) Corr.	Heat flow (mW/m²)
66.	(9S-8E-12) SW	121°46'53"	44°48'12"	— (Olallie L. CG.)	US	09/24/85	1506	70	66	3	—	—	iso.	—	—
67.	10S-5E-02 SE	122°09'25"	44°43'57"	Ingram	US	08/11/86	452	65	9	9.8	55-65	1.30e (0.15)	28.1 (1.58)	26.3	[34]
68.	10S-5E-03 SE	122°10'46"	44°43'41"	FS-DRSWW	OR	06/26/78	488	180	3	16.7	—	—	adv.	—	—
69.	10S-5E-15 NE	122°10'32"	44°42'18"	— (Southshore CG.)	US	(1,2,4): 08/03/86	518 / 487	180 / 29	— / 4.6	— / 9.1	10-170 / 24-29	[1.17] / 1.30e (0.15)	52.0 / 53.8 (1.86)	43.0 / 41.7	51 / [54]
70.	10S-7E-09 NW	121°57'57"	44°43'33"	SUN-BRA5	SU	09/30/81	1329	152	—	13.5	100-152	1.65e (0.15)	70.4 (0.68)	83.8e	[138]
71.	10S-7E-11 NE	121°54'26"	44°43'22"	RDH-DVCK	OR	11/05/79	1194	155	7	(4): 16.8	115-152 / 70-155	[1.38] / 1.40 (0.04)	68.6 / 83.2 (0.72)	92.6 / 72.3	126 / 101
72.	10S-7E-20 SW	121°59'12"	44°41'27"	SUN-BRA9	SU	09/30/81	640	154	—	(1,2,4): 20.6	70-150 / 75-150	1.40 / 1.50e (0.25)	83.5 / 112 (1.10)	72.6 / 90.3	102 / 135
73.	10S-7E-23 NW	121°55'33"	44°41'36"	SUNBRA10	SU	09/30/81	817	152	—	(4): 20.4	75-153 / 80-150	[1.38] / 1.65e (0.15)	104.3 / 115 (0.47)	78.4 / 83.3	108 / 138
74.	10S-7E-24 NE	121°53'39"	44°41'36"	SUNBRA11	SU	10/01/81	1000	147	—	(4): 16.6	85-152 / 45-145	[1.38] / 1.65e (0.15)	115.6 / 87.9 (0.47)	84.2 / 79.2	117 / 131
75.	10S-7E-34 NE	121°55'57"	44°39'54"	SUNBRA12	SU	(4): 09/30/81	975 / 780	— / 153	—	18.6	50-145 / 50-150	[1.38] / 1.65e (0.15)	87.4 / 84.8 (0.36)	78.9 / 73.7	109 / 122
76.	11S-1E-07 SE	122°43'19"	44°37'28"	RL-WW	OR	10/13/76	158	58	5-8	(4): 12.5	50-150 / 40-58	[1.38] / 1.34	84.8 / 28.1 (1.38)	71.8 / 26.7	100 / 35
77.	11S-4E-19 SE	122°22'19"	44°35'20"	—	US	08/07/86	415	28	3.7	(1,2): 9.6	40-58 / 15-28	1.34 / 1.75e (0.20)	28.1 / 28.7 (1.13)	26.7 / 19.3	35 / [34]
78.	11S-6E-22 SE	122°03'23"	44°36'01"	BUCK MTN	OR	07/31/80	1223	77	10	8.1	65-77	1.21 (0.08)	80.2 (1.85)	72.9e	[88]
79.	11S-7E-10 SE	121°56'07"	44°37'35"	(4): RDH-MTCK	OR / OR	(2): 10/08/80 / 07/31/80	1333 / 1333 / 762	152 / — / 109	— / — / 25	— / — / 16.1	30-50 / 66-76 / 45-109	— / 1.21 / 1.64 (0.13)	90.8 / 79.0 / 37.3 (1.79)	— / 91.6 / 34.9	— / 111 / 57
				(1):	OR	11/05/79	762	—	—	—	33-48	1.64	68.4	64.0	105
				(2):	OR	07/31/80	762	—	—	—	30-109	1.64	68.4	64.0	105
				(4):	OR	10/07/80	762	—	—	—	0-108	1.64	68.4	64.0	105
79a.	12S-6E-01 SE	122°01'56"	44°33'08"	Lynx Creek	US	07/08/92	1122	105	—	11.0	34-96	1.18 (0.10)	65.6 (0.2)	64.3	76
											96-105	1.60 (0.09)	51.6 (0.4)	50.1	80
80.	(12S-7E-09) SE	121°57'48"	44°32'41"	EWEB-TM	OR	05/29/80	1195	587	22	31.0	270-587	1.36 (0.08)	72.2 (0.27)	70.2	95
				(1):	OR	10/31/79	1195	—	—	—	300-600	1.36	71.4	69.4	95
				(2):	OR	05/29/80	1195	600	—	—	300-600	1.36	71.4	69.4	94

APPENDIX.—Conductive heat-flow data from the Cascade Range and adjacent areas in north-central Oregon—Continued

No.	T-R-Sec. 1/4	Longitude	Latitude	Name	Code	Date logged (mo/d/yr)	Elev. (m)	Depth (m)	Static water level (m)	Bottom-hole temp. (°C)	Interval (m)	Therm. cond. (W/m·K)	Gradient (°C/km) Uncorr.	Gradient (°C/km) Corr.	Heat flow (mW/m²)
								West of the Cascade crest—Continued							
81.	13S-1E-20 NW	122°42'58"	44°25'55"	MR-WW	OR	08/11/76	402	130	120-125	13.1	90-130	[1.34]	33.6 (1.76)	39.9	53
82.	13S-1E-35 NE	122°38'58"	44°24'08"	MWW	OR	08/11/76	310	150	17-20	(1,2): 13.8	90-130	[1.34]	33.6	39.9	53
											75-150	[1.34]	31.3 (0.28)	37.2	50
83.	13S-2E-36 SW	122°30'46"	44°23'40"	—	US	07/23/86	244	125	20.4	(1,2): 14.9	90-130	[1.34]	31.5	37.4	50
											55-125	1.30e (0.15)	32.3 (1.04)	27.6	36
84.	13S-3E-31 SE	122°29'22"	44°23'43"	—	US	08/08/86	244	78	2	12.5	21-78	1.42e (0.25)	23.1 (0.17)	18.9	27
85.	13S-6E-17 NW	122°07'17"	44°26'30"	Cougar Creek	US	07/08/92	945	143	12	18.1	37-67	1.76 (0.31)	61.6 (0.8)	46.0	81
											67-143	1.31 (0.13)	86.4 (0.3)	67.5	88
86.	13S-7E-09 NE (2):	121°58'30"	44°27'42"	DETRO-FM	OR	07/23/80	1128	55	15e	3.7	—	—	adv.	—	—
87.	13S-7E-32 SW (1,2):	121°58'58"	44°27'42"	EWEB-CL	OR	07/23/80	1128	79	20-25	24.9	485-555	1.50e (0.25)	20.8 (0.27)	37.5	[56]
		121°59'40"	44°23'24"			09/05/79	955	557			50-205	1.44	112.0	102.8	148
		44°23'19"				09/05/79	955	557			0-555	1.40	25.6	23.9	33
88.	13S-7.5E-23 SE	121°52'49"	44°25'24"	—	US	08/07/86	1453	121	—	3.2	—	—	—	—	—
89.	14S-6E-32 SE	122°07'16"	44°18'12"	WOLF MDW	OR	08/01/80	999	154	10	18.1	40-154	1.46 (0.13)	89.4 (1.17)	74.5	109
90.	(15S-6E-11) SE	122°03'15"	44°16'06"	(1):	OR	11/14/79	999	—	—	—	42-155	1.46	87.2	72.7	106
				(2):	OR	08/01/80	999	155	—	—	42-155	1.46	87.2	72.7	110
				RDHCRTBR	OR	12/15/76	716	50	—	8.0					
91.	(15S-7E-28) NE (1,2):	121°58'24"	44°14'48"	RDH-CRSM	OR	07/26/77	716	64	—	4.4	0-52	—	adv.	—	—
					OR	07/26/77	1143	53	—		—	—	—	—	—
92.	16S-2E-26 NW	122°32'30"	44°09'00"	OH-2Z	OR	11/26/75	310	34	—	(1,2): 10.3	0-53	—	adv.	—	—
											20-34	1.50e (0.25)	24.7 (0.31)	27.4	[41]
93.	16S-2E-26 NW	(2):		—	OR	11/26/75	(2): —	30	—	10.0	20-30	—	25.0	—	—
								26			20-26	—	35.5e	—	—
94.	16S-4E-14 SE	122°17'30"	44°10'27"	BH-3Z	OR	11/26/75	457	48	—	10.8	12-48	1.80 (0.33)	37.7 (0.38)	34.9	63
95.	16S-4E-29 NW (1,2):	122°21'34"	44°10'03"	—		11/26/75	457	45	—	8.7	12-45	1.80	37.8	35.0	63
			44°09'16"		US	09/03/86	339	23	11.3		—	—	iso.	—	—
96.	16S-5E-30 NE	122°14'53"	44°09'17"	DDH-15	OR	08/08/79	367	87	5-10	14.2	65-87	1.33 (0.15)	96.5 (1.38)	86.7	115
97.	16S-5E-30 NE (1,2):	122°15'00"	44°09'12"	ST DAM 1	OR	06/26/78	367	85	—	—	15-85	1.33	54.0	51.0	68
			44°09'08"		OR	08/08/79	368	80	<5	12.9	65-80	[1.33]	32.1 (3.87)	30.4	[40]
										(2):	45-70	—	55.9	53.0	—

APPENDIX.—Conductive heat-flow data from the Cascade Range and adjacent areas in north-central Oregon—Continued

	T-R-Sec. 1/4	Longitude	Latitude	Name	Code	Date logged (mo/d/yr)	Elev. (m)	Depth (m)	Static water level (m)	Bottom-hole temp. (°C)	Interval (m)	Therm. cond. (W/m·K)	Gradient (°C/km) Uncorr.	Gradient (°C/km) Corr.	Heat flow (mW/m²)
						West of the Cascade crest—Continued									
98.	16S-5E-30 NE	122°14'36"	44°09'18"	ST DAM 2	OR	08/08/79	389	61	5-10	11.7	30-61	1.32	57.1 (0.86)	53.7	71
99.	16S-5E-31 SE	122°14'29"	44°07'47"	—	US	09/04/86	(2):	87 (sic)			25-61	1.32	56.3	53.0	70
							382	79	6	10.0	—	—	adv.	—	—
100.	16S-6E-02 SW	122°02'58"	44°12'08"	RDH-CRFP	OR	09/29/76	701	150	—	14.8	115-150	1.74 (0.03)	90.1 (2.44)	94.6	165
101.	16S-6E-10 SW	122°04'33"	44°11'06"	(1,2): Bigelow	OR	08/05/76	701	150	—	—	100-150	1.74	84.1	88.3	153
					US	06/14/84	481	207	—	52.	—	—	adv.	—	—
102.	16S-6E-14 SW	122°03'06"	44°10'26"	— (Limberlost CG.)	US	08/29/86	519	23	0	8.8	17-23	1.30e (0.15)	29.5 (0.66)	23.9	[31]
103.	16S-6E-27 NW	122°04'41"	44°09'04"	RDH-CRHC	OR	09/29/76	573	152	—	21.6	70-150	1.57 (0.05)	89.8 (1.10)	66.2	104
104.	17S-3E-02 NE	122°24'46"	44°07'20"	—	US	09/03/86	288	125	3	(1,2): 13.9	30-150	1.57	96.2	70.9	111
											58-125	1.50e (0.25)	29.8 (0.07)	25.3	38
105.	17S-3E-04 SE	122°26'58"	44°06'54"	—	US	09/03/86	291	61	1	11.4	30-61	2.70e (0.25)	13.1 (0.14)	11.1	30
106.	17S-3E-10 NE	122°25'40"	44°06'37"	—	US	09/02/86	298	111	40e	11.6	40-111	2.70e (0.25)	16.6 (0.14)	14.7	40
107.	(17S-6E-08) NE	122°13'28"	44°06'24"	WALKER-CRK	OR	08/15/80	585	154	15	13.1	105-154	[1.59]	53.2 (0.78)	51.1	81
108.	(2):	122°14'00"	44°06'24"	RIDER-CRK	OR	07/24/80	585	155	—	—	105-155	[1.59]	54.1	52.0	83
	(17S-5E-20) NW	122°13'51"	44°04'54"		OR	07/31/80	536	154	10	24.8	120-154	1.64 (0.04)	127	102	166
109.	(17S-6E-25) NE	122°01'22"	44°03'54"	RDH-MQCK	OR	09/24/80	1005	151	15	(2): 11.0	60-154	2.64 (sic)	128.5	97.5	159
											129-151	1.55 (0.06)	75.3 (1.16)	88.7	137
110.	(18S-5E-11) NW	122°09'49"	44°01'07"	(2): RDH-RBCK	OR	08/01/80	1005	152	—	(1): 14.4	131-151	1.55	76.3	89.9	139
					OR	10/30/80	890	150	80		115-152	1.55	62.8	73.8	114
111.	19S-4E-29 SW	122°22'09"	43°53'00"	(1): (2): CHRS-CRK	OR	09/24/80	780	—	—	—	—	—	adv.	—	—
					OR	07/31/80	780	152	—	—	96-152	1.42	61.1	65.0	92
											55-78	1.55	34.4	36.6	56
					OR	09/17/80	579	153	20	16.8	71-153	1.75 (0.09)	64.6 (0.24)	52.8	92
112.	19S-5E-27 NW	122°12'37"	43°53'23"	(2): BRCK-CRK	OR	07/31/80	579	154	—	—	70-154	1.75	64.0	52.3	92
					OR	09/17/80	987	154	20	16.1	137-154	1.75 (0.09)	69.7 (2.26)	69.5	122
113.	(19S-6E-08) NW	122°01'51"	43°56'58"	(2): RDH-ELKCK	OR	07/31/80	987	154	—	—	135-154	1.75	65.8	65.6	115
					OR	11/05/80	877	133	5e	18.2	37-133	1.22	39.8 (0.39)	30.6	37
114.	(19S-5.5E-25) SE	122°04'07"	43°52'57"	(1): (2): N. FORK	OR	12/04/79	877	—	—	—	110-134	1.52	35.5	27.4	41
					OR	07/09/80	877	135	—	—	40-135	1.22	43.2	33.3	41
					OR	07/31/80	951	154	25-30	(2): 18.9	90-154	1.35 (0.05)	93.7 (3.16)	82.5	111
											30-154	1.35	78.4	67.5	91

APPENDIX.—*Conductive heat-flow data from the Cascade Range and adjacent areas in north-central Oregon*—Continued

No.	T.-R.-Sec. 1/4	Longitude	Latitude	Name	Code	Date logged (mo/d/yr)	Elev. (m)	Depth (m)	Static water level (m)	Bottom-hole temp. (°C)	Interval (m)	Therm. cond. (W/m·K)	Gradient (°C/km) Uncorr.	Gradient (°C/km) Corr.	Heat flow (mW/m²)
									Mount Hood area						
115.	3S-7E-03 NE	121°55'22"	45°20'38"	RDH-RD19	OR	04/12/79	512	65	—	10.2	25-65	[1.21]	61.0 (5.70)	57.1	[69]
						(3):	148 (sic)				30-65	[1.21]	57.7	54.0	66
116.	3S-8E-14 NW	121°47'42"	45°18'56"	NNG-KC-1	OR	09/25/79	983	285	<5	11.6	175-285	2.24 (0.08)	19.4 (0.05)	17.5	39
117.	3S-8E-16 SW	121°49'51"	45°18'23"	CR-LH	OR	(3): 02/07/77	953	—	—	—	100-285	2.24	18.1	16.4	37
							762	126		10.2	80-125	2.18 (0.06)	23.8 (0.49)	24.8	54
118.	3S-8E-24 NW	121°46'27"	45°18'08"	SKI-BOWL	OR	05/25/77	1106	60	artesian	(3): 8.4	50-120	2.18	26.3	28.0	61
											—	—	adv.	—	—
119.	3S-8E-24 NE	121°45'55"	45°18'14"	THNDRHDL	OR	08/19/80	1145	536	—	(3): 24.7	0-60	[1.67]	60.0	55.0	92
											494-536	[2.30]	46.1 (1.06)	>40.8	>94
120.	3S-8E-29 SE	121°50'33"	45°16'34"	RDH-SC	OR	(3): 01/05/79	1127	—	—	17.7	500-536	[2.30]	48.7 (0.81)	48.7	112
							722	151			130-150	—	25.8	—	—
121.	3S-8.5E-25 NE	121°43'41"	45°17'15"	CR-SB	OR	05/02/77	1167	82	4	(3): 7.1	100-150	2.64	34.1	25.2	67
											65-82	1.67 (0.11)	102 (5.81)	102	[170]
122.	3S-8.5E-25 SW	121°44'06"	45°16'58"	(3): NNG-TRLK	OR	02/07/77	1167	—	—	—	0-82	1.67	—	—	—
					OR	10/23/79	1109	315	5	21.0	175-315	[1.76]	54.1 (0.20)	48.3	85
123.	3S-9E-03 SW	121°39'44"	45°19'57"	MEADOWS	US	08/21/81	1634	601	29-30	(3): 29.8	180-315	[1.76]	53.9	53.9	95
											430-601	2.02 (0.08)	81.7 (1.66)	81.7	165
124.	3S-9E-06 SE	121°42'30"	45°19'53"	CR-HH	OR	09/13/77	1167	110	—	(3): 2.6	275-354	2.02	61.0	68.5	139
											—	—	iso.	—	—
125.	3S-9E-07 NE	121°42'25"	45°19'45"	(3): RDH-TBLG	OR	09/14/76	1798	—	—	—	10-115	1.85	—	—	—
					OR	12/28/78	1761	226		10.6	210-226	[1.84]	171 (1.56)	169	[311]
126.	3S-9E-07 SE	121°42'56"	45°19'18"	(3): USGS-PUC	OR	12/13/78	1761	—	—	—	195-225	[1.84]	201.7	201.7	371
					US	06/23/81	1640	1129	573	76.6	560-1129	1.79 (0.03)	67.1 (0.42)	72.4	130
127.	3S-9E-16 SW	121°40'34"	45°18'22"	(3): WHT RIVR	OR	08/15/81	1631	—	—	(3): 15.7	560-1125	1.79	67.2	67.2	121
					OR	07/02/81	1330	303	41-42		—	—	adv.	—	—
128.	3S-9E-30 NE	121°42'35"	45°16'57"	USGS-HWY	OR	10/22/79	1108	289	25	(3): 15.4	250-303	2.37	10.2	10.2	24
											75-289	[1.76]	41.5 (0.13)	38.2	67
	(3):	121°42'41"	45°17'10"			10/22/79	1108	—	—	—	80-289	[1.76]	41.5 (0.77)	41.5	73
									East of the Cascade crest						
129.	3S-11E-01 NE	121°21'35"	45°20'48"	—	OR	05/08/79	920	126	—	14.2	50-126	1.65e (0.15)	42.2 (0.27)	46.0	76
130.	3S-13E-31 NW	121°14'03"	45°16'16"	Palmer	US	05/27/88	418	87	11	21.2	34-87	1.60e (0.15)	24.7 (0.77)	21.2	34

APPENDIX.—Conductive heat-flow data from the Cascade Range and adjacent areas in north-central Oregon—Continued

	T-R-Sec. 1/4	Longitude	Latitude	Name	Code	Date logged (mo/d/yr)	Elev. (m)	Depth (m)	Static water level (m)	Bottom-hole temp. (°C)	Interval (m)	Therm. cond. (W/m·K)	Gradient (°C/km) Uncorr.	Gradient (°C/km) Corr.	Heat flow (mW/m²)
						East of the Cascade crest—Continued									
131.	3S-14E-07 SE	121°05'55"	45°19'01"	—	OR	07/14/77	835	65	40-45	12.4	45-65	1.60e (0.15)	23.8 (0.60)	23.9	38
132.	4S-9E-28 SE	121°40'08"	45°11'15"	—	OR	05/07/79	1036	145	—	4.2	—	—	iso.	—	—
133.	4S-12E-10 SE	121°16'45"	45°13'51"	—	OR	06/10/77	532	90	60-65	14.3	—	—	adv.	—	—
134.	4S-12E-17 NW	121°20'04"	45°13'29"	—	OR	06/17/77	640	150	—	12.8	115-150	1.40e (0.20)	15.1 (1.05)	<21.6	<30
135.	4S-12E-17 SW	121°20'03"	45°13'04"	—	OR	06/17/77	637	184	125-130	14.5	—	—	adv.	—	—
136.	4S-13E-01 SW	121°07'27"	45°14'55"	—	OR	06/10/77	341	75	3	16.3	—	—	adv.	—	—
137.	4S-13E-24 SW	121°07'34"	45°12'22"	—	OR	06/09/77	506	136	—	11.3	—	—	iso.	—	—
138.	4S-13E-24 SE	121°07'07"	45°12'14"	McElheran	US	10/10/87	520	140	98	11.9	—	—	iso.	—	—
139.	4S-13E-27 SW	121°10'11"	45°11'34"	—	US	10/13/87	536	104	104	15.6	—	—	—	—	—
140.	4S-13E-32 SE	121°12'06"	45°10'29"	—	OR	06/09/77	549	145	70-75	18.6	130-145	1.65e (0.15)	45.8 (2.07)	45.8	76
141.	4S-14E-19 NE	121°05'49"	45°12'38"	—	OR	06/07/77	506	105	—	11.6	—	—	iso.	—	—
142.	4S-14E-33 SW	121°04'10"	45°10'36"	—	OR	07/11/77	314	70	55-60	18.4	40-70	—	adv.	—	—
143.	5S-11E-14 SE	121°22'45"	45°07'48"	—	OR	06/14/77	733	245	—	13.0	180-245	—	53.9e / 24.1 (2.42)	—	—
144.	5S-11E-25 SE	121°22'41"	45°06'17"	Harmon	US	05/26/88	713	152	136	17.2	149-152	1.60e (0.15)	62.3 (5.56)	60.2	[96]
145.	5S-11E-26 NE	121°23'19"	45°06'28"	Kimmel	US	10/09/87	782	264	236	21.4	258-264	1.60e (0.15)	50.7 (1.00)	51.5	[82]
146.	5S-12E-08 NW	121°20'05"	45°09'19"	—	OR	06/16/77	629	35	30-35	11.7	—	—	adv.	—	—
147.	5S-12E-31 NE	121°20'20"	45°05'55"	—	OR	06/16/77	680	108	90-95	14.9	—	—	adv.	—	—
148.	6S-11E-11 SW	121°23'30"	45°03'27"	Garner/Rainbow Rock	US	10/16/87	838	72	3	16.7	30-72	1.65e (0.15)	95.2 (1.14)	92.0	152
149.	6S-14E-13 SE	120°59'46"	45°02'35"	CRITRN 1	OR	06/14/77	940	120	105-110	14.9	50-120	1.59	40.2 (1.56)	44.3	[70]
150.	6S-15E-05 NW	120°57'52"	45°04'57"	MCLEOD R	OR	06/15/77	802	70	45-50	(1): 14.4	80-120 / 50-70	[1.59] / [1.59]	44.8 / 37.8 (0.95)	44.8 / 38.6	71 / 61
151.	7S-11E-14 SW	121°23'37"	44°57'40"	Confederated Tribes	US	10/13/87	695	30	4	(1): 15.2	35-70 / 17-30	[1.59] / 1.30e (0.15)	44.3 / 97.2 (6.84)	43.3 / <80.9	70 / [<105]
152.	7S-11E-15 SE	121°24'40"	44°57'22"	Confederated Tribes Indian Health Service	US	10/13/87	798	118	104	15.3	—	—	adv.	—	—
153.	7S-12E-29 SW	121°19'45"	44°55'36"	—	US	10/14/87	823	120	93	19.3	94-110	1.35e (0.20)	75.1 (1.14)	75.6	[102]
154.	8S-12E-03 NE	121°16'56"	44°54'19"	Peters	US	10/14/87	856	90	3	13.1	49-90	1.35e (0.20)	22.9 (0.19)	20.7	28

APPENDIX.—Conductive heat-flow data from the Cascade Range and adjacent areas in north-central Oregon—Continued

	T-R-Sec. 1/4	Longitude	Latitude	Name	Code	Date logged (mo/d/yr)	Elev. (m)	Depth (m)	Static water level (m)	Bottom-hole temp. (°C)	Interval (m)	Therm. cond. (W/m·K)	Gradient (°C/km) Uncorr.	Gradient (°C/km) Corr.	Heat flow (mW/m²)
									East of the Cascade crest—Continued						
155.	8S-12E-03 SW	121°17'27"	44°54'13"	Wolfe	US	10/17/87	844	42	3	11.0	27-42	1.35e (0.20)	102 (1.26)	>98.5	>133
156.	9S-11E-02 NW	121°23'25"	44°49'26"	Williams	US	10/15/87	815	111	88	13.8	105-111	1.30e (0.15)	24.6 (1.20)	24.9	[32]
157.	9S-12E-14 SE	121°15'36"	44°47'10"	Macy	US	10/17/87	511	28	2	14.1	—	—	adv.	—	—
158.	9S-12E-31 SW	121°20'56"	44°44'36"	Perthina	US	10/14/87	591	62	3	17.5	40-62	1.30e (0.15)	77.7 (1.65)	64.5	84
159.	9S-12E-34 SW	121°17'32"	44°44'43"	—	US	05/26/88	494	24	2	11.9	—	—	adv.	—	—
160.	9S-14E-23 NW	121°01'30"	44°46'39"	—	OR	07/13/77	597	80	12-15	16.7	60-80	1.30e (0.15)	61.0 (3.58)	56.3	[73]
161.	9S-14E-30 SW	121°06'11"	44°45'15"	Vibbert	US	09/24/87	573	180	4	19.4	149-180	1.60e (0.15)	37.2 (0.90)	35.0	56
162.	11S-10E-05 NE	121°33'28"	44°38'47"	CASTLERX	OR	10/09/80	1194	153	113e	10.4	141-153	1.50e (0.25)	17.5 (0.73)	>18.8	[>28]
163.	11S-13E-01 NW	121°07'25"	44°38'51"	City of Madras	US	09/25/87	693	162	89	(2): 17.0	25-153 149-162	1.30e (0.15)	18.2 15.6 (1.31)	— 14.7	— [19]
164.	11S-13E-07 SW	121°13'34"	44°37'21"	Belle	US	09/23/87	817	242	<235	15.9	235-242	1.30e (0.15)	11.5 (0.41)	11.7	[15]
165.	11S-13E-24 NE	121°06'49"	44°36'21"	SCHNDR-1	OR	07/14/77	731	295	90-95	24.9	90-295	1.44	53.8 (0.54)	53.1	76
166.	11S-13E-24 NE	121°06'50"	44°36'06"	—	OR	07/14/77	756e	245	55-60	(1): 21.1	70-260 185-245	1.44 1.32e (0.20)	50.7 51.5 (0.33)	48.2 51.1	69 68
167.	11S-15E-22 SW	120°55'06"	44°35'35"	HAYCK RN	OR	08/10/77	963	820	—	47.7	600-820	2.72	31.3 (0.17)	30.3	82
168.	12S-9E-01 NW	121°36'25"	44°33'42"	GREENRDG	OR	07/23/80	999	105	—	(1): 16.8	605-820 60-105	2.72 [1.60]	31.3 81.0 (0.99)	31.3 64.8	85 104
169.	12S-11E-02 SW	121°22'51"	44°33'18"	Stills	US	09/24/87	(2): 774	152 175	127	— 13.3	70-105 171-175	[1.60]	79.2 adv. 12.3e	63.4	101
170.	12S-12E-04 NW	121°18'02"	44°33'41"	Wheeler	US	09/23/87	792	189	170	11.7	—	—	iso.	—	—
171.	12S-12E-20 NE	121°19'12"	44°31'02"	—	OR	08/07/80	820	217	210-212	11.6	—	—	iso.	—	—
172.	13S-8E-27 SE	121°45'41"	44°24'56"	— (by Blue L. airstrip)	US	08/12/86	1070	46	5.8	5.2	—	—	adv.	—	—
173.	13S-10E-05 NE	121°33'25"	44°28'46"	FLY CRK	OR	07/24/80	1195	105	73	7.3	—	—	iso.	—	—
174.	13S-12E-21 NE	121°17'41"	44°26'02"	Hart	US	05/28/88	(2): 850	120 177	— 165	— 10.9	—	—	iso.	—	—
175.	13S-14E-11 SW	121°01'13"	44°27'12"	—	OR	08/05/77	988	50	20-25	13.9	25-50	1.30e (0.15)	28.1 (1.83)	27.3	36
176.	13S-14E-11 SW	121°01'24"	44°26'58"	—	OR	08/03/77	978	45	30-35	14.8	—	—	adv.	—	—
177.	13S-14E-11 SW	121°01'13"	44°26'58"	—	OR	08/03/77	997	45	25-30	14.8	—	—	adv.	—	—

APPENDIX.—Conductive heat-flow data from the Cascade Range and adjacent areas in north-central Oregon—Continued

#	T-R-Sec. 1/4	Longitude	Latitude	Name	Code	Date logged (mo/d/yr)	Elev. (m)	Depth (m)	Static water level (m)	Bottom-hole temp. (°C)	Interval (m)	Therm. cond. (W/m·K)	Gradient (°C/km) Uncorr.	Gradient (°C/km) Corr.	Heat flow (mW/m²)
									East of the Cascade crest—Continued						
178.	14S-9E-08 NE	121°40'41"	44°22'37"	Kiewit Pacific Company	US	08/02/87	1030	120	89	5.7	—	—	iso.	—	—
179.	14S-9E-35 SW	121°37'52"	44°18'38"	Deschutes National Forest	US	08/03/87	1040	43	40e	6.5	—	—	adv.	—	—
180.	14S-10E-07 SW	121°35'32"	44°22'09"	—	US	09/16/87	987	180	77	8.8	—	—	iso.	—	—
181.	14S-10E-08 NW	121°34'17"	44°22'19"	Gill	US	08/05/87	984	66	22	8.2	—	—	iso.	—	—
182.	14S-10E-26 NE	121°29'43"	44°20'00"	Stangland	US	08/04/87	963	203	171	10.1	—	—	iso.	—	—
183.	14S-10E-28 SE	121°32'15"	44°19'31"	Mehring	US	08/03/87	988	49	10	10.0	—	—	adv.	—	—
184.	14S-10E-34 NW	121°31'48"	44°18'56"	Wagner	US	08/04/87	975	42	24	8.4	27-41	—	adv. 6.9e	—	—
185.	14S-11E-01 SE	121°21'04"	44°22'43"	Gillworth	US	09/17/87	840	147	106	10.5	—	—	iso.	—	—
186.	14S-11E-04 NW	121°25'51"	44°23'32"	Veeck	US	08/12/87	838	87	58	9.9	—	—	iso.	—	—
187.	14S-11E-28 NE	121°24'46"	44°20'00"	—	US	09/07/87	948	188	155e	10.2	—	—	adv.	—	—
188.	14S-11E-28 SW	121°25'20"	44°19'35"	—	US	09/17/87	933	167	133	10.1	—	—	iso.	—	—
189.	14S-13E-14 NE	121°08'08"	44°21'33"	—	OR	03/21/80	872	58	40-45	12.9	45-58	1.50e (0.25)	14.7 (1.43)	>13.4	[>20]
190.	14S-13E-29 SW	121°12'22"	44°19'33"	—	US	08/12/87	864	58	38	12.3	40-58	—	adv. 8.8e	—	—
191.	14S-14E-18 SW	121°06'19"	44°21'09"	SWIFT	OR	04/18/80	874	60	45-50	12.3	—	—	iso.	—	—
192.	15S-10E-02 SE	121°29'40"	44°17'34"	—	US	08/29/87	959	70	66	(5): 9.4	25-60	—	4.5	—	—
193.	15S-10E-05 NW	121°34'22"	44°18'19"	CENTWEST	OR	04/05/80	978	102	30-35	9.7	—	—	iso.	—	—
194.	15S-10E-06 NW	121°35'16"	44°18'13"	Reed	US	08/04/87	(2): 989	106 / 61	— / 43e	— / 8.8	10-30 / —	—	104.8 / iso.	—	—
195.	15S-10E-11 NW	121°30'12"	44°17'23"	—	US	08/05/87	957	69	52	9.4	—	—	iso.	—	—
196.	15S-10E-36 SE	121°28'24"	44°13'29"	—	OR	08/19/81	997	95	—	10.3	—	—	adv.	—	—
197.	15S-11E-07 NW	121°28'05"	44°17'09"	—	OR	03/17/80	944	130	105-110	10.2e	—	—	adv.	—	—
198.	15S-11E-09 NW	121°25'26"	44°17'28"	—	US	08/25/87	933	123	96e	10.4	—	—	adv.	—	—
199.	15S-11E-16 NW	121°25'33"	44°16'24"	Mid-Oregon Crushing Co.	US	08/29/87	890	86	43	7.0	—	—	iso.	—	—
200.	15S-12E-03 NW	121°17'13"	44°18'03"	—	US	08/29/87	872	88	77	7.2	—	—	iso.	—	—
201.	15S-12E-04 NE	121°17'42"	44°17'58"	—	US	08/29/87	866	104	88	7.1	—	—	iso.	—	—

APPENDIX.—Conductive heat-flow data from the Cascade Range and adjacent areas in north-central Oregon—Continued

	T-R-Sec. 1/4	Longitude	Latitude	Name	Code	Date logged (mo/d/yr)	Elev. (m)	Depth (m)	Static water level (m)	Bottom-hole temp. (°C)	Interval (m)	Therm. cond. (W/m·K)	Gradient (°C/km) Uncorr.	Gradient (°C/km) Corr.	Heat flow (mW/m²)
						East of the Cascade crest—Continued									
202.	15S-12E-09 NW	121°18'03"	44°17'13"	—	OR	09/04/80	922	156	100–105	10.5	—	—	adv.	—	—
203.	15S-12E-23 NW	121°15'43"	44°15'39"	—	OR	03/19/80	907	88	70–75	11.0	—	—	adv.	—	—
204.	15S-13E-02 SW	121°08'42"	44°17'31"	—	US	08/25/87	920	88	85	15.9	—	—	adv.	—	—
205.	15S-13E-03 SE	121°09'06"	44°17'35"	—	OR	03/25/80	916	154	80–85	17.2	35–154	1.65e (0.15)	42.3 (1.85)	42.3	70
206.	15S-13E-03 SE	121°09'06"	44°17'35"	—	OR	04/09/80	916	88	60–65	12.9	—	—	adv.	—	—
207.	15S-13E-04 SW	121°10'52"	44°17'52"	—	US	08/26/87	900	85	68	12.5	—	—	iso.	—	—
208.	15S-13E-18 NW	121°13'40"	44°16'12"	—	OR	04/04/80	916	64	64e	11.2	55–64	—	adv. 12.6e	—	—
209.	15S-13E-22 NE	121°09'25"	44°15'42"	—	US	08/26/87	934	220	93e	11.4	—	—	iso.	—	—
210.	15S-14E-15 SE	121°01'41"	44°15'55"	CRABTREE	OR	04/16/80	930	81	35–40	12.2	—	—	adv.	—	—
211.	15S-14E-36 NE	120°59'36"	44°13'14"	FHRNBKWW	OR	09/22/78	1023	157	(5): 135–140	121.8 (sic) 31.7	—	—	—	—	—
212.	15S-15E-11 SW	120°53'48"	44°16'50"	—	OR	12/17/80	991	142	124	(1,5): 19.6	20–155 / 120–142	[1.46] / 1.58e (0.25)	128.4 / 45.4 (4.28)	120.5 / 45.1	176 / 71
213.	15S-15E-28 NE	120°55'42"	44°14'37"	KOOPS	OR	08/11/80	998	149	80–85	20.3	40–149	1.50e (0.25)	50.9 (0.50)	49.7	74
214.	15S-15E-31 NE	120°58'31"	44°13'41"	DEASON	OR	04/06/80	1067	244	240–244	(5): 30.0	40–149 / 140–244	— / 1.65e (0.15)	51.0 / 54.1 (1.50)	51.3	85
215.	16S-11E-34 NW	121°23'37"	44°09'04"	—	OR	08/20/81	1049	66	55–60	(5): 11.5	40–244	—	68.7	—	—
216.	16S-11E-34 SW	121°24'07"	44°08'25"	—	OR	08/19/81	1068	49	—	9.6	—	—	adv.	—	—
217.	16S-11E-34 SW	121°23'50"	44°08'24"	—	OR	08/19/81	1068	178	160–165	9.7	—	—	iso.	—	—
218.	16S-11E-35 NE	121°21'48"	44°09'08"	—	OR	08/20/81	1030	208	110–120	10.3	—	—	iso.	—	—
219.	16S-12E-20 NE	121°18'38"	44°10'37"	Dearing	US	08/12/87	1018	169	149	11.1	—	—	iso.	—	—
220.	16S-12E-26 NW	121°15'38"	44°09'37"	—	US	09/—/87	993	171	154	10.6	166–171	1.30e (0.15)	49.3 (5.71)	>47.6	[>62]
221.	16S-12E-29 SW	121°18'58"	44°09'25"	—	OR	04/04/80	984	163	140–145	10.9	—	—	iso.	—	—
222.	16S-12E-31 SW	121°20'25"	44°08'39"	—	OR	03/25/80	1024	100	75–80	10.3	—	—	adv.	—	—
223.	16S-12E-31 SE	121°19'38"	44°08'37"	La Moin Brandt	US	07/29/87	969	55	49	10.7	—	—	iso.	—	—
224.	16S-13E-16 NE	121°09'56"	44°11'31"	Heierman	US	08/25/87	964	146	133	10.6	—	—	iso.	—	—

APPENDIX.—Conductive heat-flow data from the Cascade Range and adjacent areas in north-central Oregon—Continued

	T-R-Sec. 1/4	Latitude	Longitude	Name	Code	Date logged (mo/d/yr)	Elev. (m)	Depth (m)	Static water level (m)	Bottom-hole temp. (°C)	Interval (m)	Therm. cond. (W/m·K)	Gradient Uncorr. (°C/km)	Gradient Corr. (°C/km)	Heat flow (mW/m²)
				East of the Cascade crest—Continued											
225.	16S-14E-16 NE	44°11'38"	121°02'59"	—	OR	02/06/81	995	460	120-125	56.4	200-460	1.50e (0.25)	76.4 (0.57)	73.7	111
226.	16S-14E-17 SE	44°10'52"	121°04'00"	ST HWY 1	OR	10/20/80	975	150	20	16.2	—	—	adv.	—	—
227.	16S-14E-20 NE	44°10'29"	121°04'20"	(5): MILLER	OR OR	11/25/80 08/12/80	975 963	— 30	— 5-10	16.2 12.6	— —	— —	— adv.	— —	— —
228.	16S-14E-20 SE	44°10'22"	121°03'58"	SLVDLR R	OR	08/12/80	972	149	5-10	(5): 16.9	10-30 125-149	— —	-30.4 110 (10.4)	— —	— —
229.	16S-14E-35 SW	44°08'34"	121°01'05"	SBUTTE 2	OR	12/10/80	1035	142	—	(5): 24.0	10-149 95-142	1.65e (0.15)	-12.5 47.4 (0.84)	45.9	[76]
230.	16S-15E-20 SW	44°10'10"	120°57'55"	(5): SBUTTE 1	OR OR	10/20/80 12/10/80	1035 1190	— 142	— —	24.1 14.8	90-140 40-142	1.65e (0.15)	47.3 29.4 (0.36)	28.4	47
231.	16S-15E-26 SW	44°08'56"	120°54'18"	(5): H MARTIN	OR OR	10/20/80 08/19/80	1190 1076	— 168	— 145-150	14.8 20.9	40-140 150-168	1.50e (0.25)	29.1 36.7 (2.71)	36.8	[55]
232.	16S-15E-29 SW	44°08'58"	120°57'38"	SHMWAY W	OR	09/24/80	1104	96	20	(5): 20.9	40-165 75-96	1.50e (0.25)	55.9 82.8 (1.50)	80.3	120
233.	(5): 17S-12E-09 SE	44°10'10" 44°06'36"	120°57'54" 121°17'23"	Gisler	OR US	10/20/80 09/04/80	1104 1050	— 251	— 215e	21.3 10.5	20-95 —	—	105.6 iso.	—	—
234.	17S-13E-08 NW	44°07'20"	121°11'52"	—	OR	05/01/80	1014	183	160-165	10.9	—	—	adv.	—	—
235.	17S-14E-23 NE	44°05'08"	121°00'57"	LEWIS	OR	08/20/80	1021	187	175-180	18.3	—	—	adv.	—	—
236.	17S-15E-20 SW	44°04'40"	120°57'40"	BOWEN	OR	04/16/80	1036	215	195-200	(5): 26.2	135-170	—	68.7 adv.	—	—
237.	18S-11E-23 SW	43°59'46"	121°22'53"	Wolf	US	08/27/87	1193	128	120	(5): 9.0	10-120 123-128	1.55e (0.35)	34.2 35.8 (0.20)	35.1	[54]
238.	18S-11E-25 NW	43°59'22"	121°21'24"	PATTRSON	OR	06/03/76	1195	130	—	9.2	—	—	adv.	—	—
239.	18S-11E-27 NW	43°59'17"	121°24'10"	City of Bend	US	08/20/87	1200	116	50	(1): 9.1	0-130	—	iso.	—	—
240.	18S-11E-36 NE	43°58'28"	121°21'12"	Deschutes County	US	08/24/87	1200	108	104	9.1	—	—	iso.	—	—
241.	18S-12E-05 NW	44°02'48"	121°19'03"	BS-WW	US	08/20/87	1102	223	106	10.3	—	—	adv.	—	—
242.	19S-11E-16 NE	43°55'48"	121°24'47"	(1): U.S.F.S.	OR US	05/02/76 08/22/87	1102 1276	— 77	— 13	— 7.1	0-230 —	—	— adv.	—	—
243.	19S-11E-25 NW	43°54'24"	121°21'30"	LAVBUTTE	OR	10/01/75	1373	123	—	9.2 (1):	93-123 93-123	[1.59] [1.59]	39.5 (3.22) 38.3	>38.4 38.3	[>61] 26 (sic)

Appendix.—Conductive heat-flow data from the Cascade Range and adjacent areas in north-central Oregon—Continued

T-R-Sec. 1/4	Longitude	Latitude	Name	Code	Date logged (mo/d/yr)	Elev. (m)	Depth (m)	Static water level (m)	Bottom-hole temp. (°C)	Interval (m)	Therm. cond. (W/m·K)	Gradient (°C/km) Uncorr.	Gradient (°C/km) Corr.	Heat flow (mW/m²)
								East of the Cascade crest—Continued						
244. 19S-14E-02 SE	121°00'33"	43°57'06"	Moon	US	08/22/87	1184	264	253e	22.3	—	—	adv.	—	—
245. 19S-14E-24 SE	120°59'11"	43°54'25"	Crane	OR	12/15/81	1280	384	360	21.7	250–380	1.65e (0.15)	30.9 (1.17)	30.9	51
246. (20S-7E-34) NE	121°51'51"	43°48'02"	U.S.D.A.	US	07/30/87	1410	53	17	6.8	46–53	1.55e (0.35)	14.1 (0.33)	>12.6	[>20]
247. 20S-14E-13 NE	120°59'12"	43°50'43"	—	OR	12/02/80	1314	108	—	13.1	70–108	1.50e (0.25)	30.9 (1.12)	32.0	48
248. 20S-14E-25 NE	120°59'21"	43°48'53"	BFZ-PMW	OR	08/17/76	1428	125	—	14.3	65–125	1.65e (0.15)	33.0 (0.27)	32.2	53
249. 21S-11E-25 NW	121°21'42"	43°43'56"	BFZ-MB	OR	08/04/76	1515	35	—	(1): 8.3	45–125 / 28–35	<1.84 / 1.51	34.4 / 67.6 (2.08)	34.4 / >64.8	<63 / [>98]
250. 21S-13E-31 SW	121°13'31"	43°42'26"	— (Newberry 2)	US	—/—/81	1950	932	8–9	(1,2): 265	28–35 / 842–932	1.51	65.3 / 449 (29.6)	65.3	100
251. 21S-13E-31 SW	121°13'25"	43°42'23"	— (RDO-1)	OR	10/06/83	1960	351	<15e	158	—	—	adv.	—	—
252. 21S-15E-16 NE	120°55'11"	43°45'12"	BFZ-PMS	OR	08/17/76	1476	152	—	14.5	70–152	1.76 (0.15)	54.6 (0.36)	52.2	92
253. 22S-14E-03 NE	121°02'15"	43°41'55"	BFZ-CH	OR	08/04/76	1580	75	—	(1): 5.8	70–150 / 52–75	1.76 / 1.55e (0.35)	55.0 / 9.0 (0.24)	55.0 / 8.0	96 / 12
254. 22S-15E-35 NE	120°52'36"	43°37'30"	BFZ-QM	OR	08/04/76	1660	40	—	(1): 7.6 ... (1):	0–75 / 15–40 / 20–40	1.65e (0.15)	18.9 (1.01) / 20.5	18.0 / 20.5	30